Investigation of Inositol dehydrogenase-related enzymes

A Thesis Submitted to the

College of Graduate Studies and Research

in Partial Fulfillment of the Requirements for the

Degree of Master of Science in the Department of Chemistry

University of Saskatchewan

Saskatoon

by

Hari Babu Aamudalapalli

Keywords: Inositol, Inositol dehydrogenase, *Lactobacillus plantarum* WCFS1, *Lactobacillus casei* BL23, gene cloning, gene expression, protein purification, and enzyme kinetics.

PERMISSION TO USE

In presenting this dissertation in partial fulfillment of the requirements for a Masters degree from the University of Saskatchewan, I agree that the libraries of this University may make it freely available for inspection. I further agree that permission for copying of this dissertation in any manner, in whole or in part, for scholarly purposes may be granted by the professor who supervised my dissertation work or, in their absence, by the Head of the Department or the Dean of the College in which my thesis work was done. It is also understood that any copying or publication or use of this dissertation or parts thereof for financial gain shall not be allowed without my written permission. It is also understood that due recognition shall be given to me and to the university of Saskatchewan in any scholarly use which may be made of any material in my dissertation

Request for permission to copy or make other use of material in this dissertation in whole or in part should be addressed to:

Head of the Department of Chemistry
University of Saskatchewan
110 Science Place, Saskatoon, SK S7N 5C9
CANADA

ABSTRACT

Inositol dehydrogenase (IDH) catalyzes the oxidation of *myo*-inositol to *scyllo*-inosose using NAD^+ as the coenzyme. IDH-related genes (*Lp_iolG1* to *Lp_iolG4*) from *Lactobacillus plantarum* WCSF1 and (*Lc_iolG1* and *Lc_iolG2*) from *Lactobacillus casei* BL23 were cloned into the vector *pQE-80L,* expressed in *E. coli* host cells and the proteins were purified to homogeneity. IDH activity of the purified enzymes was explored with *myo*-inositol and other structurally related compounds. It was found that IDH-related enzymes from *L. plantarum* WCSF1 did not exhibit any activity with tested substrates but, LcIDH1 and LcIDH2 from *L. casei* BL23 showed activity with *myo*-inositol and other related compounds. pH-rate profile studies have demonstrated the optimum pH for the reactions catalyzed by the active enzymes. Steady-state kinetics of the active enzymes was performed as with IDH from *Bacillus subtilis* (BsIDH), revealing that LcIDH1 is a *myo*-inositol dehydrogenase and LcIDH2 is a *scyllo*-inositol dehydrogenase. Both LcIDH1 and LcIDH2 are observed to be NAD^+-dependent. Kinetic isotopic effect experiments for LcIDH1 have demonstrated that the chemical step in the reaction is partly rate-limiting. Substrate spectrum of LcIDH1 and LcIDH2 was explored and compared to BsIDH. Finally, a multiple sequence alignment of IDH-related enzymes was performed and the proposed consensus sequence motifs were considered to understand the activity differences between these enzymes.

ACKNOWLEDGEMENTS

I would like to express my deep sense of gratitude to Dr. David Robert Joseph Palmer, Associate Professor and Head of the Department of Chemistry, University of Saskatchewan, for giving me this opportunity to work under his supervision. His valuable guidance and constant encouragement has enabled me to successfully complete this research project.

I would also like to thank my advisory committee member, Dr. David A. R. Sanders, Associate Professor, and committee chair, Dr. Dale E. Ward, Professor, for their valuable advices and helpful comments during the course of my graduate studies and the research work. I express my sincere thanks to all the Professor and Associate Professors of the Department of Chemistry and the College of Pharmacy and Nutrition, who helped me in successful completion of my graduate courses.

I enjoyed working with my lab members (Natasha Vetter, Yulia Skovpen, Anil Krishnamurthy, Dr. Shazia Anjum, Dr. Rajendra Jagdhane, and Julie Boisvert) and the members of Dr. David A. R. Sanders lab (Dr. Inder Sheoran, Dr. Karen E. Van Straaten, Dr. Sean Dalrymple, Jijin Raj Ayanathkuttiyatveetil, Carla Protsko, Drew Bertwistle, Sarathy K. P., Josiah Obiero and Ryan Stubbins). I thank each and every one for sharing their knowledge, for their encouraging support and for their great friendship. They made my stay during these years very blissful and memorable.

I express my sincere gratitude to the Department of Chemistry, the College of Graduate Studies and the University of Saskatchewan for giving me this opportunity and the financial support.

I am indebted to my friends, Suresh K. R. Chemicala, Harsha Rayudu, Vijay K. Mamillapalle, Anil Krishnamurthy, Jijin Raj Ayanathkuttiyatveetil, Vinay Chella and Tirupathiswamy Nidamanuri, who always there with me, spent their valuable time and supported me in my difficult situations.

Finally, I would like to thank my great parents, Janaki Aamudalapalli, Ram Murthy Aamudalapalli, and sister, Vijaya Lakshmi and her family for their endless affection and support without which I wouldn’t have been what I am today.

TABLE OF CONTENTS

LIST OF TABLES

LIST OF SCHEMES

LIST OF FIGURES

LIST OF ABBREVITONS

A_{280}	Absorbance measured at a wavelength of 280 nm
ADP	adenosine diphosphate
AMP	adenosine monophosphate
ATP	adenosine triphosphate
ATCC	American Type Culture Collection
AU	absorbance unit
BSA	bovine serum albumin
CECT	Spanish Type Culture Collection
CHES	*N*-cyclohexyl-2-aminoethanesulfonic acid
CV	column volumes
ddH_2O	distilled, deionized water
DMSO	dimethyl sulfoxide
DNA	deoxyribonucleic acid
dNTP	deoxynucleoside triphosphate
DTT	1, 4-dithio-D-threitol or dithiothreitol
ε	molar extinction coefficient
EDTA	ethylenediaminetetraacetic acid
FCC	flash column chromatography
GDP	guanidine diphosphate
GFOR	glucose-fructose oxidoreductase
h	hour
IDH	*myo*-Inositol-2-dehydrogenase or Inositol dehydrogenase
IMAC	Immobilized Metal ion Affinity Chromatography
IPTG	isopropyl-β-D-thiogalactoside

k_{cat}	turnover number
k_{cat}^{app}	apparent turnover number
k_{cat}/K_m	specificity constant
$(k_{cat}/K_m)^{app}$	apparent specificity constant
kDA	kilo Daltons
KEGG	Kyoto Encyclopedia of Genes and Genomes
KIE	kinetic isotopic effect
K_m	Michaelis constant
K_m^{app}	apparent Michaelis constant
LAB	Lactic acid bacteria
LB	Lauria Bertani
M	molecular weight
MCS	multiple cloning sites
MRS	De Man, Ragosa and Sharpe
MSA	malonic semialdehyde
m.p.	melting point
MWCO	molecular weight cut off
NAD	β-nicotinamide adenine dinucleotide
NADP	β-nicotinamide adenine dinucleotide phosphate
NCIMB	National Collection of Industrial and Marine Bacteria
NMR	nuclear magnetic resonance
OD_{600}	optical density measured at a wavelength of 600 nm
PCR	Polymerase chain reactions
PDB	Protein data bank
rt	room temperature
s	second
[S]	concentration of a substrate

SDS-PAGE	sodium dodecyl sulphate-polyacrylamide gel electrophoresis
TB	Terrific broth
TE	Tris EDTA
THcHDO	3D-(3,5/4)-trihydroxycyclo hexane-1,2-dione
T_m	melting temperature of DNA
Tris	2-amino-2-(hydroxymethyl)-propane-1, 3-diol
v_0	initial velocity
V_{max}	maximum velocity
V_{max}^{app}	apparent maximum velocity
WCFS	Wageningen Centre for Food Sciences

1. INTRODUCTION

1.1 Inositol and its importance

Inositol (cyclohexanehexol) exists in nine possible stereoisomers (**Figure 1.1**), *myo*-inositol, *scyllo*-inositol, D-*chiro*-inositol, L-*chiro*-inositol, *muco*-inositol, *allo*-inositol, *epi*-inositol, *cis*-inositol and *neo*-inositol (*1*). Among these isomers, *myo*-, D-*chiro*- *scyllo*-, L-*chiro*-, *muco*-, and *neo*- inositols are found in nature, while *allo*-, *epi*-, and *cis*- inositols can be obtained by chemical synthesis only. D-*chiro*- & L-*chiro*-inositols are enantiomers while other isomers are optically inactive (*2*). *myo*-Inositol (*cis*-1,2,3,5-*trans*-4,6-cyclohexanehexol), is the predominant form of inositol in nature (*3*).

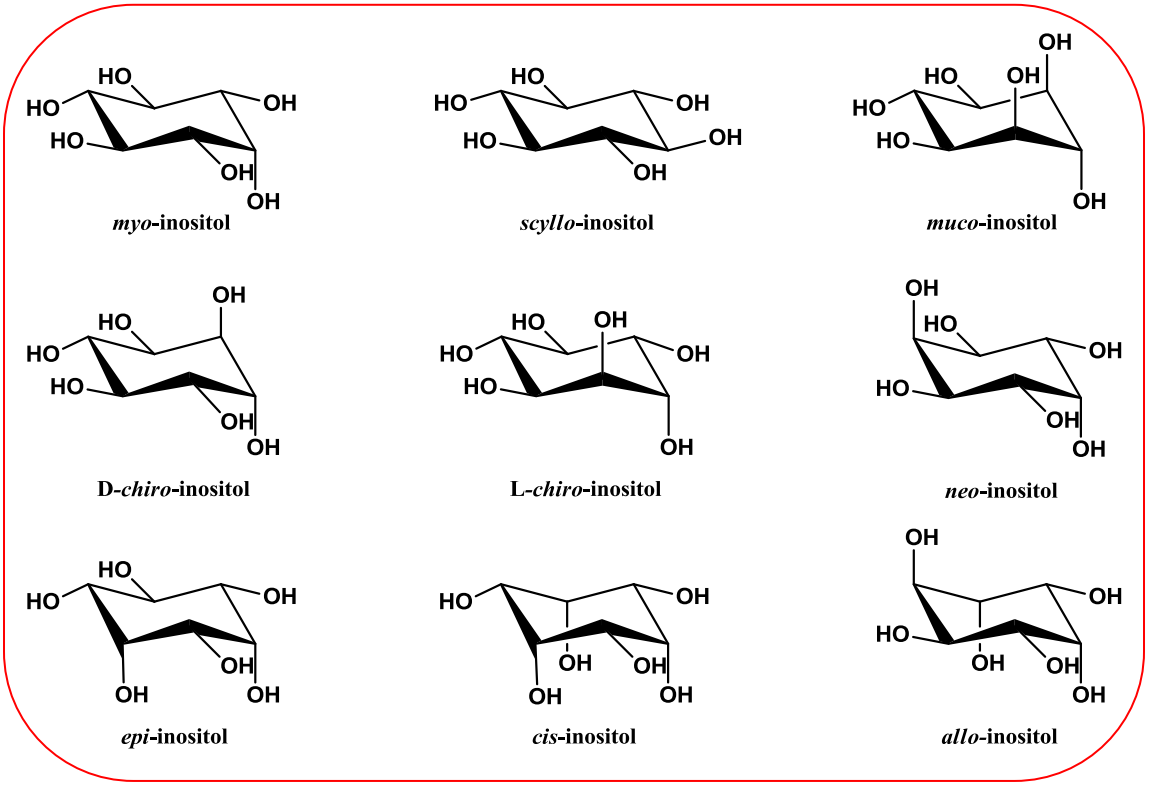

Figure 1.1: Structure and nomenclature of possible stereoisomers of inositol.

myo-inositol and its phosphate derivatives play an important role as secondary messenger molecules in diverse cellular activities, such as cell growth, apoptosis, cell migration, cell differentiation, stress response, seed germination, gene expression,

hormone function, protein trafficking etc, (*4-10*). Recently, D-*chiro*-inositol has been identified as a potential drug for the treatment of type-2-diabetes and polycystic ovary syndrome (*11, 12*). Phytic acid, or inositol hexakisphosphate is the principal storage form of phosphorus in plant tissues(*13, 14*). It is also found in high concentrations in many food items; including cereal grains, nuts, and seeds. Phytic acid is a metal chelator that can suppress the damage caused by metal-catalyzed redox reactions, making it a natural antioxidant (*15*). *myo*-inositol in the form of phytic acid has been proposed as a possible agent in the treatment of colon-cancer (*16*).

1.2 Inositol catabolism in bacteria

Inositol metabolism in eukaryotes is not discussed in this thesis as this work is entirely related to bacterial species. However, it has been reported that eukaryotic *myo*-inositol catabolic pathway is different from that which occurs in bacteria (*17*). *myo*-Inositol catabolism was reported for the first time in *Aerobacter aerogenes* (reclassified as *Enterobacter aerogenes*/*Klebsiella mobilis*) (*18*). Later, it was Anderson *et al.,* who demonstrated that acetyl-CoA, dihydroxyacetone phosphate (DHAP) and carbon dioxide are the end products of *myo*-inositol degradation in *A. aerogenes* (*19*). Further, it was reported that several microorganisms, including *Cryptococcus melibiosum* (*20*), *Rizobium leguminosarum by. viciae* (*21*), *Bacillus subtilis* (*22*), *Sinorhizobium meliloti* (*23*), *Salmonella enteric* serovar Typhimurium (*24*), *Sinorhizobium fredii* (*25*), *Corynebacterium glutamicum* (*26*) and *Lactobacillus casei* strain BL23 (*27*) are able to utilize *myo*-inositol as the sole carbon source for their metabolism.

However, a detailed *myo*-inositol catabolic pathway was reported from *B. subtilis* (*22*). In this organism, the *iol* divergon containing *iolABCDEFGHIJ, iolRS,* and *iolT* operons (clusters of genes) are involved in *myo*-inositol catabolism. Furthermore, it was demonstrated that *B. subtilis* can also utilize D-*chiro*-inositol as the carbon source (*28*). Recently, it was demonstrated that *B. subtilis* can also grow on *scyllo*-inositol as a sole carbon source and that this organism has two different *scyllo*-inositol dehydrogenase enzymes (*29*). The enzymes encoded by *iolX* and *iolW* (earlier called as *yisS* and *yvaA* respectively) catalyze the reversible oxidation of *scyllo*-inositol to *scyllo*-inosose using NAD^+ and $NADP^+$ as coenzymes respectively. Inositol catabolic pathways proposed for *A. aerogenes, B. subtilis* are indicated in **Figure 1.2.**

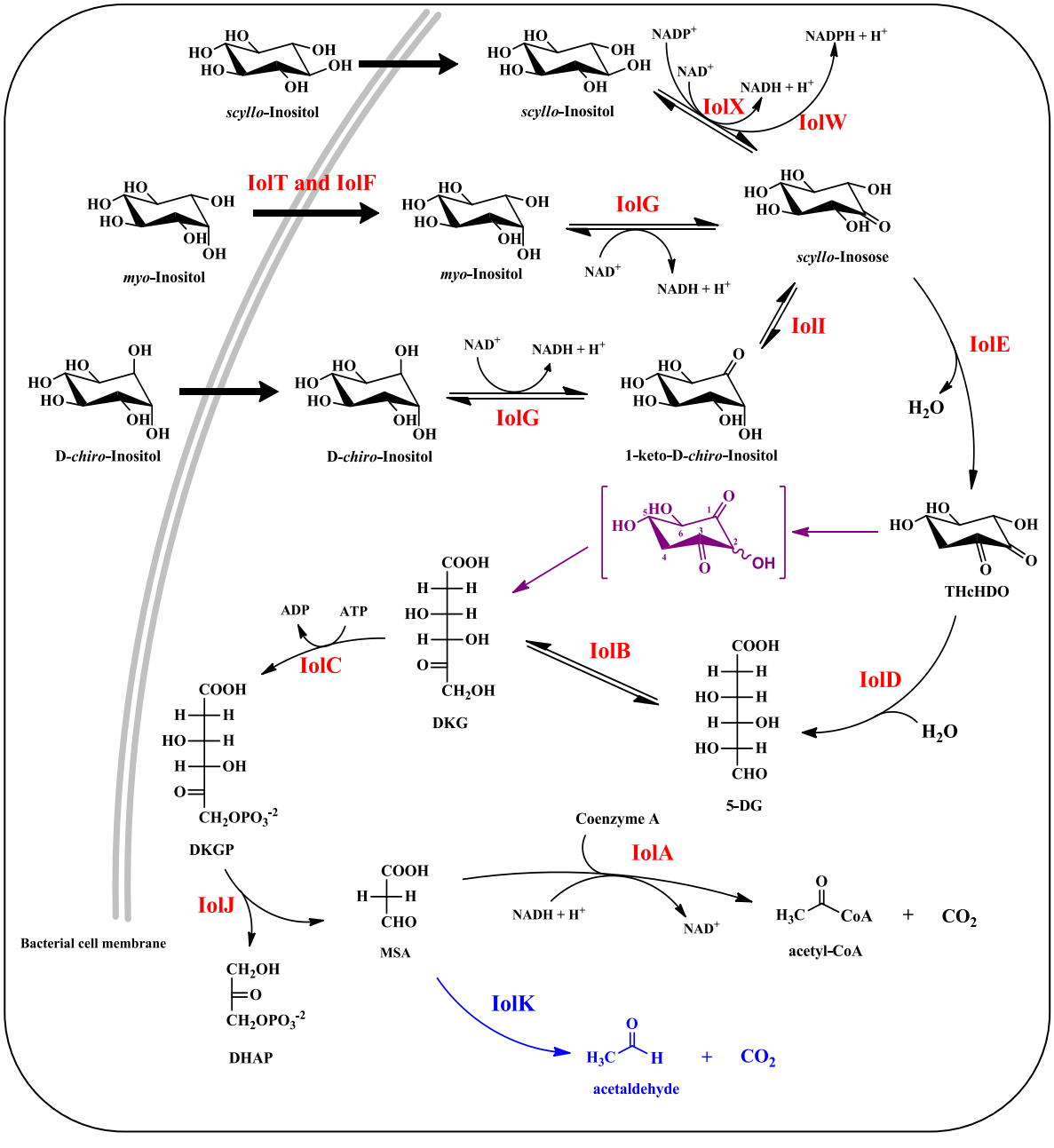

Figure 1.2: The proposed inositol catabolic pathway in bacteria. The proposed pathways from *A. aerogenes*, *B. subtilis* and *L. casei* BL23 are represented in colors. The pathway for *B.subtilis* is represented in all black; the pathway for *A. aerogenes* is indicated in green and the *iolK* pathway for *L. casei* BL23 is indicated in blue. The enzyme catalyzing each reaction is indicated in red. Compounds: THcHDO = 3D-(3, 5/4)-trihydroxycyclo hexane-1, 2-dione; 5-DG = 5-*deoxy*-glucuronic acid; DKG = 5-*deoxy*-2-keto-gluconic acid; DKGP = 5-*deoxy*-2-keto-gluconic acid-6-phosphate; DHAP = dihydroxy acetone phosphate; MSA = malonic semialdehyde.

As reported, *B. subtilis* takes up *myo*-inositol and other related compounds with the help of inositol transporters, IolT and IolF (*30*). Once the inositol is inside the cell, IolG catalyzes the first step of this catabolic pathway, the oxidation of *myo*-inositol to *scyllo*-inosose sometimes called as 2-keto-*myo*-inositol, and D-*chiro*-inositol to 1-keto-D-

chiro-inositol. IolI catalyzes the conversion of 1-keto-D-*chiro*-inositol to *scyllo*-inosose. IolX and IolW catalyze the conversion of *scyllo*-inositol to *scyllo*-inosose (*29*). The second step of the pathway is catalyzed by IolE, a 2-keto-*myo*-inositol dehydratase (*31*). According to Anderson *et al.*, the product of the second step, 3D-(3, 5/4)-trihydroxycyclohexane-1, 2-dione, (THcHDO) [earlier called as D-2, 3-diketo-4-*deoxy*-*epi*-inositol], isomerizes to an intermediate (indicated in green in **Figure 1.2**) by keto-enol tautomerization and leads to formation of 2-*deoxy*-5-keto-D-gluconic acid (DKG). But it was proposed to be different in *B. subtilis myo*-inositol catabolic pathway in which, THcHDO gets hydrolyzed to 5-*deoxy*-glucuronic acid (5-DG) catalyzed by IolD, a hydrolase. Isomerization of 5-DG to DKG is a fourth reaction catalyzed by IolB, an isomerase.

From the fifth reaction, the pathways in both *A. aerogenes* and *B. subtilis* are similar. IolC, a kinase, phosphorylates DKG to from 2-deoxy-5-keto-D-gluconic acid-6-phosphate (DKGP) in the presence of ATP. DKGP is cleaved into DHAP and malonic semialdehyde (MSA) by the action of IolJ, an aldolase. The final step of the pathway is catalyzed by a malonic semialdehyde decarboxylase, that was reported to be encoded by the product of *iolA* (*32*). The function of IolH has not been characterized but it was found that IolH is paralogous to IolE and IolI suggesting that IolH may act as either a dehydratase or an isomerase. However, it was demonstrated that IolH did not possess the dehydratase activity. Finally, it was demonstrated that *iolS* from *iolRS* operon encodes a pyridoxal reductase (*30*), which was earlier reported to be homologous to pyridoxal reductase of *Schizosaccharomyces pombe* (*33*).

The *iol* operon similar to *B. subtilis* has been identified in *L. casei* BL23 (*27*). However, some of the genes such as *iolI*, *iolH*, *iolS* and one of the inositol transporter genes, *iolF* are not present in the *iol* operon of *L. casei* BL23. But the presence of *iolK*, predicted to be a malonic semialdehyde decarboxylase, suggested that this organism may have two different pathways for malonic semialdehyde metabolism. The additional *iolK* pathway in *L. casei* BL23 is indicated in blue in **Figure 1.2.** Moreover, *L. casei* BL23 has two IDH-related genes, *iolG1* and *iolG2* in its operon.

1.3 Lactic acid bacteria and their importance

Lactic acid bacteria are a group of gram-positive, non-sporulating, non-respiring cocci (round shaped), or bacilli (rod shaped) that produce lactic acid during the fermentation of different carbohydrates (*34*). *Lactobacillus, Leuconostoc, Pediococcus, Lactococcus* and *Streptococcus* forms the main genera of this group. However, other organisms such as *Aerococcus, Carnobacterium, Enterococcus, Oenococcus, Sporolactobacillus, tetragenococcus* and *Weisella* are considered as the principle lactic acid bacteria based on their practical application in food and fermentation industries. Lactic acid bacteria are called either homofermentative or heterofermentative bacteria based on their method of carbohydrate metabolism. Homofermentative bacteria follow the Embden-Meyerhof-Parnas (EMP) pathway to metabolize sugars and produce high amounts of lactic acid (>85%) as the sole end product, while heterofermentative bacteria follow the pentose-phosphate pathway, alternatively called the phosphoketolase pathway or the phosphogluconate pathway and produces CO_2, ethanol/acetate and relatively less amount of lactic acid (*34*).

The genus *Lactobacillus* constitutes the largest group among lactic acid bacteria with over 100 species and subspecies. These microbes can be found in a variety of ecological niches such as plants, animals, raw milk and fermented food materials. Earlier, the *Lactobacillus* group was divided into three phylogenetic groups, the *Lactobacillus casei-Pediococcus, Lactobacillus delbrueckii* and *Leuconostoc* group, based on their 16S/23S rRNA gene sequence analysis (*35*). Later, the group *L. delbrueckii* was renamed as *L. acidophilus* and the *L. casei-Pediococcus* group was divided into *L. plantarum, L. casei, L. reuteri, L. bcuchneri* and *L. salivarius* groups (*36*). *Lactobacillus* species have been associated with food fermentation and dairy industries for many years. The ability to metabolize many sugars results in the production of several natural compounds, including organic acids (lactic acid, acetic acid, formic acid, phenyllactic acid, caproic acid), carbon dioxide, hydrogen peroxide, diacetyl, ethanol, bacteriocins, reuterin and reutericyclin. These compounds have been reported to have antimicrobial properties which help in preventing the growth of other bacteria and fungi (*37, 38*).

Probiotics are defined as “live microorganisms which, when administered in adequate amounts, confer health benefit on the host” (*39*). In order to consider a microorganism as a probiotic, it must have certain functional properties for example, it

must show tolerance to the acidic environment of human gut, adherence to epithelial surfaces, persistence in the human gastrointestinal (GI) tract, immune stimulation, antagonistic activity toward intestinal pathogens and the capacity to stabilize and modulate the intestinal microbes (*40, 41*). Probiotics must be non-pathogenic and non-toxic and should not carry acquired, genetically exchangeable antibiotic resistance.

Furthermore, it has been reported that probiotic *Lactobacillus* species have many beneficial effects on animal and human health. It has been demonstrated that LAB fermented milk and yoghurt supplemented with *L. bulgaricus* and *Streptococcus thermophilus* cultures have anti-mutagenic effects; that is, these bacteria degrade the harmful chemical mutants that are produced as a result of metabolism (*42, 43*). Studies on animal models and humans have demonstrated that probiotic *Lactobacillus* species such as *L. acidophilus* and *L. casei* (*44, 45*), *L. cremori* (*46*), *L. bulgaricus* (*47*), and *Bifidobacteria bifidum* (*48*) have been observed to reduce the serum cholesterol levels and decrease the risk of heart diseases. Consumption of sour milk fermented by *L. helveticus* and *Saccharomyces cerevisiae* cultures resulted in significant reduction of blood pressure in hypertensive patients (*49-51*), and many more applications of *Lactobacillus* have been reported.

1.3.1 *Lactobacillus plantarum* WCFS1

Lactobacillus plantarum WCFS1 is a microaerophilic, heterofermentative organism, usually found as a natural inhabitant of fermented vegetables and meat products (*52*). The strain WCFS1 is a single colony isolate of *L. plantarum* NCIMB8826, which was initially isolated from human saliva. The whole genome sequence of this organism has been determined. It contains two small, cryptic plasmids (2365 bp and 1917 bp) and a larger plasmid (36069 bp) encoding all genes involved in conjugal plasmid transfer and several other functions. The genome contains 3052 predicted protein coding genes and the putative biological functions were assigned to 2120 (70%) of these predicted gene products based on the sequence homology with other bacteria.

Presence of the 3.3 Mbp genome (largest among lactic acid bacteria), and majority of the predicted proteins that are related to various sugar transporters and sugar metabolism suggests that *L. plantarum* WCFS1 is able to ferment different sugars and can survive in various environmental habitats. Moreover, it has been reported that this

organism along with other *Lactobacilli* can survive passage through the stomach and is able to live for at least a week in the human GI tract and can adhere to epithelial surfaces of the GI tract. This property makes them to use as the vehicles for the delivery of active pharmaceutics, antibodies, enzymes and vaccines (*53*, *54*). In contrast to other vaccine carriers such as *Salmonella*, *E. coli*, and *Vaccinia* etc., *Lactobacilli* are considered highly safe for these purposes.

myo-Inositol catabolism has not been reported for this organism. Although, the *iol* operon looks incomplete, it consists of four predicted IDH-related genes (*Lp_iolG1* to *Lp_iolG4*). A diagram showing the *iol* operon of *L. plantarum* WCFS1 is indicated in **Figure 1.3**. In this thesis, the products of these genes are represented as LpIDH1 to LpIDH4 respectively.

1.3.2 *Lactobacillus casei* BL23

L. casei BL23 is a probiotic strain of genus *Lactobacillus*. It was identified while trying to obtain a plasmid free *L. casei* ATCC 393 (reclassified as *L. zeae*) (*55*). It is also a gram-positive, heterofermentative lactic acid producing bacteria. Its complete genome sequence reveals that it has a single circular chromosome of 3.08 Mbp (*55*). The genome of *L. casei* BL23 has an extra 12.8 K bp of DNA, compared to *L. casei* ATCC 334 and it is involved in *myo*-inositol catabolism (*27*). Based on these findings, the *myo*-inositol catabolic pathway has been proposed (**Figure 1.2**). The *iol* operon of this organism, as shown in **Figure 1.3**, consists of two IDH-related genes (*Lc_iolG1* and *Lc_iolG2*).

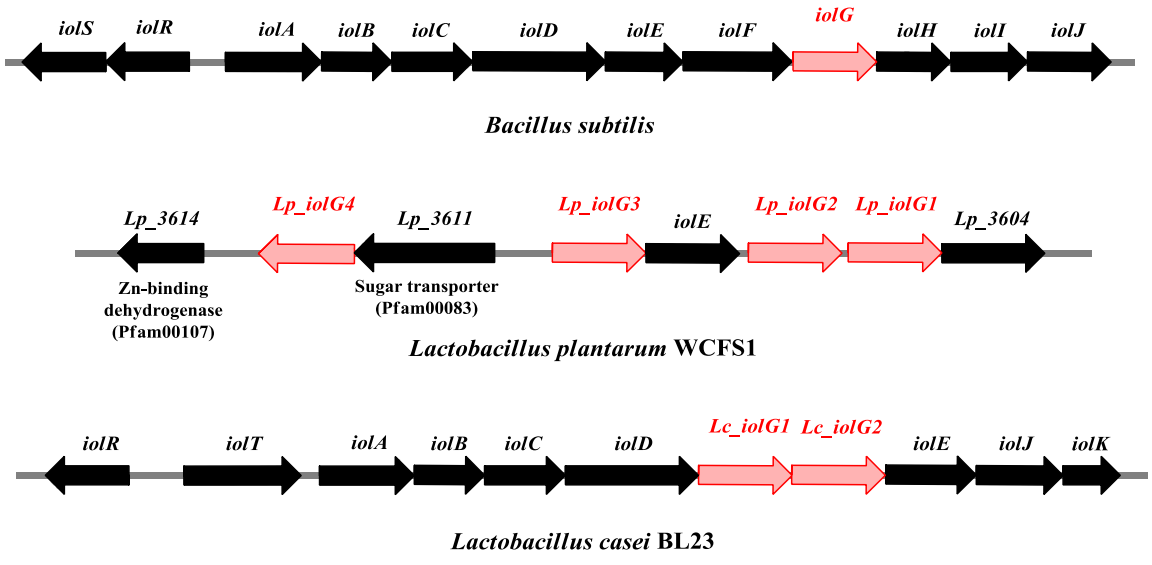

Figure 1.3: The *iol* operon showing the organization of the genes involved in *myo*-inositol catabolism. IDH-related genes are indicated in red. The image is generated using ChemDraw Pro 12.0 Version based on the information reported in *Appl. Environ. Microbiol.* (2000), 73: 3850-3858.

1.4 BsIDH as a model enzyme

In *B. subtilis*, IDH is encoded by *iolG* and hereafter this enzyme is called as BsIDH throughout this thesis. BsIDH (EC 1.1.1.18) belongs to the oxidoreductase class of enzymes because it catalyzes the oxidation-reduction reaction by transferring a hydride group between the substrate and the coenzyme, NAD^+. BsIDH was first isolated and characterized by Ramaley *et al.*, in 1979 (*56*). The active enzyme is a homotetramer with an apparent molecular weight of 160 kDa and each monomer of 40 kDa. The pH-rate profile indicated that the maximum activity for the forward reaction occurs at pH 9.0 and for the reverse reaction occurs at pH 7.0. Our lab has also studied the biochemical and mechanistic features of this enzyme to a great detail in collaborating with Dr. David A. R. Sanders lab and confirmed that BsIDH is an NAD^+-dependent enzyme and catalyzes the oxidation of the C2 axial hydroxyl group of *myo*-inositol to form *scyllo*-inosose, and simultaneous reduction of NAD^+ to NADH by transferring the C2 equatorial hydride of *myo*-inositol to the C4 of the nicotinamide ring of NAD^+, which is the first step in the *myo*-inositol catabolism for *B. subtilis* **(Scheme 1.1)** (*56, 57*).

Kinetic studies have demonstrated that the reaction catalyzed by BsIDH follows a sequentially ordered Bi-Bi mechanism (*56*, *58*). The enzyme shows a broad substrate spectrum and at the same time it is highly stereoselective between the substrates (*57*, *59*). This enzyme predominantly oxidizes *myo*-inositol and can also accept other related compounds such as D-glucose and D-xylose as its substrates, but shows no activity with *scyllo*-inositol (*56*). Previous results from our laboratory have revealed that 4-*O*-substituted *myo*-inositol and 6-*O*-substituted D-glucose derivatives were also substrates for BsIDH (*60*). In addition, it shows trace activity with D-ribose and D-fructose, but cannot oxidize compounds such as D-galactose, D-sorbitol, D-mannose, D-mannitol, GDP-D-mannose, *scyllo*-inosose, ADP-D-glucose, D-mannose-6-phosphate, CDP-D-glucose, D-glucose-6-phosphate, *myo*-inositol-4-*O*-phosphate, D-glucosamine, 2-deoxy-D-glucose-6-phosphate, D-erythrose, D-erythritol and N-acetyl-D-glucosamine (*56*, *61*). Recently it is was reported that, BsIDH can also oxidize D-*chiro*-inositol (*28*), and pinitol, (3-*O*-methyl-D-*chiro*-inositol) (*62*).

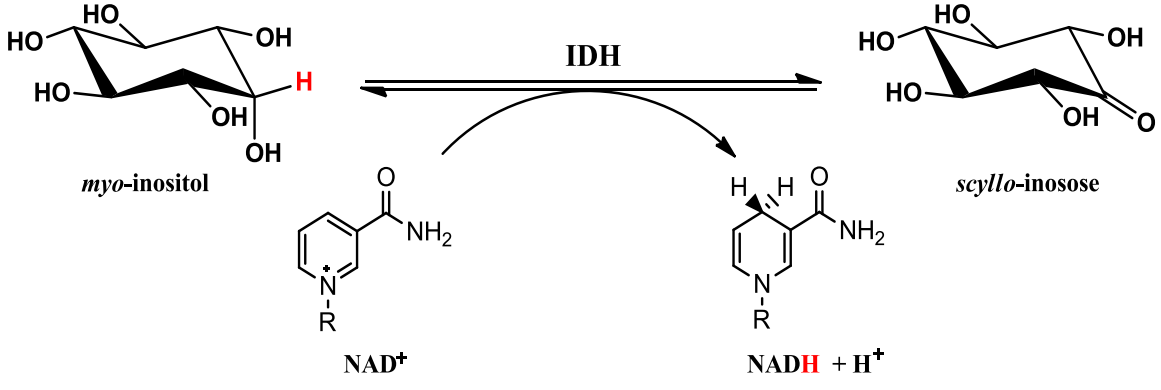

Scheme 1.1: Reaction catalyzed by BsIDH

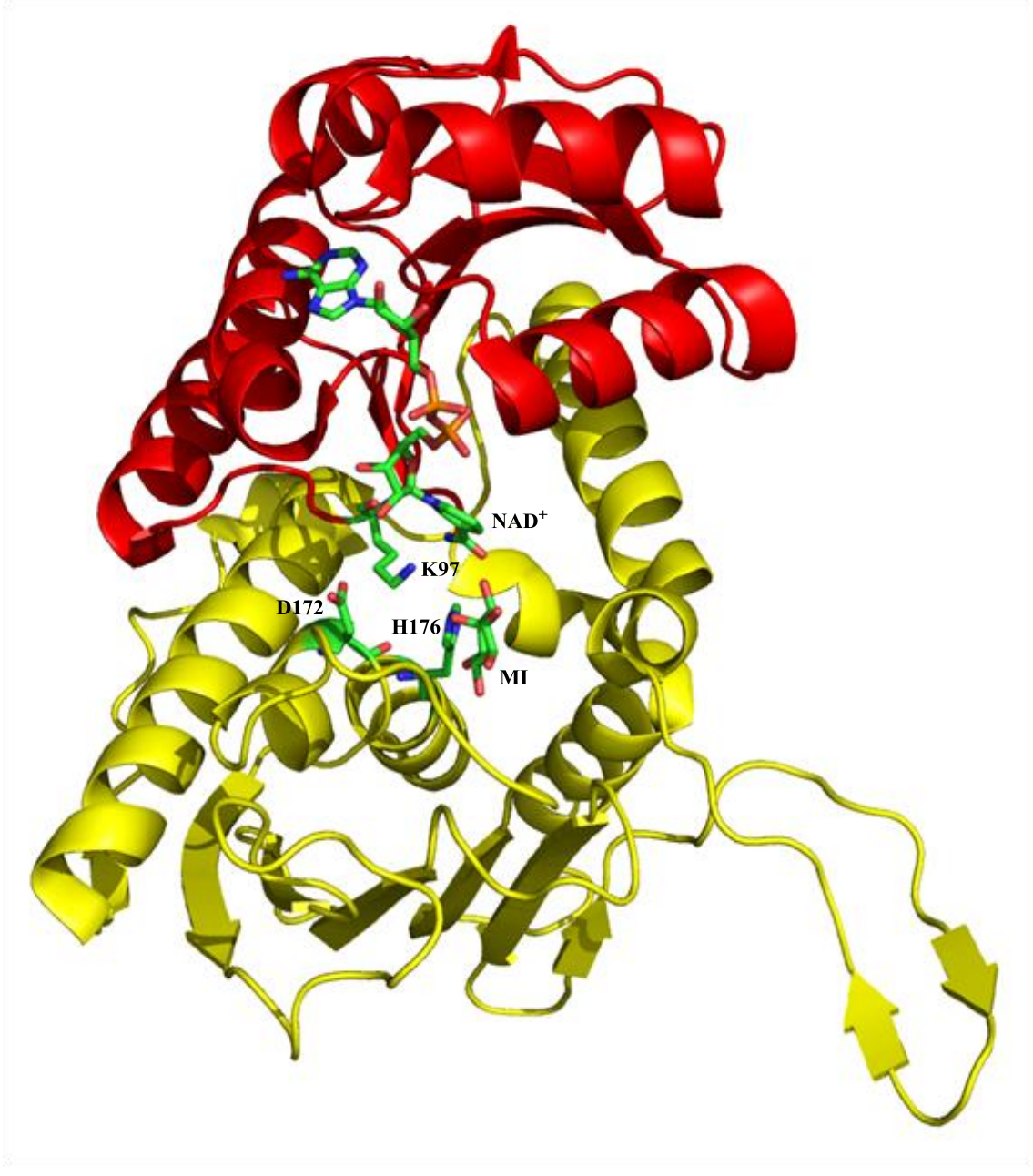

Figure 1.4: Structure of BsIDH (PDB code: 3NT4). The N-terminal domain with bound NAD^+ is indicated in red and the C-terminal domain with *myo*-inositol (MI) in the active site is shown in yellow. Active site residues, (K97, D172 and H176) and NAD^+ and substrate are highlighted.

BsIDH is assigned to the GFOR/IDH/MocA family of homologous dehydrogenases (*63*) and its active site residues Asp172 and H176 were predicted based on the sequence alignment analysis (*61*), homology model building and manual docking studies (*60*). The structures for apo-enzyme, holo-enzyme and apo-K97V mutant and the

ternary complexes with *myo*-inositol and *scyllo*-inosose were determined (*63*, *64*). These structural studies have revealed that, K97 is also involved in a proton transfer to D172 through a water molecule during catalysis. Each monomer shows two structurally distinct domains (**Figure 1.4**). The N-terminal domain spans up to 124 amino acid residues and it forms a characteristic dinucleotide binding Rossmann fold with a centrally arranged parallel β-sheet surrounded by α-helices. The rest of the protein sequence (125-337 residues) forms the C-terminal domain. It consists of 6 α-helices, an antiparallel oriented 6-stranded β-sheets and an antiparallel oriented two-stranded short β-sheet which extends out from the core monomer. This extended structure of each monomer is held together to form a tetramer. The coenzyme (NAD^+) binds to the N-terminal domain with its nicotinamide ring pointing towards the active site present at the interface of the two domains, where the substrate binds.

1.5 IDH-related enzymes

Genome sequencing and multiple sequence alignment analysis of many bacterial DNA have demonstrated the presence of multiple genes encoding for IDH-related enzymes. For example, *Lactobacillus casei* BL23 (*Lc_iolG1 and Lc_iolG2*) (*27*), *Salmonella enteric*a serovar Typhimurium (*St_iolG1 and St_iolG2*) (*65*), *Corynebacterium glutamicum* (*Cg_iolG1 to Cg_iolG3*) (*26*), and *Lactobacillus plantarum* WCFS1 (*Lp_iolG1 to Lp_iolG4*) (*52*).

Multiple sequence alignment of these IDH-related enzymes with the sequence and structure of BsIDH has led to the identification of six different consensus sequence motifs of which motifs I and II are involved in NAD^+/NADH binding while the other four motifs define the binding pocket of the active site for these enzymes (*63*). Based on these findings, the putative IDH-related enzymes were classified into four subgroups. A multiple sequence alignment of IDH-related enzymes from *L. plantarum* WCFS1 and *L. casei* BL23 with BsIDH is shown in **Figure 1.5**.

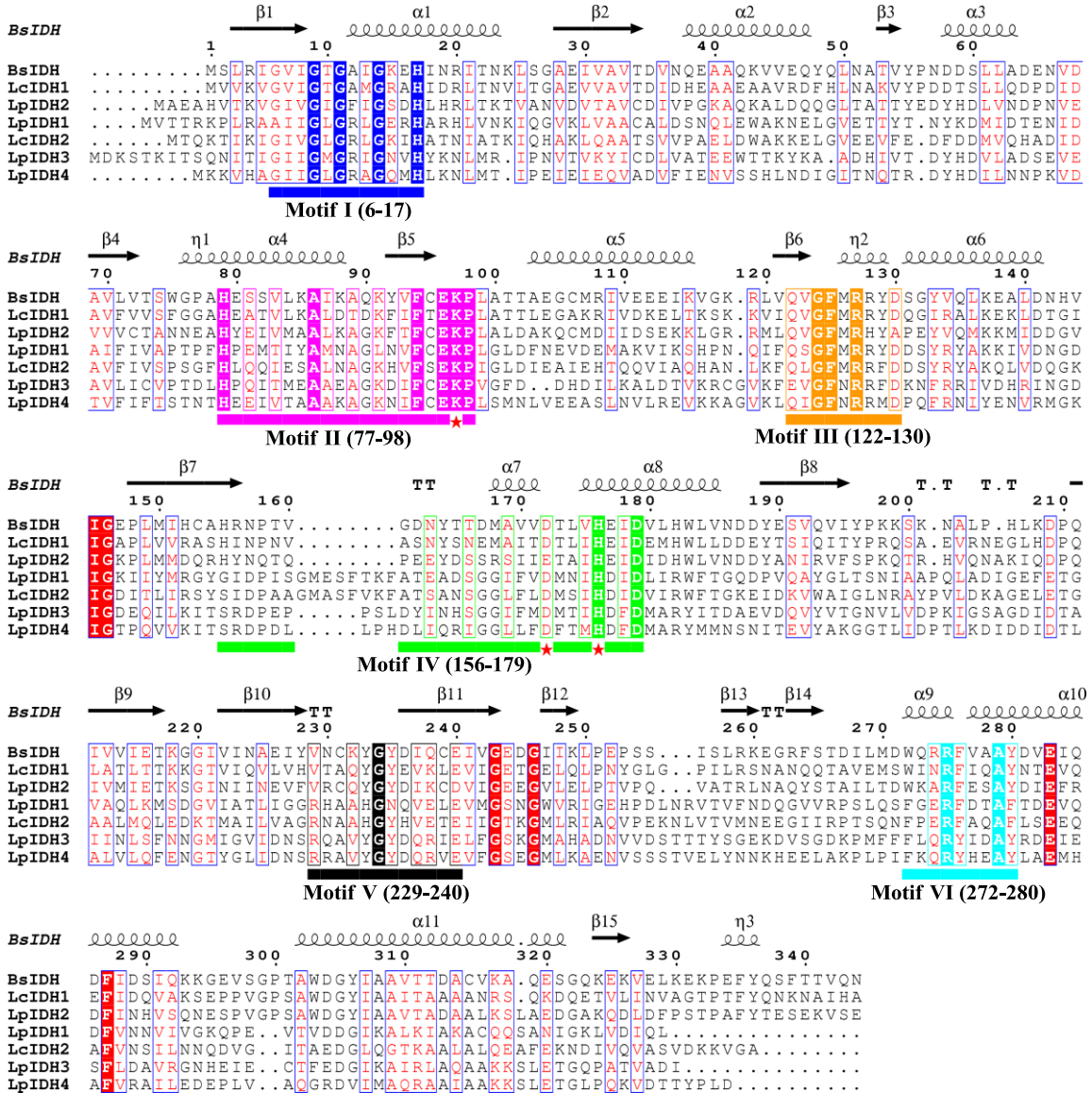

Figure 1.5: Multiple sequence alignment IDH-related enzymes from *L. plantarum* WCFS1, *L. casei* BL23 and BsIDH. The consensus sequence motifs are highlighted in colors, the active site residues (K97, D172 and H176) are indicated with red star. The image is generated using ClustalW2 and ESPript V2.2 softwares based on the information reported in *Biochemical Journal* (2010), 432, 237-247.

BsIDH, StIDH and LpIDH2 are included in subgroup I, in which the amino acid residues involved in substrate binding are highly conserved indicating that they are probably *myo*-inositol dehydrogenases. It was reported that the protein sequence of LcIDH1 has high percentage of sequence identity with BsIDH and considered as the actual IDH for *L. casei* BL23 (*27*). The enzymes that showed high percentage sequence identity with LpIDH1 are included in subgroup II and LcIDH2 has 46% sequence identity with LpIDH1.

Subgroup III includes TmIDH, CgIDH, LpIDH3 and IDHA from *Rhizobium* and *Brucella* species, and MocA from various species of *Brucella*. These enzymes have a proline-rich loop between β-strand 7 and α-helix 7 in their substrate binding pocket, which forms a flexible left-handed poly-proline helix (PP_II helix) (*66*). It was proposed that this loop may make the adjacent α-helix to close the active site after the substrate or coenzyme binding (*67*). Also found was that these members have high sequence identity among themselves than compared to other group members. LpIDH4 is included in subgroup IV. Although, the structure is not available for this subgroup, the consensus sequence motifs I, II, III, V and VI of these members show similarity to subgroup III, but only motif IV is different. Recent studies by Zhang *et al* have identified *iol* operons from several species of *Lactobacillus* by comparing the genome sequences with *B. subtilis* and reported that most of the *L. casei* species show similar kind of *iol* operons (*68*).

1.5.1 Studies on LpIDH1

Before I started this research project, the protein structure for LpIDH1 was known, (PDB code: 3CEA). The clone was obtained from the Joint Center for Structural Genomics. In our lab LpIDH1 was first expressed and purified by Hongyan Zheng and its functional characterization had been studied to a little extent by Natasha Vetter and Grey Wilkinson, undergraduate students from this lab. It was established that LpIDH1 reacts with *scyllo*-inososе. The product of this reaction shows a UV absorption peak at 304 nm. Different buffers with varying pH conditions were tested for LpIDH1 activity and the kinetic assays were performed in 100 mM Bis-Tris buffers pH 6.5 at 25^{o}C. In 1979 Angyal *et al* has reported that in basic solutions *scyllo*-inososе isomerizes into enediols that show UV absorption peak at 304 nm (*69*). This suggested that buffers with basic pH are not suitable for measuring LpIDH1 activity. The effect of NAD^+ and NADH in this reaction seems to be little or even negligible. Later, Ryan Stubbins, another undergraduate student from Dr. David A. R. Sanders lab has determined the crystal structures for wild type and the mutants and found that the NAD^+ was intrinsically bound to the purified LpIDH1. However, the product of this reaction was not identified and the role of NAD^+ bound to this enzyme is not known. **Figure 1.6** shows the structure of LpIDH1 with NAD^+.

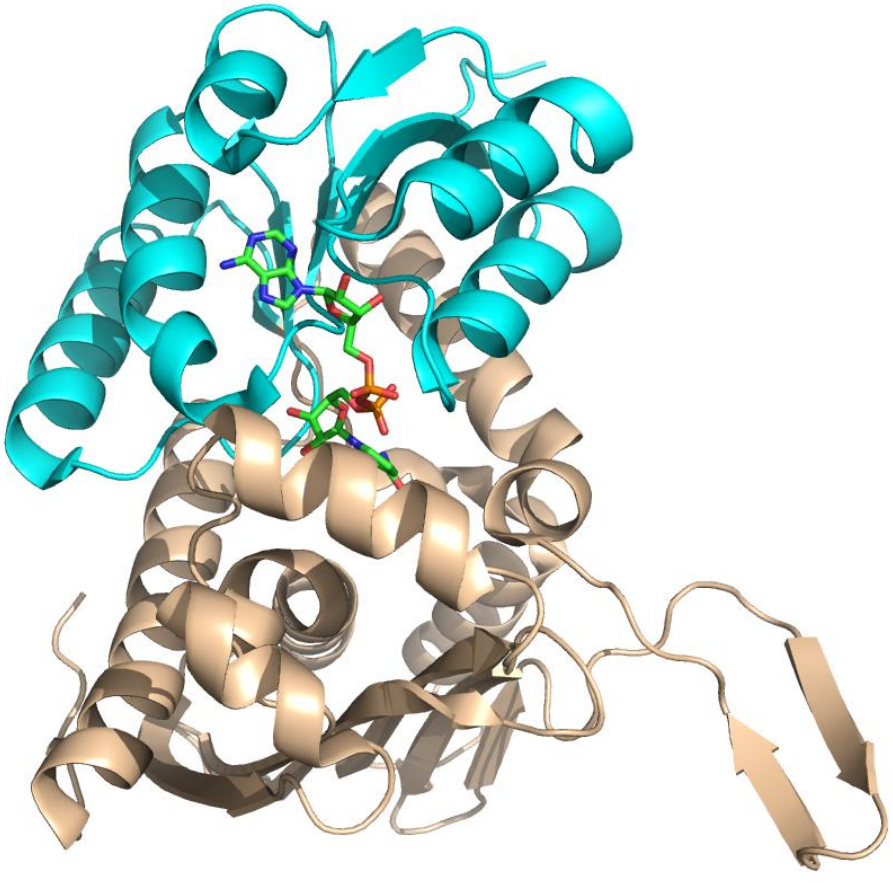

Figure 1.6: Structure of LpIDH1 (PDB code: 3CEA). The N-terminal domain with bound NAD^+ is indicated in cyan and the C-terminal domain is shown in brown.

1.6 Mechanisms of two substrate reaction

The enzyme catalyzed reactions involving two substrates and two products are called as Bi-Bi reactions (*70*). An example of a Bi-Bi reaction is shown in **Scheme 1.2.**

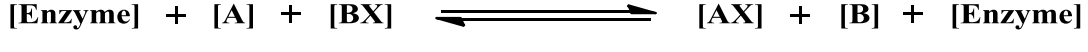

Scheme 1.2: Bi-Bi reaction

Where, [A] and [BX] are substrates and [AX] and [B] are products respectively. On the basis of the binding order of the substrates and the releasing order of products, the Bi-Bi reactions are identified to follow three types of mechanisms and named as random ordered, compulsory or sequentially ordered, and Ping-Pong mechanisms. In random ordered mechanism, either substrate A or BX will bind first to the enzyme before catalysis, after catalysis either product AX or B will release first, as shown in **Scheme**

1.3. The binding of first substrate is independent of the binding of the second substrate. The conversion of glucose to glucose-6-phosphate by hexokinase, using ATP is an example of random ordered mechanism.

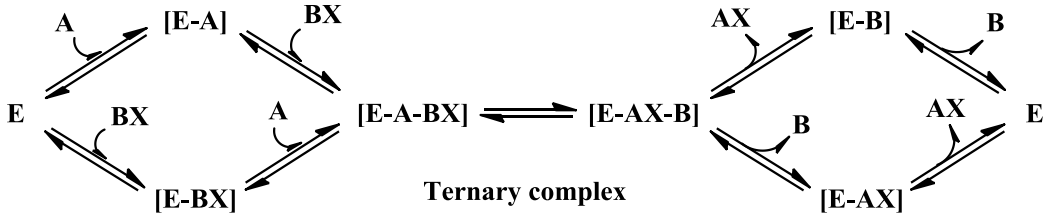

Scheme 1.3: Random ordered mechanism for a Bi-Bi reaction.

In compulsory ordered or sequentially ordered mechanism, substrate A will bind first followed by the second substrate BX to the binary complex [E–A] and forms a ternary complex [E-A-BX] before catalysis, as shown in **Scheme 1.4**. After catalysis, the ternary complex containing products, [E-AX-B] will breaks down to release the product B first followed by AX. Dehydrogenase enzymes are reported to follow this type of mechanism. As described in section **1.4,** the reaction catalyzed by BsIDH is a Bi-Bi reaction and it follows a sequentially ordered mechanism during catalysis (*56*) (*58*). Here the substrate NAD^+ binds first to BsIDH followed by *myo*-inositol. After catalysis, the product *scyllo*-inosose is released first followed by NADH.

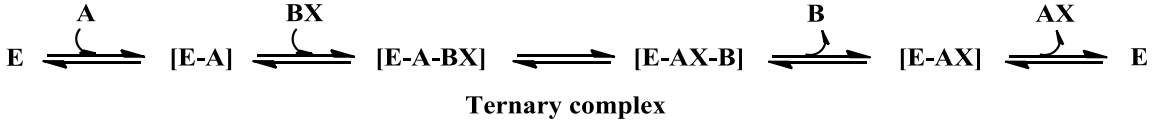

Scheme 1.4: Compulsory ordered mechanism for a Bi-Bi reaction

In Ping-Pong mechanism, the enzyme converts the first substrate BX into the product B. During this conversion, an atom or a group of BX remains attached to the enzyme, shown as [EX] in the **Scheme 1.5.** Then the second substrate A binds to [EX] and gets converted into AX. In this way an atom or a group from BX is transferred to A. Aminotransferase is an example of a Ping-Pong mechanism.

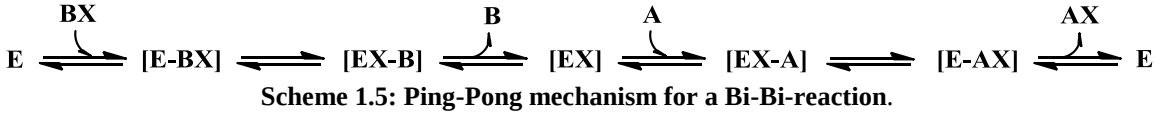

Scheme 1.5: Ping-Pong mechanism for a Bi-Bi-reaction.

These mechanisms can be distinguished by double reciprocal plot of the kinetic data. That is, the initial velocity data is plotted as 1/[initial velocity] versus 1/[substrate] and if the plot displays a set of lines intersecting towards the left of the y-axis, it indicates that the reaction follows an ordered (either random or sequential) mechanism and if the plot displays a set of parallel lines, it indicates that the reaction follows a Ping-Pong mechanism in the Bi-Bi-reactions. Two inhibition methods such as dead end inhibition and product inhibition can further distinguish the random ordered and the compulsory ordered mechanism.

1.7 Kinetic isotopic effect (KIE)

Kinetic isotopic effect (KIE) can be explained as the change in the rate of a reaction when an atom of the substrate is substituted by its isotope and used in the same reaction. Isotopic substitution affects only the mass dependant properties such as vibrational frequency of the atoms (*71*). Mathematically, the theoretical and the experimental KIE can be represented as the ratio of k_H/k_D, where k_H is the rate constant of the reaction when performed with normal substrate and k_D is the rate constant of the reaction when performed with the isotope substituted substrate (*72*). The magnitude of the KIE value depends on the relative mass difference between the atom and its isotope and in most of the KIE experiments hydrogen is substituted with deuterium or tritium. KIE is classified into primary KIE and secondary KIE based on the position of the isotope relative to the site of bond making or bond breaking in the rate determining step of a reaction mechanism (*73*). When the isotopic substitution is at the site of bond making or breaking in the rate determining step, it is called as the primary KIE and when the isotopic substitution is adjacent to the site of bond making or breaking in the rate determining step, it is called as the secondary KIE. The secondary KIE is always lesser than the primary KIE, and the maximum theoretical values for the primary deuterium KIE is 6.9, the secondary deuterium KIE is 1.2, whereas the primary tritium KIE is 18 (*72*). The concept of kinetic isotopic effect can be applied to enzyme catalyzed reactions to determine the rate determining step of the reaction mechanism. The KIE of an enzyme catalyzed reaction can be represented as ${}^{X}V_{max}$, ${}^{X}(V_{max}/K_m)$, or ${}^{X}(k_{cat}/K_m)$, where the superscript X is the isotopic substitution.

2. RESEARCH OBJECTIVES

Although IDH-related enzymes from different bacteria have been identified and their functions were hypothesized, it is not clear whether these predicted enzymes have similar functions, share the same structural features or display different specificities towards inositol isomers or other structurally related compounds. Therefore, this research project was aimed at the investigation of IDH-related enzymes from *Lactobacillus plantarum* WCFS1 and *Lactobacillus casei* BL23. BsIDH was chosen as a comparative model in this study because it has been characterized structurally and functionally to a great detail in our lab collaborating with Dr. David A. R. Sanders laboratory. Here are the objectives of this research:

1. clone all genes that encode inositol dehydrogenase from *L. plantarum* WCFS1 (*Lp_iolG1 to Lp_iolG4*) and *L. casei* BL23 (*Lc_iolG1 and Lc_iolG2*);
2. express and purify IDH-related enzymes (LpIDH1 to LpIDH4, and LcIDH1 & LcIDH2) in their active form;
3. observe dehydrogenase activity with *myo*-inositol and/or other related compounds;
4. study the pH-rate profiles, determine the true kinetic constants and identify the substrate spectrum for all enzymes that are showing dehydrogenase activity;
5. compare the pH-rate profiles, the true kinetic constants and the substrate spectrum of the active enzyme/s with BsIDH;
6. if possible, rationalize the activity differences between these enzymes by comparing their sequences and/or structures to each other and to BsIDH.

3. MATERIALS AND METHODS

3.1 Materials and instrumentation

Lactobacillus plantarum WCFS1 was purchased from the American Type Culture Collection (ATCC # BAA-793) and *Lactobacillus casei* BL23 was purchased from the Spanish Type Culture Collection (CECT # 5275). *Gluconobacter oxydans* was purchased from American Type Culture Collection (ATCC # 621H). *Escherichia coli* XL1 Blue and *E.coli* BL21 Gold (DE3) competent cells were purchased from Novagen®, EMD Biosciences, ON, Canada. MRS broth media was purchased from Sigma-Aldrich, (ON, Canada) and other culture media ingredients such as Yeast Extract, Peptone, Tryptone and Agar were purchased from Becton, Dickinson and Company, (BD) USA and/or EMD Biosciences, ON, Canada. DNA primers used in PCR were purchased from Integrated DNA Technologies (IDT), IW, USA. *PfuUltra*® HiFi DNA polymerase (Stratagene, Agilent Technologies Ltd) and/or KAPA HiFi DNA polymerase (KAPA Biosystems, MA, USA.) were used for gene amplification reactions. QIAprep Spin Miniprep Kit, QIAprep PCR Purification Kit and QIAprep Gel Extraction Kit and the vector *pQE-80L* were purchased from QIAGEN Inc, ON, Canada.

Restriction enzymes, T4 DNA Ligase and other reagents used in gene cloning experiments were purchased from New England Biolabs (NEB), MA, USA. A HiTrap-IMAC FF 1mL columns and a Chelating Sepharose™ Fast Flow resin were purchased from GE Healthcare, QC, Canada. A Spectra/Por® # 7 (25 kDa MWCO) protein dialysis membrane was purchased from Spectrum Laboratories, CA, USA. Chemical compounds like *scyllo*-inosose, 2-^{1}H-*myo*-inositol and 2-^{2}H-*myo*-inositol used for kinetic isotopic effect (KIE) experiments were prepared as described previously in Hongyan Zheng's PhD thesis (*61*). All other materials and reagents used in this research were purchased from Sigma-Aldrich (ON, Canada), VWR (ON, Canada), Alfa Aesar (MA, USA) or TCI America (OR, USA).

Bacillus subtilis iolG (*Bs_iolG*) gene was previously cloned into *NdeI* and *BamHI* sites in the multiple cloning sites (MCS) of *pET-28b* vector (EMD Biosciences) by Mike Laliberte, a summer student form this laboratory. *E. coli* host cell containing *pET-28b*-

Bs_iolG plasmid was used for the expression of BsIDH. Bacterial culture media was sterilized using either a table top sterilizer (VWR) or a Castle® 233LS vacuum steam sterilizer (GETINGE Canada Ltd., ON Canada). Distilled deionized water (ddH_2O) was obtained from a Barnstead NANOpure® DIamond™ Life Science (UV/UF) ultrapure water system. A Beckman Coulter microfuge-18R table-top centrifuge was used during genomic DNA and plasmid DNA purification processes. A Mastercycler® Gradient (Eppendorf) is a PCR device used to amplify inositol dehydrogenase related genes by the polymerase chain reaction (PCR) method. DNA concentrations were measured using a NanoDrop™ 1000 Spectrophotometer (Thermo Scientific). DNA analyses of PCR amplified DNA fragments, plasmid DNA samples and all other DNA samples during gene cloning experiments were performed using a Sub-cell® GT agarose gel electrophoresis unit (Bio-Rad).

Temperature controlled orbital shaker incubators were used for bacterial cell culturing and protein expression. A Virsonic 600 ultrasonic cell distrupter (VirTis Company) was used for cell lysis during protein isolation. A Beckman Coulter Avanti J-E high speed centrifuge was used during, cell harvesting, protein separation from cell debris, and protein concentrations. A HiTrap-IMAC FF 1 mL column and an XK 16 column (GE Healthcare) packed with Chelating Sepharose™ Fast Flow resin was used for protein purification. A Mini-PROTEAN 3 electrophoresis unit (Bio-Rad) was used to perform SDS-polyacrylamide gel electrophoresis. Protein concentration measurements and enzyme kinetic assays were performed using a Beckman DU640 UV-VIS spectrophotometer connected to a temperature controlled circulating-water bath. DNA sequencing was performed at DNA Technologies Unit, National Research Council, Plant Biotechnology Institute (NRC-PBI), Saskatoon, SK, Canada.

3.2 Preparation of substrates

3.2.1 Biotransformation of *myo*-inositol to *scyllo*-inosose [74]

A loop full of *Gluconobacter oxydans* from the glycerol stock was transferred into a test tube containing 10 mL revitalizing media (1.0 g D-sorbitol, 0.05 g yeast extract) and incubated by shaking aerobically at 200 rpm and 30 ^{o}C overnight. A flask containing 300 mL of sterile revitalizing *myo*-inositol media (0.3 g D-sorbitol, 1.5 g yeast extract, and 8.25 g *myo*-inositol was inoculated with 2.5 mL of overnight culture and incubated at

the same conditions for 4 days (96 h). After 96 h incubation, the cells were harvested by centrifugation at 3,500 ×*g* for 30 min and the supernatant was collected into a clean 500 mL round bottomed flask. The supernatant was reduced to half of its original volume by evaporation at 40^{o}C. An equal volume of ice-cold MeOH was added to the resultant supernatant and kept at -20^{o}C for 2 more days. The precipitate was filtered, washed with 10 mL fresh ice-cold MeOH and air dried to afford *scyllo*-inosose as a white powder. The overall yield obtained was 4.65 g, (56%). m.p: 190 - 192 ^{o}C, Lit (*74*) m.p: 188 - 192 ^{o}C, 1H-NMR (D_2O): δ 4.36 (2H, d, *J* = 10 Hz), 3.77 (1H, t, *J* = 9.5 Hz), 3.5-3.2 (2H, m) ppm.

3.2.2 Preparation of 2-^{2}H-*myo*-inositol and *myo*-inositol

Chemical compounds such as 2-^{2}H-*myo*-inositol and *myo*-inositol were prepared according to the procedure described in Hongyan Zheng's PhD thesis (*61*). The overall yield for 2-^{2}H-*myo*-inositol and *myo*-inositol was 28% and 33% respectively. The ^{1}H NMR for 2-^{2}H-*myo*-inositol (D_2O): δ 3.58 (2H, t, *J* = 9.8 Hz,), 3.49 (2H, d, *J* = 10 Hz), 3.25 (1H, t, *J* = 9.3), and *myo*-inositol (D_2O): δ 4.01 (1H, t, *J* = 2.8 Hz), 3.58 (2H, t, *J* = 9.7 Hz), 3.49 (2H, dd, *J* = 2.9 Hz and 10 Hz), 3.23 (1H, t, *J* = 9.4 Hz) ppm.

3.3 Microbiology methods

3.3.1 Preparation of culture media

L. plantarum WCFS1 and *L. casei* BL23 strains were cultured in De Man, Ragosa and Sharpe (MRS) media. *E. coli* XL1 Blue or BL21 host cells containing a recombinant plasmid were regularly performed in a Luria-Bertani (LB) media. Terrific Broth (TB) was used for routine gene expression experiments. MRS and LB agar plates were prepared by adding 1.5% (w/v) agar to the liquid media (also called as broth) before sterilization. After sterilization, the media was cooled to about 45-50 ^{o}C; antibiotics such as ampicillin (50 µg/mL) or kanamycin (50 µg/mL) were added as required and then, the media was poured into petri plates and allowed them to solidify under aseptic conditions. Finally, the sterile media (broth and agar plates) was stored at 4 ^{o}C for future use. The compositions for all types of media used in this research were indicated in **Appendix-A.**

3.3.2 Preparation of the glycerol stocks of bacterial strains

Lyophilized cell pellets of *L. plantarum* WCFS1 and *L. casei* BL23 were resuspended separately in 0.5 mL of MRS broth by following the supplier's instructions. A loop full of each suspension was streaked separately on MRS agar and the plates were incubated at 37 ^{o}C overnight. Remaining samples were transferred into separate test tubes containing 5 mL of fresh and sterile MRS broth and the tubes were incubated by shaking aerobically at 250 rpm and 37 ^{o}C overnight. The agar plates having colonies were wrapped with the parafilm and stored at 4 ^{o}C for future use. The cells were harvested from the 5 mL overnight culture by centrifugation at 18,000 ×*g* for 1 min and the cell pellets was resuspended in 1 mL of 80% sterile glycerol. The glycerol stocks were preserved at -80 ^{o}C for future use.

3.3.3 Preparation of competent cells

E. coli competent cells were prepared according to the method adopted from Hongyan Zheng's PhD thesis (*61*). *E. coli* XL1 Blue and BL21 cells were initially grown on LB agar plate at 37 ^{o}C overnight. A single colony of each type was transferred into separate test tubes containing 5 mL of sterile LB broth and tetracycline (50 µg/mL) and the tubes were incubated by shaking aerobically at 250 rpm and 37 ^{o}C overnight.

The overnight culture (1 mL each) was transferred separately into 500 mL flasks containing 150 mL of fresh LB broth and 50 µg/mL of tetracycline and incubated at the same conditions as above, until the cell growth reached ~ 0.4 AU, measured at A_{600}. The growth of the cells was not allowed to exceed 0.4 AU. At this point, the cultures were transferred into pre chilled 50 mL falcon tubes and incubated on ice for 10 min. Following the incubation, the cultures were centrifuged at 1,500 ×*g* for 20 min at 4 ^{o}C and the supernatant was discarded. The tubes were held upside-down for several minutes to remove the supernatant completely. Then cell pellets were resuspended in 20 mL of sterile ice-cold transformation buffer (25 mM Tris-Cl pH 7.5, 20 mM $CaCl_2.2H_2O$) and incubated on ice for 30 min. After incubation, the samples were centrifuged again at 1,500 ×*g* for 20 min at 4 ^{o}C, the supernatant was discarded and cell pellets were resuspended in 5 mL of sterile ice-cold transformation buffer. To this cell suspension, 5 mL of 80% sterile glycerol was added and mixed by vortex. Finally, the glycerol stocks

of the competent cells were prepared into 100 µL aliquots and stored at -80 ^{o}C for future use.

3.4 Molecular biology methods

3.4.1 Isolation of genomic DNA and plasmid DNA

***L. plantarum* WCFS1:** A single colony of *L. plantarum* WCFS1 was taken from an agar plate, transferred into a test tube containing 5 mL MRS broth and cultured by shaking aerobically at 250 rpm and 37 ^{o}C overnight. Cells were harvested from the overnight culture by centrifugation at 18,000 ×*g* for 1 min at room temperature. The genomic DNA was isolated by using an UltraClean® Microbial DNA Isolation Kit, *MO BIO* Laboratories, Inc., CA, USA. This kit was generously provided by Vanessa Pittet and Professor Dr. Barry Ziola from Department of Microbiology and Immunology, University of Saskatchewan along with the technical assistance. Hence, the genomic DNA of the *L. plantarum* WCFS1 was prepared, according to the manufacturer's protocol. The DNA sample was immediately used for further experiments or stored at -20 ^{o}C for future use. All the steps in the above protocol were performed at room temperature.

***L. casei* BL23:** A test tube containing 5 mL of sterile MRS broth was inoculated with a loop full of *L. casei* BL23 taken from the glycerol stock and cultured by shaking aerobically at 250 rpm and 37 ^{o}C overnight. Genomic DNA was isolated using a phenol: chloroform: isoamyl alcohol (25:24:1) protocol, adopted from Dr. Bonnie Chaban, research associate in Dr. Janet Hill's laboratory, Department of Veterinary Microbiology, Western College of Veterinary Medicine, University of Saskatchewan.

According to this protocol, *L. casei* BL23 cells were pelleted from a 5 mL overnight culture, by centrifugation at 18,000 ×*g* for 1 min and resuspended in a 1.5 mL Eppendorf tube using 630 µL of TE buffer (100 mM Tris-HCl pH 8.0, 10 mM EDTA). To this suspension, 70 µL of 10% SDS (w/v) was added, mixed by inverting 2-3 times and incubated at 37 ^{o}C for 10 min. Following the incubation, 17.5 µL of lysozyme (100 mg/mL) and 4 µL of RNase (10 mg/mL) were added, mixed by inverting 2-3 times and incubated again at 37 ^{o}C for 30 min. To this sample mixture, 8 µL of Proteinase K (20 mg/mL) was added, mixed by inverting 2-3 times and then incubated again at 50-55 ^{o}C for 45 min. After incubation, the crude sample containing genomic DNA was extracted

with 700 µL of phenol: chloroform: isoamyl alcohol (25:24:1). The resultant sample was centrifuged at 18,000 ×*g* for 3 min, using a table top centrifuge. The top aqueous layer was carefully transferred into a fresh Eppendorf tube and extracted again with 350 µL of chloroform: isoamyl alcohol (24:1). Again the top aqueous layer was collected into a fresh Eppendorf tube. To this aqueous sample, $1/10^{th}$ volume of 5 M NaCl and 2 volumes of ice cold 95% ethanol were added and mixed by inverting several times. The Eppendorf tube was incubated at -20 ^{o}C of 30 min, during which time the genomic DNA gets precipitated out. Following the incubation, the sample was centrifuged at 18,000 ×*g* and 4 ^{o}C for 10 min to separate the supernatant. Then, 100 µL of 70% ethanol was added and the tube was gently inverted 2-3 times and centrifuged at 18,000 ×*g* for 3 min. Once the supernatant was removed, the Eppendorf tube was completely air dried for about 5-10 min, by keeping tube in inverted position. Finally, the DNA pellet was resuspended in 50 µL of sterile ddH_2O and the concentration was measured by using a NanoDrop™ 1000 Spectrophotometer.

Plasmid DNA: *E. coli* host cells harboring either *pQE-80L* or recombinant constructs (*pQE-80L*-IDH-related gene*)* were cultured by shaking aerobically at 250 rpm and 37 ^{o}C overnight. Cells were harvested from the overnight culture by centrifugation at 18,000 ×*g* for 1 min at room temperature and the plasmid DNA was isolated using a QIAprep Spin Miniprep Kit, according to the manufacturer's protocol, but with a change that the plasmid DNA was eluted with 30 µL sterile ddH_2O.

3.4.2 Primer designing

To amplify the IDH-related genes from *L. plantarum* WCFS1 and *L. casei* BL23 genomic DNA, a forward primer and a reverse primer specific to each gene were designed, based on their sequences available from online database, Kyoto Encyclopedia of Genes and Genomes (KEGG) (*75*)**.** The DNA sequence for each gene was obtained by a specific entry name. Inositol dehydrogenase-related genes from *L. plantarum* WCFS1, *L. casei* BL23 and *B. subtilis* are indicated with their KEGG database entry names in **Table 3.1.**

Table 3.1: IDH-related genes and their identification names in KEGG database

Bacteria genes	**KEGG entry name**
***Lactobacillus plantarum* WCFS1**	
Lp_iolG1	lp_3605
Lp_iolG2	lp_3606
Lp_iolG3	lp_3608
Lp_iolG4	lp_3612
***Lactobacillus casei* BL23**	
Lc_iolG1	LCABL_02210
Lc_iolG2	LCABL_02220

Restriction sites compatible with the MCS of the *pQE-80L* vector**,** were inserted in the primer sequences to flank the ends of each gene after PCR amplification. An online OligoAnalyzer tool from Integrated DNA technologies was used to optimize parameters such as length, melting temperature (T_m), %GC, and formation of dimer and hairpin etc. All the primers used for cloning IDH-related genes are provided in **Table 3.2.**

Table 3.2: Primers used for cloning IDH-related genes from *L. plantarum* WCSF1 and *L. casei* BL23.

Primer	Nucleotide sequence (5'end -to - 3'end)	Size (bases)	T_m (°C)	% GC	Restriction sites at ends of the amplified gene
lp_iolG1_forward	GAGGAGGA*GGATCC*ATGGTAACCACAAGA	29	62.4	51.7	*BamHI* - *Lp_iolG1* - *PstI*
lp_iolG1_reverse	GCCATCATCC*CTGCAG*CTATAGCTGAATATC	31	61.6	48.3	
lp_iolG2_forward	GGAGATT*GGATCC*ATGGCTGAAGCACAT	28	62.4	50.0	*BamHI* - *Lp_iolG2* - *SphI*
lp_iolG2_reverse	GAAGCAATGTC*GCATGC*TTACTCTGAGAC	29	61.0	48.2	
lp_iolG3_forward	GTAAAGGGGC*GGATCC*ATGGATAAAAGC	28	61.2	50.0	*BamHI* - *Lp_iolG3* - *XmaI*
lp_iolG3_reverse	CCTCCTAG*CCCGGG*TTAAATATCTGCTAC	29	61.3	51.7	
lp_iolG4_forward	GGTGGTCT*GCATGC*ATGAAAAAAGTACATGC	31	61.9	45.1	*SphI* - *Lp_iolG4* - *XmaI*
lp_iolG4_reverse	CCTCTTTCTA*CCCGGG*TTAATCTAAAGGA	29	59.1	44.8	
lc_iolG1_forward	AAAGGAGTG*GGATCC*ATGGTTGTCAAAGTTGG	32	63.3	46.8	*BamHI* - *Lc_iolG1* - *XmaI*
lc_iolG1_reverse	CTATTTTGTCTAA*CCCGGG*CTAAGCATGAATCGC	34	63.1	47.0	
lc_iolG2_forward	GGAGGAGGTAATT*GGATCC*ATGACTCAAAAAACG	34	61.6	44.1	*BamHI* - *Lc_iolG2* - *PstI*
lc_iolG2_reverse	CCCAATTCAATC*CTGCAG*TTAAGCACCTAC	30	61.0	46.6	

Note: Restriction sites were italicized and underlined; each restriction site and its respective name were indicated in color

3.4.3 Polymerase chain reaction (PCR)

3.4.3.1 Amplification of IDH-related genes form *L. plantarum* WCFS1

Lp_iolG1 to Lp_iolG4 genes were amplified using their respective forward and reverse primers. Reactions were prepared in 12 × 200 µL PCR tubes to a final volume of 50 µL, as mentioned in **Table 3.3**. All four gene amplification reactions were carried out in a Mastercycler™ Gradient using the program mentioned in **Table 3.4**.

Table 3.3: PCR mixture for the amplification of *Lp_iolG1* to *Lp_iolG4* genes.

Polymerase chain reaction mixture	
Sterile ddH_20	40.5 µL
10X *PfuUltra*® Buffer*	5 µL
10 mM *dNTP* mix	1 µL
10 µM forward primer	1 µL
10 µM reverse primer	1 µL
Genomic DNA template *(~0.8 ng/µL)*	1 µL
PfuUltra® HiFi DNA polymerase	0.5 µL
Total volume	**50 µL**

*** (200 mM Tris–HCl, pH 8.8, 100 mM KCl, 100 mM $(NH4)_2SO_4$, 20 mM MgSO4, 1% TritonX-100, and 1.0 mg/mL BSA)**

Table 3.4: PCR program for the amplification of *Lp_iolG1* to *Lp_iolG4* genes.

PCR Program			
1.	Initial denaturation	T = 95 ^oC	5 min
2.	Denaturation	T = 98 ^oC	20 sec
3.	Annealing	T = 55 ^oC	15 sec
4.	Extension	T = 72 ^oC	35 sec
	Go to step-2 and repeat for 39 cycles		
5.	Final extension	T = 72 ^oC	5 min
Hold at 4 ^oC or end program			

3.4.3.2 Amplification of IDH-related genes from *L. casei* BL23

Lc_iolG1 & Lc_iolG2 genes were amplified using their respective forward and reverse primers Reactions were prepared in 12 × 200 µL PCR tubes to a final volume of

25 µL, as mentioned in **Table 3.5.** The two genes were amplified by using a gradient annealing temperature program, in a Mastercycler^{TM} Gradient, as mentioned in **Table 3.6.**

Table 3.5: PCR mixture for the amplification of *Lc_iolG1* and *Lc_iolG2* genes.

Polymerase chain reaction mixture	
Sterile ddH_20	36 µL
5X KAPA High Fidelity Buffer	10 µL
10 mM *dNTP* mix	1 µL
10 µM forward primer	0.75 µL
10 µM reverse primer	0.75 µL
Genomic DNA template *(~7.6 ng/µL)*	1 µL
KAPA HiFi DNA polymerase	0.5 µL
Total volume	**50 µL**

Table 3.6: PCR program for the amplification of *Lc_iolG1* and *Lc_iolG2* genes

PCR Program			
1.	Initial denaturation	T = 95 ^oC	5 min
2.	Denaturation	T = 98 ^oC	20 sec
3.	Gradient annealing	T = 50-60 ^oC	15 sec
4.	Extension	T = 72 ^oC	35 sec
	Go to step-2 and repeat for 34 cycles		
5.	Final extension	T = 72 ^oC	5 min
Hold at 4 ^oC or end program			

After PCR, 2-3 µL of the reaction mixture was analyzed by 1% agarose gel electrophoresis and the rest of the samples were purified by using a QIAquick PCR Purification Kit, according to the manufacturer's protocol, but with a change that final pure DNA was eluted with 30 µL sterile ddH_2O.

3.4.4 Restriction digestion

All the PCR products (*Lp_IolG1* to *Lp_iolG4* and *Lc_iolG1 & Lc_iolG2 genes*) were digested separately with their respective restriction enzymes. Similarly, *pQE-80L* was also digested with the corresponding enzymes to generate compatible cohesive ends. The digestion reaction mixtures were prepared on ice. A total volume of 50 µL in 200 µL PCR tubes, containing 1X concentration of an appropriate buffer, ~200-400 ng/µL of DNA sample, and 20-50 units of restriction enzymes. Bovine Serum Albumin (1 µL of 10 mg/mL concentration) was added to the reaction mixture as required. The reactions were carried out in a Mastercycler™ Gradient with a program set at 37 ^{o}C for 2 h. The combination of restriction enzymes used to digest the PCR products and the vector is indicated in **Table 3.7.**

Table 3.7: Combination of enzymes used in restriction digestion process

PCR product and the native vector	Combination of the restriction enzymes
Lp_iolG1 and *pQE-80L*	*BamHI and PstI*
Lp_iolG2 and *pQE-80L*	*BamHI and SphI*
Lp_iolG3 and *pQE-80L*	*BamHI and XmaI*
Lp_iolG4 and *pQE-80L*	*SphI and XmaI*
Lc_iolG1 and *pQE-80L*	*BamHI and XmaI*
Lc_iolG2 and *pQE-80L*	*BamHI and PstI*

After restriction digestion, the DNA samples were purified from 0.7% agarose gel by using a QIAquick Gel Extraction Kit, following the manufacturer's protocol, but with a change that final pure DNA was eluted with 30 µL sterile ddH_2O.

3.4.5 DNA ligation

The purified gene inserts (*Lp_iolG1 to Lp_iolG4*, *Lc_IolG1* & *Lc_iolG2*) with their cohesive ends were ligated into the MCS of *pQE-80L* that was digested with corresponding enzymes, as mentioned in section **3.4.4**. The ligation reaction mixture was prepared in a typical volume of 10 µL containing 1.0 µL of 10X T4 Ligation buffer, 3:1 molar ratio of insert to plasmid, 1.0 µL of T4 DNA Ligase enzyme. A negative control reaction was prepared simultaneously by adding everything to the reaction mixture

except the insert. All the ligation reaction mixtures were prepared on ice, mixed by taping and the reaction was carried out at room temperature for about 1 h. After the ligation reaction, the sample was transformed into *E. coli* competent cells.

3.4.6 Transformation

Frozen stocks of competent cells (*E. coli* XL1-Blue and/or BL21-Gold) were thawed on ice before starting the transformation. The reaction mixture after ligation reaction was added and incubated on ice for 30 min. Following the incubation, the cells were subjected to heat-shock for 1 min in a water bath maintained at 42 ^{o}C. Immediately after heat-shock, the sample was kept on ice for 2 min and then transferred into a sterile 1.5 mL Eppendorf tubes containing 900 µL LB media. The tubes were incubated by shaking at 250 rpm and 37 ^{o}C for 1 h. After incubation, the sample was plated onto LB agar containing 50 µg/mL of ampicillin, and incubated at 37 ^{o}C overnight.

3.4.7 Screening and selection of viable clones

To confirm successful ligation, 6-8 colonies for each clone were selected for restriction analysis. The selected colonies were cultured in test tubes, containing 5 mL LB broth and 50 µg/mL of ampicillin, by shaking aerobically at 250 rpm and 37 ^{o}C overnight. A loop full of each culture was streaked on LB agar containing 50 µg/mL of ampicillin and the plates were incubated at 37 ^{o}C overnight and kept for future use. The remaining culture was harvested by centrifugation at 18,000 $\times g$ for 1 min and the recombinant constructs were isolated using a QIAprep Spin Miniprep Kit, according to the manufacturer's protocol.

Restriction enzymes that could cut the plasmid DNA through the inserted gene were chosen. After restriction digestion the DNA fragments of different size were analyzed by 1% agarose gel electrophoresis. A virtual restriction analysis of all the recombinant constructs was performed using DNADynamo software and compared to the restriction digest results. Clones with results matching to the expected virtual analysis were submitted for DNA sequencing. Finally, clones having the correct DNA sequence were made into stocks and stored at -80 ^{o}C in 80% sterile glycerol.

3.5 Gene expression

E. coli host cells harboring the recombinant vector (for example: *pQE80L-Lp_iolG1*) were taken from their frozen stocks and streaked onto LB agar containing 50 µg/mL concentration of ampicillin and incubated at 37 ^{o}C overnight. Kanamycin at 50 µg/mL concentration was used during the expression of *pET-28b-Bs_iolG*. A test tube containing 5 mL of sterile TB was inoculated with a single colony picked from the agar plate and incubated by shaking aerobically at 250 rpm and 37 ^{o}C overnight. A 1 mL of overnight culture was transferred into a 500 mL flask containing 100 mL of fresh TB and incubated by shaking aerobically at 250 rpm and 37 ^{o}C. Growth was monitored by measuring the turbidity of the culture spectrophotometrically at 600 nm (OD_{600}) at regular time intervals. When the OD_{600} reached about 0.6-0.8 AU, isopropyl β-D-thiogalactoside (IPTG) was added to a final concentration of 1 mM to induce overexpression of the gene. The culture was further incubated overnight at 15 ^{o}C and 250 rpm. Finally, the cells were harvested by centrifugation at 3500 $\times g$ for 30 min and the cell pellet was either immediately used for protein isolation and purification or stored at -80 ^{o}C for future use.

3.6 Protein isolation and purification

Fresh or frozen cell pellet was thawed on ice and resuspended in 5 mL of binding buffer (25 mM Tris-HCl pH 8.0, 0.5 M NaCl, 10 mM imidazole, and 10% glycerol), lysozyme and DNase were added in 1:1000 volume ratio, then cell lysis was performed using a Virsonic 600 ultrasonic cell disrupter with a program (5 s pulse on and 20 s pulse off) for 2 min. After sonication, the crude supernatant was separated from the cell debris by centrifugation at 15000 rpm and 4 ^{o}C for 30 min. The crude protein extract was filtered through a 0.2 µm sterile syringe filter and loaded on to a 1 mL HiTrap-IMAC FF column which had been charged with 5 column volumes (CV) of charge buffer (50 mM $NiSO_4$, pH 4.0) and equilibrated with 5 CV of binding buffer. Once the crude protein was loaded, the column was washed with 10 CV of wash buffer (25 mM Tris-HCl pH 8.0, 0.5 M NaCl, 60 mM imidazole, and 10% glycerol). Then, protein bound to the column was eluted with either 10 CV of elution buffer (25 mM Tris-Cl pH 8.0, 0.5 M NaCl, 500 mM imidazole, and 10 % glycerol) or 10 CV of strip buffer (25 mM Tris-Cl pH 8.0, 500 mM NaCl, 100 mM EDTA and 10% glycerol).

For protein eluted with strip buffer, the column was charged and equilibrated again for the next use. The purity of the eluted fractions of protein was verified by 12% SDS-PAGE. The pure protein fractions were combined and concentrated using a 30 kDa AMICON filter, by centrifuging at 3,500 ×*g*, dialyzed 2-3 time against dialysis buffer (25 mM Tris-HCl pH 8.0, 40% (v/v) glycerol and 0.1 mM D-dithiothreitol (DTT)). Purified protein was separated into 100 µL aliquots, flash frozen in liquid nitrogen and immediately stored at -80 ^{o}C. For enzyme kinetic experiments, a single frozen aliquot of protein was thawed on ice and the concentration was adjusted to 1 mg/mL with fresh dialysis buffer.

3.6.1 Purification of LpIDH2 from inclusion bodies

Fresh or frozen cell pellet from 100 mL of overnight culture was washed with ddH_2O and resuspended in 5 mL denaturing buffer (100 mM NaH_2PO_4, 10 mM Tris-HCl pH 8.0, 8M Urea), then the sample was incubated for 30 min at room temperature. Supernatant was collected by centrifugation at 15000 rpm and 4 ^{o}C for 30 min. Denatured sample was filter using a 0.2 µM syringe filter and dialyzed against 500 mL refolding buffer (100 mM Tris-HCl pH 8.0, 1mM EDTA, 1mM PMSF, 400mM L-Arginine, 5% sucrose, 0.1mM DTT and 10% glycerol) with buffer change twice a day for 2 days. After dialysis the protein sample was purified by using a 1 mL HiTrap-IMAC FF column as mentioned in section **3.5**. BsIDH was also purified by this method.

3.6.2 Determination of protein concentration

The concentration of protein samples was determined by A_{280} method, using a Beckman DU640 UV-VIS spectrophotometer. The absorbance was measured at two different dilutions of protein in 1 mL volume and the concentration for each dilution was calculated by using the **Equation 3.1.** The theoretical molar extinction coefficients (ε_{280}) were obtained by submitting the protein sequences in the expasy protparam online tool. The average value of the two different concentrations obtained from the two dilutions was taken as the final concentration of the protein.

$$C = A_{280}\,(AU) \,/\, [\varepsilon_{280}\,(M^{-1}cm^{-1}) \times L\,(cm)] \qquad \textbf{Equation 3.1}$$

3.7 Protein sequence analysis

Multiple sequence alignment of the primary protein sequences of IDH-related enzymes was performed with that of BsIDH using ClustalW2 multiple sequence alignment program (*76, 77*). The aligned sequences were compared to the structure of BsIDH and visualized by using ESPript V 2.2 software (*78, 79*).

3.8 Enzyme kinetics

3.8.1 Inositol dehydrogenase activity assay

The activity assays for the soluble IDH-related enzymes from *L. plantarum* WCFS1 and *L. casei* BL23, were performed in 1 mL cuvettes containing 100 mM Tris-HCl pH 9.0, 50 mM *myo*-inositol, 2 mM NAD^+ or $NADP^+$ and 1 µL of enzyme (1 mg/mL). According to the reaction mentioned in **Scheme 1.1,** formation of NADH or NADPH was monitored at λ = 340 nm (ε_{340} for NADH or NADPH is 6220 $M^{-1}cm^{-1}$) using a Beckman DU640 UV-VIS spectrophotometer at 25 ^oC. Similarly, other substrates such as *scyllo*-inositol, D-c*hiro*-inositol, D-glucose, L-glucose (mixed anomers) and D-xylose, L-xylose, D-galactose, D-mannose, D-sorbitol, D-mannitol and *scyllo*-inosose were also assayed.

3.8.2 Initial velocity measurement assay

All the kinetic assays in this research were performed in a total reaction volume of 1 mL, containing 100 mM concentration of an appropriate buffer at optimum pH. For determining the apparent kinetic constants NAD^+ was kept constant at 2 mM while varying the other substrate. The reaction samples containing all the components were prepared except the enzyme and it was read as the blank sample. The reaction was initiated by adding the enzyme and the formation of NADH or NADPH was measured at 340 nm, as mentioned in section **3.8.1,** at 2 s intervals for a total time of 2 min. Data recorded by the spectrophotometer was converted into a Microsoft Excel file using DU600/700 File-Utility software (version 1.0), and then a plot of absorbance (A_{340}) *vs* time was generated (**Figure 3.1**).

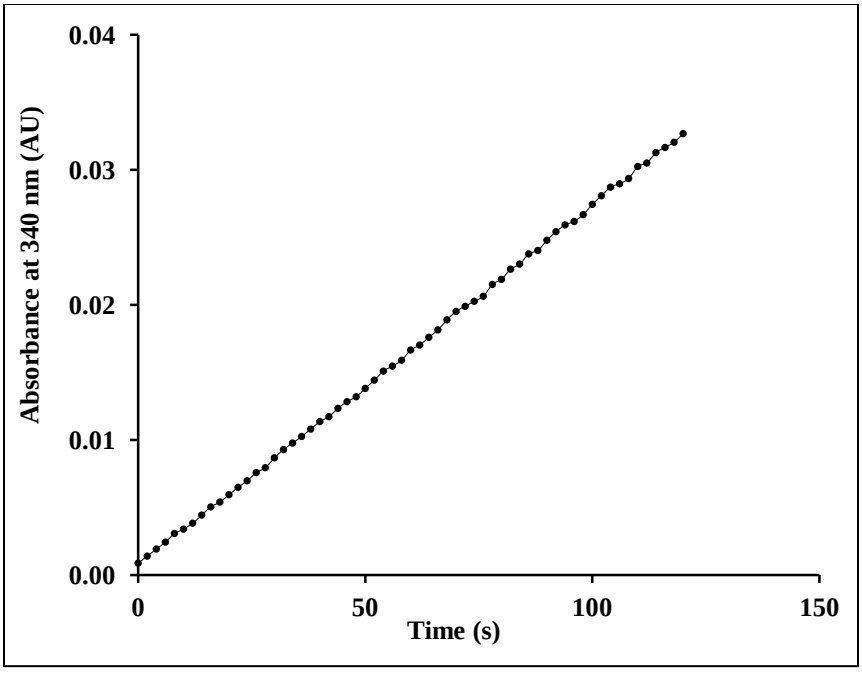

Figure 3.1: Absorbance versus time plot obtained from an IDH catalyzed reaction. Reaction conditions: 50 mM *myo*-inositol, 2 mM NAD^+ in 100 mM appropriate buffer at optimum pH and at 25°C.

The data representing the linear portions of the absorbance curve was used to determine the slope (in $AU\ s^{-1}$) and the initial velocity, (v_0) was calculated from the slope by using the **Equation 3.2** as shown below:

Initial velocity (v_0) = Slope (AU s^{-1}) / 6220 (M^{-1} cm^{-1}) x L (cm) **Equation 3.2**

Hence, the initial rate of formation of NADH or NADPH in an IDH catalyzed reaction was calculated in nM s^{-1} for convenient representation in graphs. Each data points in this thesis represent the average value of at least two measurements taken from the spectrophotometer.

3.8.3 Determination of optimum pH and the pH-rate profiles

To determine the optimum pH and to establish the pH-rate profiles for the active enzymes (LcIDH1 and LcIDH2), including BsIDH, the initial rate of reactions containing a fixed concentration of *myo*-inositol (50 mM) and NAD^+ (2 mM) in 100 mM of suitable buffer was measured at a series of pH values. A pH range from 9.0 to 10.5 with 0.1 unit difference was maintained by using the following buffers; CHES (*N*-cyclohexyl-2-

aminoethanesulfonic acid) (Useful pH range: 8.6-10.0) and glycine-NaOH (Useful pH range: 8.8-10.6). The pH of the reaction mixture was measured before and after the reaction. The initial rate at each pH value was calculated as described in **section 3.8.2**, and the rate coefficients were plotted against the selected pH range of the reaction to generate pH-rate profiles.

3.8.4 Determination of true kinetic constants (K_m , k_{cat} and k_{cat}/K_m)

Kinetic assays for LcIDH1, LcIDH2 and BsIDH were performed in their respective buffer at optimal pH. To determine the true kinetic constants the assays were performed by varying the concentrations of *myo*-inositol or sugar at different fixed concentrations of NAD^+ or vice-versa. Initial rates were determined as described in section **3.8.2**, and the data was fitted to **Equation 3.3** using Leonora software (*80*).

$$v_0 = \frac{V_{max}[A][B]}{K_{iA}K_{mB} + K_{mB}[A] + K_{mA}[B] + [A][B]} \qquad \textbf{Equation 3.3}$$

where, v_0 represents the initial velocity of the reaction, V_{max} is the maximum velocity of the reaction when both substrates are at saturation concentrations, [A] is the concentration of the substrate (NAD^+) that binds first to the enzyme, [B] is the concentration of the second substrate (*myo*-inositol or other related compounds), K_{mA} and K_{mB} are Michaelis constants for substrates A and B respectively, and K_{iA} is the dissociation constant for the enzyme-NAD^+ binary complex. Michaelis-Menten saturation curves (v_0 *vs [S]*), Lineweaver-Burk Plots (also called double reciprocal plots) ($1/v_0$ *vs* $1/[S]$) and the kinetic constants (K_{mA}, $K_{mB,}$ and K_{iA}) were obtained from Leonora. The other parameters such as turnover number (k_{cat}) and specificity constant $k_{cat}/K_{m(A)}$ and $k_{cat}/K_{m(B)}$ were manually calculated using the total enzyme concentration used in the reaction mixture.

3.8.5 Determination of apparent kinetic constants (K_m^{app}, k_{cat}^{app} and k_{cat}/K_m^{app})

Apparent kinetic assays were performed by varying the concentrations of the *myo*-inositol and other related compounds at fixed saturation concentration of NAD^+ (2 mM). All the reactions were performed at least in duplicates to obtain the consistency in

data points. Initial rates were determined as described in section **3.8.2**, and the data was fitted to **Equation 3.4** using Leonora software.

$$v_0 = \frac{V_{max}^{app}[S]}{K_m^{app} + [S]} \qquad \textbf{Equation 3.4}$$

where, v_0 represents the initial velocity of the reaction, V_{max}^{app} is the apparent maximum velocity of the reaction at saturation concentrations of the varied substrate, [S] is the concentration of the substrate (*myo*-inositol and other related compounds) and K_m^{app} is apparent Michaelis constants for the varied substrate. Michaelis-Menten saturation curves (v_0 *vs* *[S]*), double reciprocal plots ($1/v_0$ *vs* *1/[S]*) and the apparent kinetic constants (K_m^{app}) were obtained from Leonora. The other constants such as the apparent turnover number k_{cat}^{app} and the apparent specificity constant $(k_{cat}/K_m)^{app}$ were manually calculated using the total enzyme concentration used in the reaction mixture.

4. RESULTS AND DISCUSSION

4.1 Gene cloning

4.1.1 Isolation of genomic DNA and plasmid DNA

In order to clone IDH-related genes from *L. plantarum* WCFS1 and *L.casei* BL23, their genomic DNA that serves as a template during the PCR was necessary. Hence, the genomic DNA of *L. plantarum* WCFS1 was isolated by using an UltraClean® Microbial DNA Isolation Kit, as described in **3.4.1**. In this method, the bacterial cells were lysed by the combination of heat, detergent, and mechanical forces against micro beads in a MicroBead tube provided in the kit. Following the cell lysis, the released DNA was allowed to bind to silica membrane in the spin filter column. The filter was washed, and finally, the pure genomic DNA was eluted with sterile ddH_2O to obtain 8 µg of DNA from 2 mL bacterial culture.

The genomic DNA from *L. casei* BL23 was isolated by using a phenol: chloroform: isoamyl alcohol (25:24:1) protocol, as mentioned in section **3.4.1**. The bacterial cells were lysed by heating the cell suspension in the presence of 10% SDS (w/v), RNase (10 mg/mL) and Proteinase-K (20 mg/mL). SDS disrupts the integrity of the bacterial cell wall and helps in cell lysis, RNase digests all types of RNA present in the crude sample and Proteinase-K is a serine protease that exhibits broad cleavage specificity and therefore digests all the proteins in the sample. The genomic DNA was then extracted using a phenol: chloroform: isoamyl alcohol (25:24:1) solution. The DNA dissolves in the top aqueous layer and gets separated from the organic-soluble components. Following the extraction, the DNA was further purified by precipitation with 5 M NaCl, ice cold 95% ethanol, and 70% ethanol. Finally, pure genomic DNA was dissolved in ddH_2O to obtain 385 µg of DNA from 5 mL bacterial culture.

The *pQE-80L* plasmid (**Figure 4.1**) was selected for cloning all the genes because it carries different gene elements that are essential for its maintenance and efficient expression of highly stable N-terminal 6x-Histidine tagged recombinant proteins in the host cells. A lambda phage T5 promoter and *lac* operator elements are essential for regulating the protein expression (*81*). The *E. coli* RNA polymerase recognizes the T5

promoter sequence and initiates transcription. This region also has a strong ribosomal binding site (RBSII) which is required for efficient translation of mRNA. The *pQE-80L is a cis*-repressed plasmid, that is, it carries *lacI*^{q} gene element within its sequence which encodes *lac* repressor protein (*82*). The *lac* repressor protein binds to the *lac* operator and inhibits the transcription of the gene of interest.

The *pQE-80L* vectors can express proteins in any *E. coli* host cells. Protein overexpression can be achieved by the addition of isopropyl β-D-thiogalactoside (IPTG) into the growing culture. IPTG binds to the *lac* repressor protein and prevents it from binding to the *lac* operator region. This inactivation of *lac* repressor leads to successful transcription, and translation of the recombinant protein. The β-lactamase gene (*bla*) product confers resistance against ampicillin (*83*). Hence, *E. coli* host cells carrying this plasmid can survive in 50-100 mg/L concentration of ampicillin containing broth or agar plates. The other elements of this plasmid includes *ColE1*-Origin of replication(*83*), two strong transcription termination regions (t_0 and *T1*) (*84*) and a chloramphenicol acetyl transferase (CAT) gene in between the transcription termination regions.

IDH-related genes from *L. plantarum* WCFS1 and *L. casei* BL23 strains were cloned into suitable cloning sites in the MCS region of *pQE-80L* overexpression plasmid. The *pQE-80L* plasmid and the recombinant constructs were isolated by using a QIAprep Spin Miniprep Kit to obtain about 12-15 µg of pure DNA at each time performed from a 5 mL overnight culture. The DNA samples were diluted as required with sterile ddH_2O and used in further experiments.

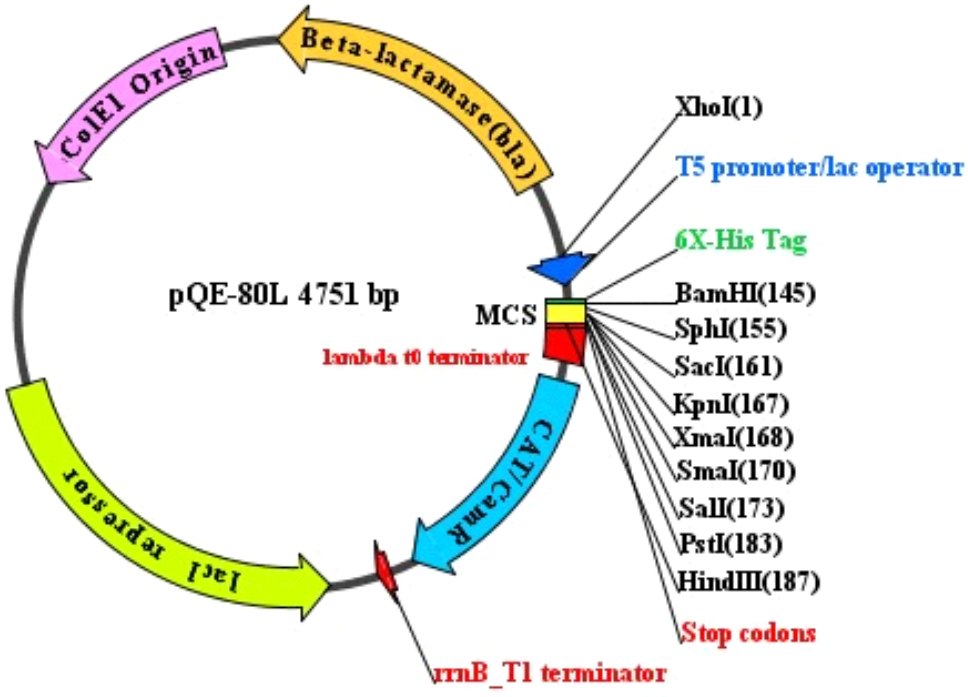

Figure 4.1: The DNA map of *pQE-80L* plasmid. (Gene elements are indicated in different colors, the arrow head indicates the direction of replication and transcription. The sequence encoding 6X-His Tag is towards the 5' end of the multiple cloning sites (MCS) and the stop codons at 3' end. The number adjacent to the restriction enzymes indicates their cut sites, *XhoI* site is the start of numbering. The image was generated using DNADynamo software.

4.1.2 Amplification of IDH-related genes

Polymerase chain reaction (PCR) was performed in a series of 35-40 cycles with each cycle operating at three different temperature steps (*85*). When the temperature of the reaction was maintained at 95-98 ^{o}C, the double stranded genomic DNA (template) was denatured into two single stranded DNA. Following denaturation, the temperature was lowered to 50-55 ^{o}C, where both forward and reverse primers annealed to their complementary sequence in the single stranded DNA template. The temperature of the reaction was then changed to 72 ^{o}C, where the new DNA strands were synthesized by DNA polymerase from the 3' end of the annealed primers, in the elongation process. After a specific number of repeated cycles, the gene of interest will increase in its copy number, which was analyzed by performing agarose gel electrophoresis.

IDH-related genes, *(Lp_iolG1* to *Lp_iolG4, and Lc_iolG1* and *Lc_iolG2)* from the *L. plantarum* WCFS1 and *L. casei* BL23 were amplified using their respective primers **(Table 3.2).** Initially, amplification trials were failed due to conditions such as the

presence of more DNA template in the reactions, primer annealing temperature and the amount of primers in the reactions. The PCR reactions were repeated by optimizing these conditions to achieve successful amplification of *Lp_iolG1* to *Lp_iolG4* genes. In case of *Lc_iolG1* and *Lc_iolG2*, non-specific DNA amplifications were observed. The reactions were performed at gradient annealing temperature and with additives such as 5% DMSO and 5% formamide to minimize the non-specific DNA amplifications. These trials resulted in no amplification at all. Therefore, another trial was performed at gradient annealing temperature without any additives. The required gene was carefully excised from the agarose gel and the samples were purified by using a QIAquick PCR Purification Kit.

4.1.3 Restriction digestion

Restriction digestion is a process of cleaving the DNA fragment at specific sequences (restriction sites) recognized by a type of enzyme called a restriction enzyme. These enzymes are named after the bacteria from which they were isolated. Purified PCR products containing inserted restriction sites on either ends were digested with respective enzymes to create cohesive ends that are compatible to the MCS in *pQE-80L* plasmid **(Figure 4.1).**

The digested samples were purified from 0.6% agarose gel using QIAquick Gel Extraction kit protocol to obtain relatively pure DNA, which is essential for a ligation experiment. Ligation is a process of covalently linking two ends of a DNA fragment or two DNA fragments at their ends. Chemically, it is the formation of a phosphodiester bond between 3' hydroxyl group of one nucleotide and the 5' phosphate group of the other nucleotide. This reaction was catalyzed by an enzyme called T4 DNA Ligase in presence of Mg^{2+} and ATP at room temperature. The digested PCR products were ligated into their corresponding vectors according to the procedure mentioned in section **3.4.5.**

Diagrams of all the genes showing 5' and 3' cohesive ends after digestion and *pQE-80L* with a part of its DNA sequence showing the transcription start site, sequence for 6x-His Tag, MCS, and transcription stop codons are indicated in **Figure 4.2,** and the DNA maps of the recombinant constructs showing start of transcription, 6X-His Tag and the cloning sites for each gene are indicated in **Appendix-B.** The recombinant constructs so prepared were transformed into a suitable host, for its maintenance and efficient

overexpression of the protein. Hence, *pQE-80L-Lp_iolG1*, *pQE-80L-Lp_iolG2*, *pQE-80L-Lp_iolG3*, *pQE-80L-Lp_iolG4*, *pQE-80L-Lc_iolG1* and *pQE-80L-Lc_iolG2*) were transformed into *E. coli* XL1 Blue and/or BL21 Gold competent cells as described in section **3.3.6.**

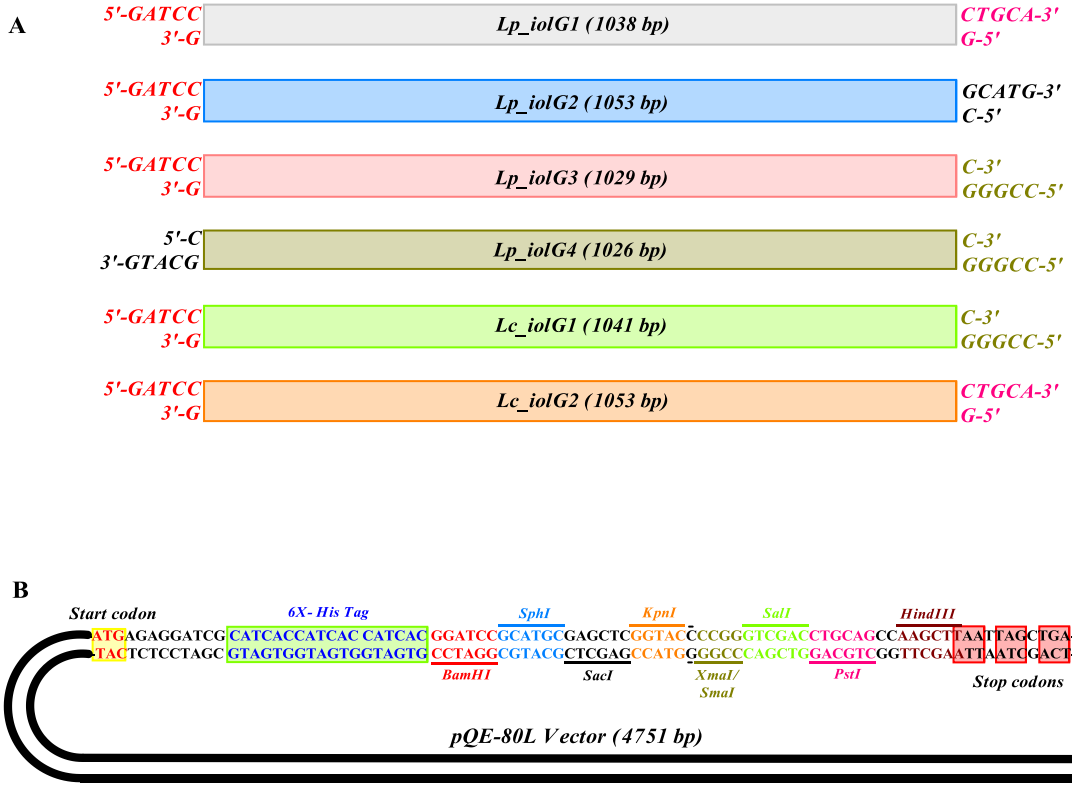

Figure 4.2: A). PCR products after restriction digestion (5'- and 3'- overhangs at the ends of each gene are shown in different colors that are matching with MCS of *pQE-80L*. **B). *pQE-80L* vector showing the DNA sequence of important regions (**starting from the transcription start codon to the stop codons, is shown). MCS is located at 3' end of the 6X-His Tag sequence and the sequences for each restriction enzyme were highlighted in different colors. The diagrams were prepared using ChemDraw Pro 12.0 Version.

4.1.4 Screening and selection of viable clones

Successfully transformed *E. coli* host cells were verified for the presence of a properly ligated gene sequence in *pQE-80L*. The native *pQE-80L* and the recombinant constructs were isolated from the host cells. Restriction digestion was performed with selected restriction enzymes.

pQE-80L has a single *EcoRV* restriction site at 1530 bp in its sequence and *Lp_iolG1* also has the same site at 654 bp towards the 3' end. The insertion of *Lp_iolG1* into *pQE-80L* has resulted in two *EcoRV* sites at 804 bp and 2540 bp, and thus *EcoRV*

digestion of *pQE-80L* (4751 bp) resulted in a single DNA fragment of 4751 bp, while *pQE-80L-Lp_iolG1* (5761 bp) resulted in two DNA fragments of 4025 bp and 1736 bp as shown in **Figure 4.3(A)**. An agarose gel showing the corresponding DNA fragments of digested *pQE-80L* and pQE-*80L-Lp_iolG1* is indicated in **Figure 4.3(B)**.

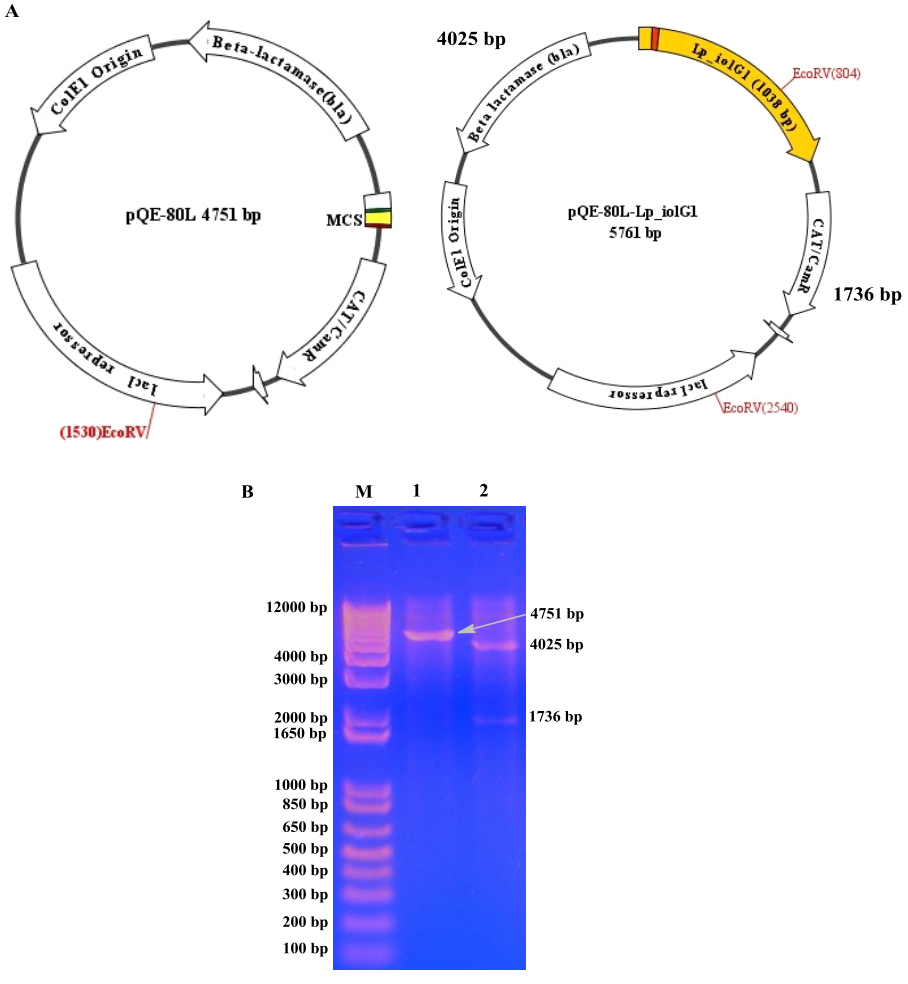

Figure 4.3: A). Restriction DNA map of *pQE-80L* and *pQE-80L-Lp_iolG1* showing restriction site for *EcoRV* enzyme. The image was generated using DNA Dynamo software. **B). A GelRed™ stained 1% agarose gel showing the DNA bands of *pQE-80L* and *pQE-80L-Lp_iolG1* digested with *EcoRV* enzyme** (Lane M:1Kb plus DNA marker; Lane 1: *pQE-80L and* Lane 2: *pQE-80l-Lp_iolG1*).

Similarly, *pQE-80L* has a single *EcoRI* restriction site at 88 bp in its sequence and the *Lp_iolG2* also has the same site at 862 bp towards the 3' end. The insertion of *Lp_iolG2* into *pQE-80L* has resulted in two *EcoRI* sites at 88 bp and 1012 bp, and thus *EcoRI* digestion of *pQE-80L* (4751 bp) resulted in a single DNA fragment of 4751 bp, while *pQE-80L-Lp_iolG1* (5804 bp) resulted in two DNA fragments of 4880 bp and 924

bp as shown in **Figure 4.4(A)**. An agarose gel showing the corresponding DNA fragments of digested *pQE-80L* and pQE-*80L-Lp_iolG1* is indicated in **Figure 4.4(B)**.

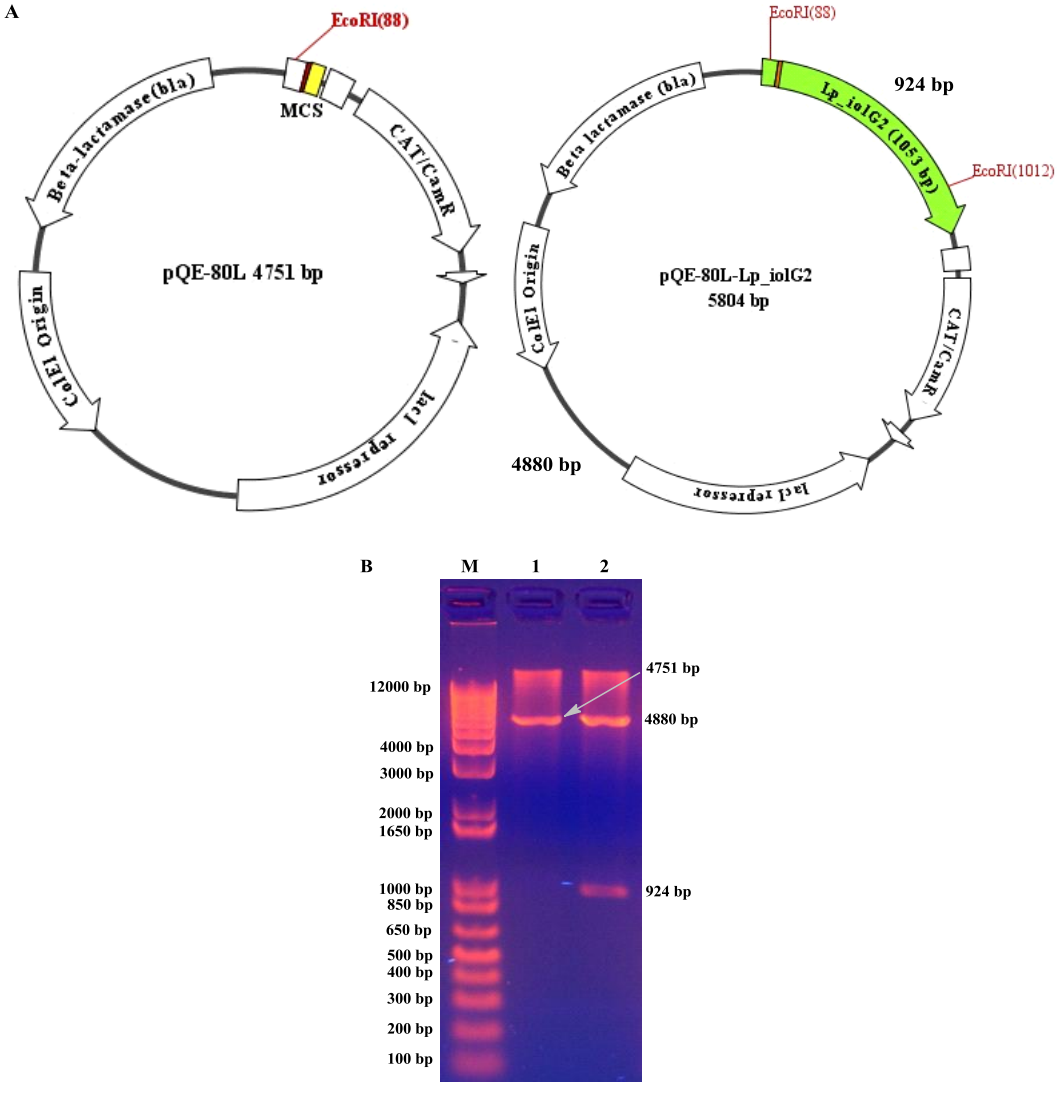

Figure 4.4: A). Restriction DNA map of *pQE-80L* and *pQE-80L-Lp_iolG2* showing restriction site for *EcoRI* enzyme. The image was generated using DNA Dynamo software. **B). A GelRed™ stained 1% agarose gel showing the DNA bands of *pQE-80L* and *pQE-80l-Lp_iolG1* digested with *EcoRI* enzyme** (Lane M:1Kb plus DNA marker; Lane 1: *pQE-80L* and Lane 2: *pQE-80L-Lp_iolG2*).

The *NcoI* enzyme cuts *pQE-80L* at a single site at 860 bp while it cuts *pQE-80L-iolG3* at two sites at 149 bp and 1872 bp as shown in **Figure 4.5(A)**. Hence, *NcoI* digestion of *pQE-80L* (4751 bp) resulted in a single DNA fragment of 4751 bp, while *pQE-80L-Lp_iolG3* (5763 bp) resulted in two DNA fragments of 4040 bp and 1723 bp. An agarose gel showing the corresponding DNA fragments of digested *pQE-80L* and pQE-*80L-Lp_iolG3* is indicated in **Figure 4.5(B)**.

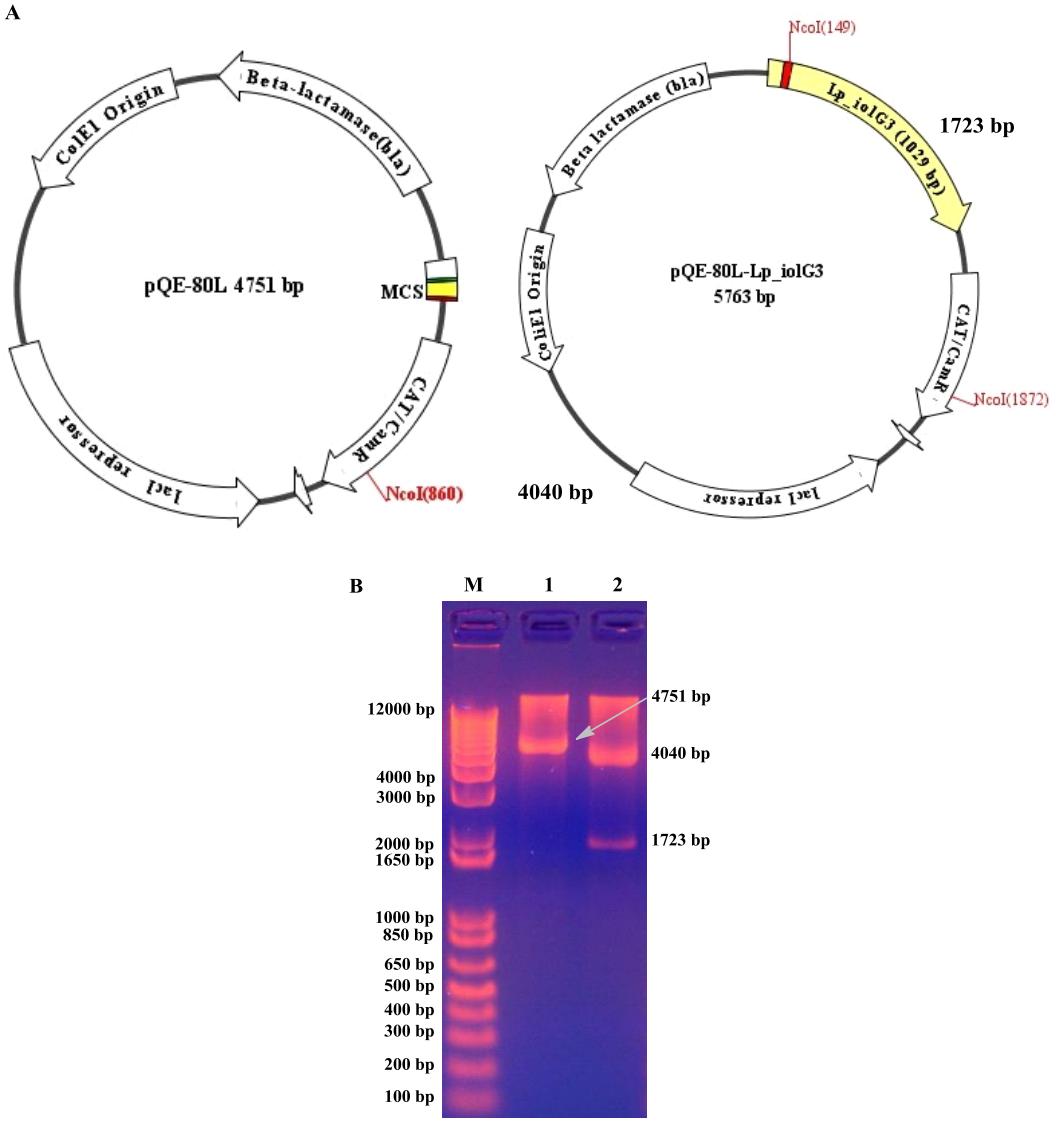

Figure 4.5: A). Restriction DNA map of *pQE-80L* and *pQE-80L-Lp_iolG3* showing restriction site for *NcoI* enzyme. The image was generated using DNA Dynamo software. **B). A GelRed™ stained 1% agarose gel showing the DNA bands of *pQE-80L* and *pQE-80l-Lp_iolG3* digested with *NcoI* enzyme** (Lane M:1Kb plus DNA marker; Lane 1: *pQE-80L* and Lane 2: *pQE-80L-Lp_iolG3*).

The *EcoRV* digestion maps for *pQE-80L* and *pQE-80L-Lp_iolG4* are shown in **Figure 4.6(A).** In this digestion, the *pQE-80L* (4751 bp) resulted in a single DNA fragment of 4751 bp, while *pQE-80L-Lp_iolG4* (5766 bp) resulted in two DNA fragments of 3521 bp and 2245 bp. An agarose gel showing the corresponding DNA fragments of digested *pQE-80L* and pQE-*80L-Lp_iolG4* is indicated in **Figure 4.6(B)**.

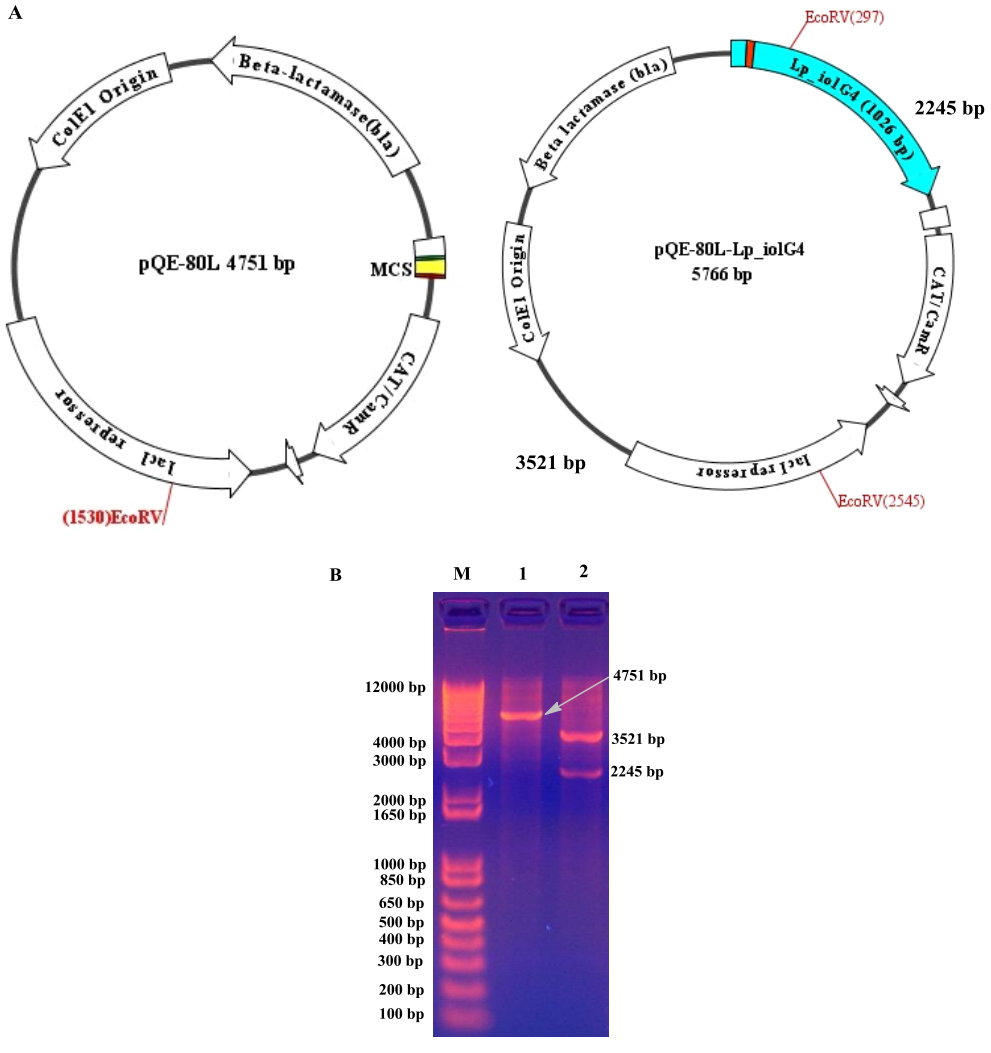

Figure 4.6: A). Restriction DNA map of *pQE-80L* and *pQE-80L-Lp_iolG4* showing restriction site for *EcoRV* enzyme. The image was generated using DNA Dynamo software. **B). A GelRed™ stained 1% agarose gel showing the DNA bands of *pQE-80L* and *pQE-80l-Lp_iolG1* digested with *EcoRV* enzyme** (Lane M:1Kb plus DNA marker; Lane 1: *pQE-80L and* Lane 2: *pQE-80L-Lp_iolG4*).

The insertion of *Lc_iolG1* into *pQE-80L* has resulted in two *NcoI* sites as shown in **Figure 4.7(A)**. Hence, *NcoI* digestion of *pQE-80L* (4751 bp) resulted in a single DNA fragment of 4751 bp, while *pQE-80L-Lc_iolG1* (5775 bp) resulted in two DNA fragments of 4040 bp and 1735 bp. An agarose gel showing the corresponding DNA fragments of digested *pQE-80L* and pQE-*80L-Lp_iolG1* is indicated in **Figure 4.7(B)**.

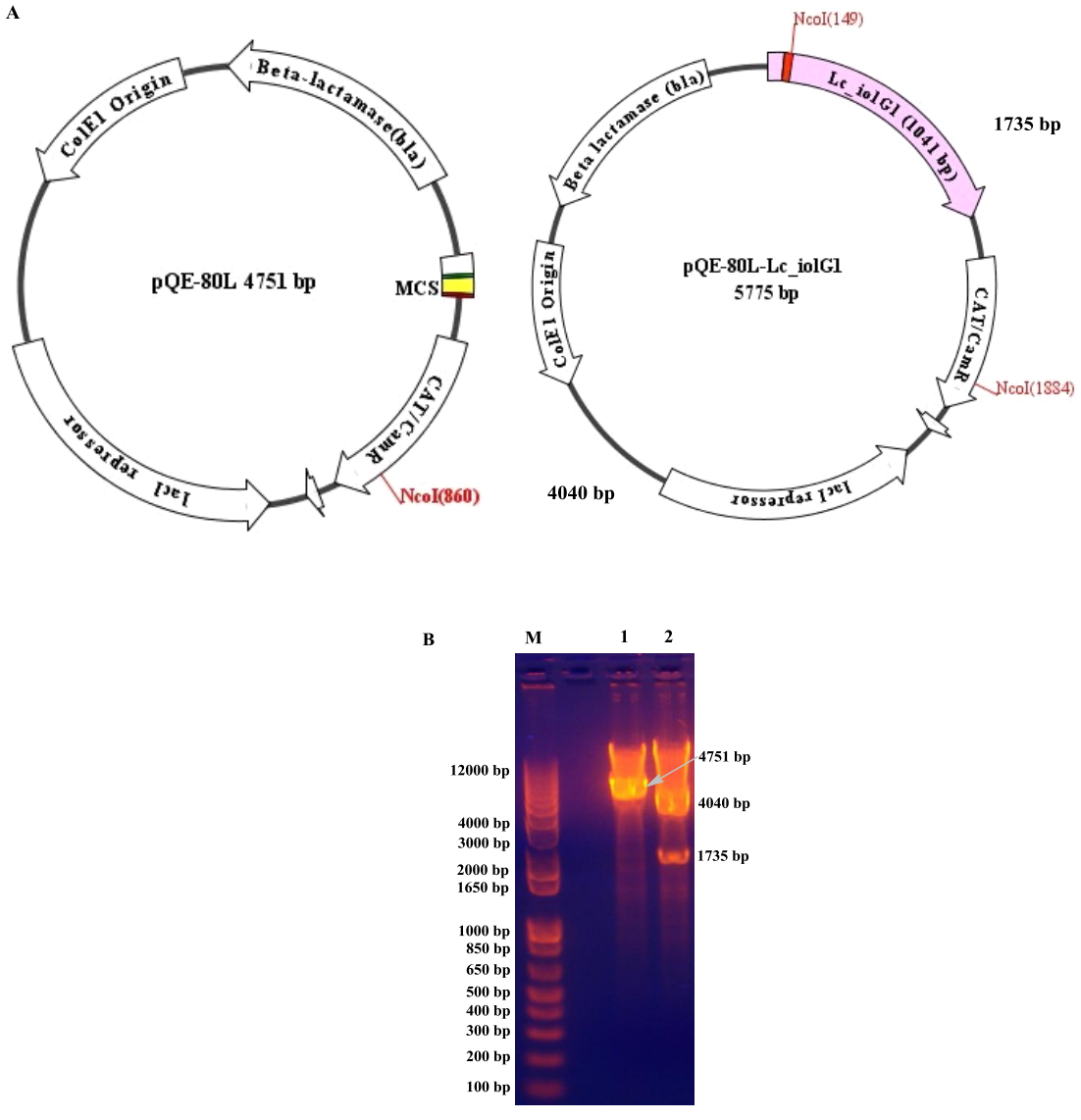

Figure 4.7: A). Restriction DNA map of *pQE-80L* and *pQE-80L-Lc_iolG1* showing restriction site for *NcoI* enzyme. The image was generated using DNA Dynamo software. **B). A GelRed™ stained 1% agarose gel showing the DNA bands of *pQE-80L* and *pQE-80l-Lc_iolG1* digested with *NcoI* enzyme** (Lane M:1Kb plus DNA marker; Lane 1: *pQE-80L and* Lane 2: *pQE-80L-Lc_iolG1*).

pQE-80L-Lc_iolG2 (5776 bp) clones were verified by *KpnI* digestion. The *KpnI* digestion maps for *pQE-80L* and *pQE-80L-Lc_iolG4* are shown in **Figure 4.8(A).** Here, the *pQE-80L* has a single cut site at 167 bp for *kpnI* enzyme, but has none in *pQE-80L-Lc_iolG2* as a result *pQE-80L* shows a single DNA band of size 4751 bp while *pQE-80L-Lc_iolG2* appears as an uncut vector on the agarose gel **Figure 4.8(B)**. Finally, DNA sequencing had confirmed the successful cloning of all genes encoding IDH-related enzymes.

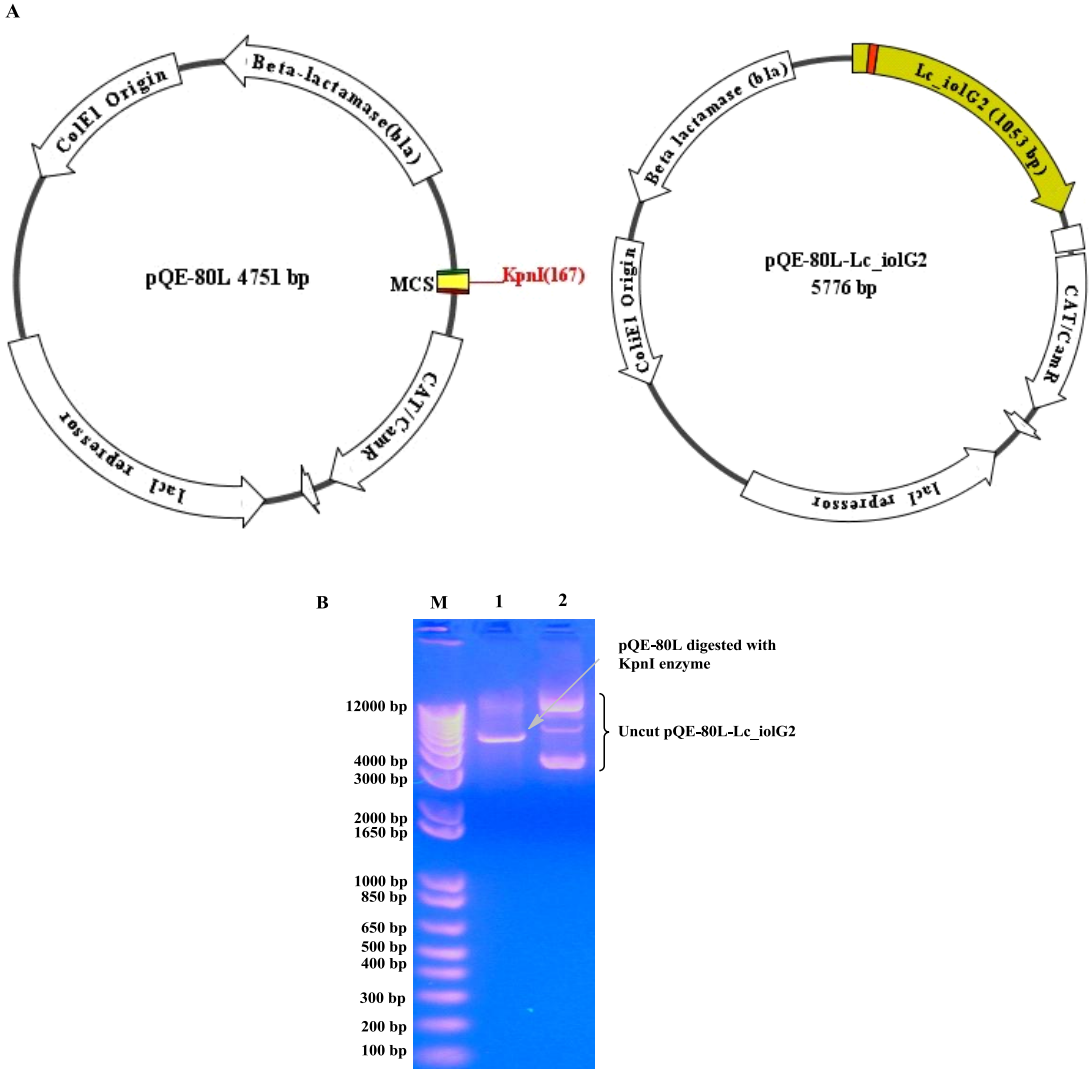

Figure 4.8: A). Restriction DNA map of *pQE-80L* and *pQE-80L-Lc_iolG2* showing restriction site for *KpnI* enzyme. The image was generated using DNA Dynamo software. **B). A GelRed™ stained 1% agarose gel showing the DNA bands of *pQE-80L* and *pQE-80L-Lc_iolG2* digested with *KpnI* enzyme** (Lane M:1Kb plus DNA marker; Lane 1: *pQE-80L and* Lane 2: *pQE-80L-Lc_iolG2*).

4.2 Gene expression

To identify the expression of all the genes, the crude cell lysates were analyzed by a 12% SDS-polyacrylamide gel electrophoresis as shown in **Figure 4.9**.

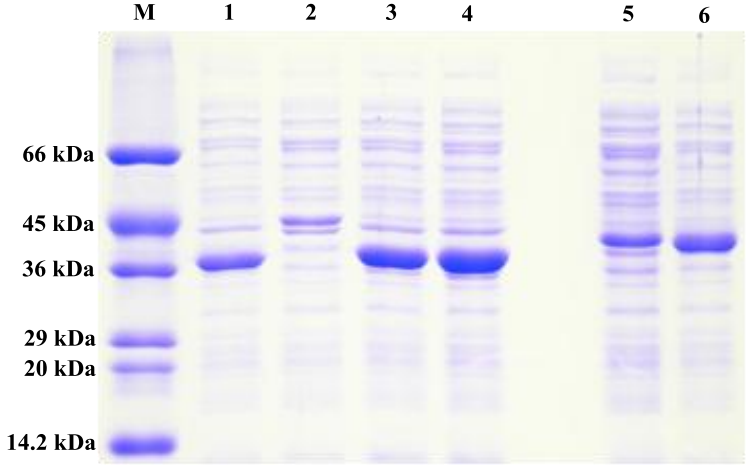

Figure 4.9: A Coomassie Brilliant-Blue stained 12% SDS Polyacrylamide gel showing crude cell lysates of IDH-related enzymes (Lane M: Low-range protein marker; Lane 1: LpIDH1, Lane 2: LpIDH2, Lane 3: LpIDH3, Lane 4: LpIDH4, Lane 5: LcIDH1 and Lane 6: LcIDH2).

From **Figure 4.9**, it is apparent that all the IDH-related genes, except *Lp_iolG2*, were able to express soluble proteins. The expression of *Lp_iolG2* had resulted in the formation of inclusion bodies or protein aggregates. Protein misfolding, alterations in the primary protein sequence as a result of mutations, or translational misincorporation of the amino acid residues are the possible reasons for protein aggregation (*86*, *87*). Formation of inclusion bodies affects the solubility and the stability of the expressed protein. Therefore, expression and purification of LpIDH2 was unsuccessful.

4.3 Protein isolation and purification

IDH-related enzymes from *L. plantarum* WCFS1 (LpIDH1, LpIDH3 & LpIDH4), *L. casei* BL23 (LcIDH1 & LcIDH2) and BsIDH were isolated as crude extracts from their respective cell pellets and purified separately using HiTrap-IMAC FF 1 mL columns as mentioned in section **3.5**. Immobilized-metal affinity chromatography (IMAC) method was first introduced in 1975 (*88*).The metal-chelating ligand iminodiacetic acid was charged with divalent metal cations such as Zn^{2+}, Cu^{2+} and Ni^{2+} to purify different proteins and peptides (*89*). Here, Nickel (Ni^{2+}) provided good binding affinity to the

hexahistidine tag at the N-terminal region of all these expressed proteins. However, binding of other non-specific proteins containing histidine clusters was obvious. Hence, the crude protein extracts were prepared in binding buffer containing 10 mM imidazole, as it minimizes binding of nonspecific proteins onto the column. Imidazole at 60 mM concentration in wash buffer was used to further remove the non-specific proteins (along with small amounts of desired protein) from the column. EDTA (metal chelator) at 100 mM concentration was used to elute pure proteins from the column. Protein dialysis using a 25 kDa MWCO dialysis membrane has provided maximum purity. A 10% (v/v) glycerol and 0.5 M NaCl was maintained throughout the purification process and 40% (v/v) glycerol and 0.1 mM 1, 4-dithio-D-threitol (DTT) in the dialysis buffer to prevent protein precipitation, especially at higher concentrations, and to maintain stability.

As described in section **3.5.1**, LpIDH2 was purified from inclusion bodies using a previously reported method (*90*). The bacterial cell pellet containing LpIDH2 inclusion bodies were solubilized using 8M urea. Bacterial cell debris was separated by centrifugation; the denatured protein sample was filtered and dialyzed against the refolding buffer. The dialysis process was done for 2 days with regular buffer changes, to ensure proper refolding of proteins. During dialysis some of the non-specific proteins and small peptides were separated. The refolded LpIDH2 was further purified by using HiTrap-IMAC FF 1 mL column. The pure protein fractions were pooled together and dialyzed against the regular dialysis buffer as described in section **3.5**. In order to show that a refolded enzyme can be active, BsIDH was also purified by this method and assayed.

The concentration of all the proteins was determined by A_{280} method as described in section **3.6.2**. Approximately 300 mg of LcIDH1 and 500 mg of LcIDH2 were purified from 1 L and 2 L bacterial cultures respectively. A Coomassie Brilliant-blue stained 12% SDS-polyacrylamide gel showing the purified LpIDH1, LpIDH3, LpIDH4, LcIDH1, LcIDH2 and BsIDH is indicated in **Figure 4.10**.

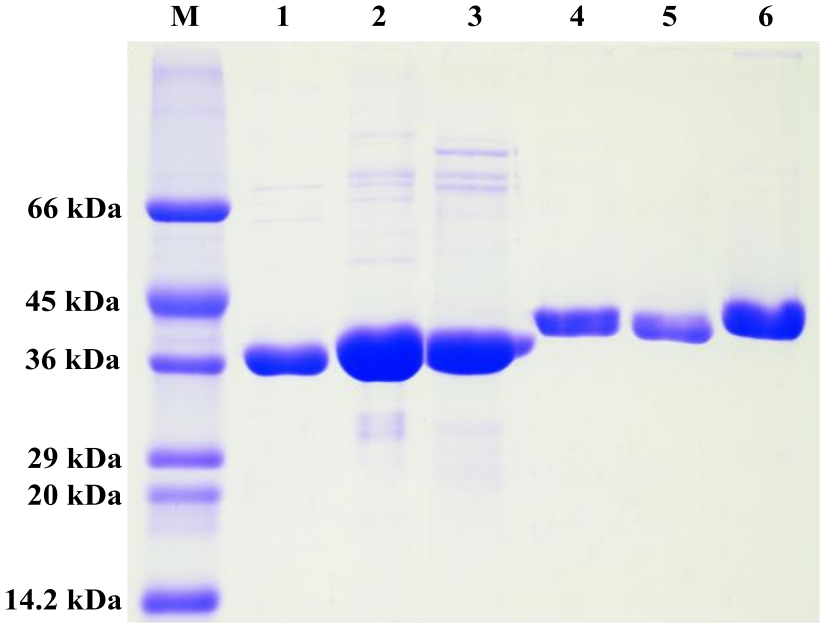

Figure 4.10: A Coomassie Brilliant-Blue stained 12% SDS Polyacrylamide gel showing the purified IDH-related enzymes (Lane M: Low-range protein marker; Lane 1: LpIDH1; Lane 2: LpIDH3; Lane 3: LpIDH4; Lane 4: LcIDH1; Lane 5: LcIDH2 and Lane 6: BsIDH).

4.4 Enzyme kinetics

4.4.1 Inositol dehydrogenase activity

BsIDH from *Bacillus subtilis* catalyses the first step in *myo*-inositol catabolism and optimal conditions for its activity have been reported earlier (*56*). Accordingly, the soluble enzymes from *L. plantarum* WCFS1 (LpIDH1, LpIDH3 & LpIDH4) and *L. casei* BL23 (LcIDH1, LcIDH2*)* were tested for *myo*-inositol dehydrogenase activity at 50 mM *myo*-inositol and 2 mM NAD^+ in 100 mM Tris-HCl pH 9.0 at 25 ^oC as described in **3.8.1.** Surprisingly, IDH-related enzymes from *L. plantarum* WCFS1 (LpIDH1, LpIDH3 & LpIDH4) did not exhibit any activity when assayed with *myo*-inositol, but LcIDH1 and LcIDH2 from *L.casei* BL23 showed dehydrogenase activity similar to BsIDH. When NAD^+ was replaced with $NADP^+$, all enzymes failed to show inositol dehydrogenase activity, suggesting that they are exclusively NAD^+-dependent inositol dehydrogenases as reported for BsIDH (*56, 58*). The absorbance versus time plots showing the activities of IDH-related enzymes with *myo*-inositol and NAD^+ is indicated in **Figure 4.11**.

Inositol dehydrogenase activity was also tested for the LpIDH2 and BsIDH that were purified by unfolding and refolding experiments. LpIDH2 did not exhibit any activity. However, BsIDH showed significantly less activity when compared to that of

BsIDH purified by normal method. An absorbance versus time plots showing the activities of unfolded and refolded LpIDH2 and BsIDH with 50 mM *myo*-inositol and 2 mM NAD^+ is indicated in **Figure 4.12**.

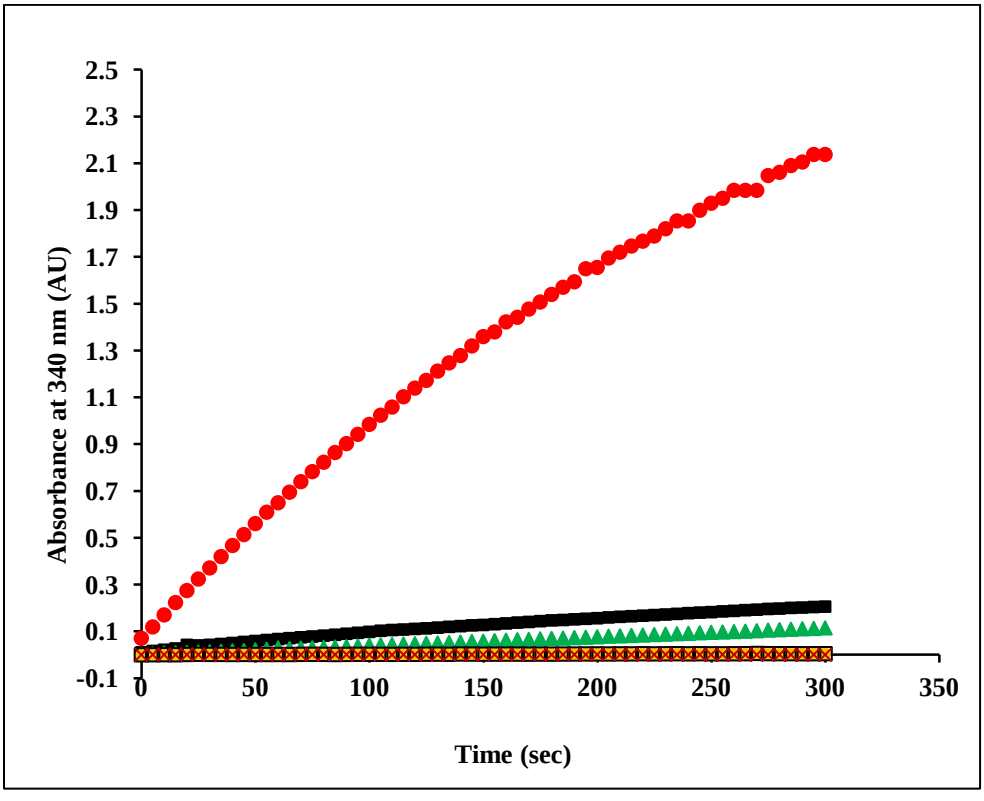

Figure 4.11: Absorbance *vs* time plot showing the activities of BsIDH and IDH-related enzymes from *L. plantarum* WCFS1 and *L. casei* BL23. Conditions: 50 mM *myo*-inositol, 2 mM NAD^+, 100 mM Tris-HCl pH 9.0 at 25 ^oC, (●) BsIDH, (■) LcIDH1, (▲) LcIDH2, (♦) LpIDH1, (□) LpIDH3 and (×) LpIDH4. The amount of enzyme in each reaction was 1 µL of 1 mg/mL.

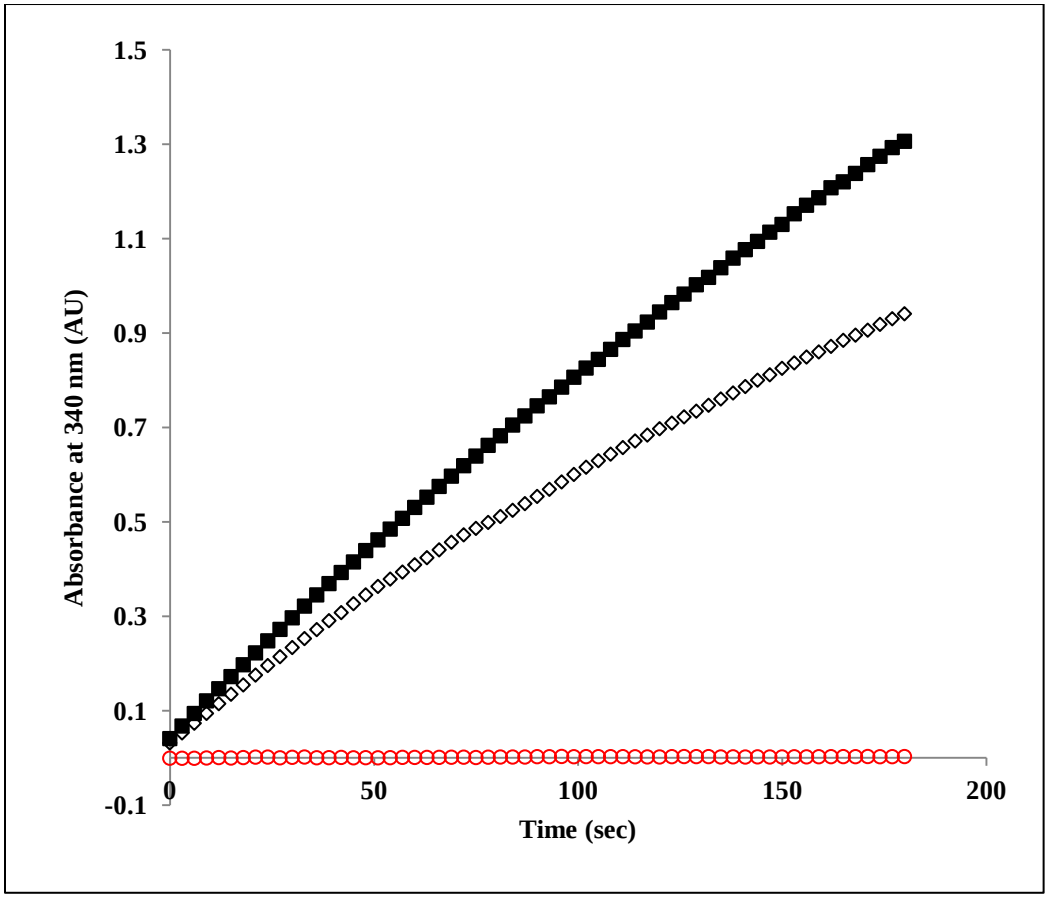

Figure 4.12: Absorbance *vs* time plot showing the activities of BsIDH and LpIDH2 purified by unfolding and refolding experiment. Conditions: 50 mM *myo*-inositol, 2 mM NAD^+, 100 mM Tris-HCl pH 9.0 at 25 ^oC, (■) BsIDH purified by normal method, (◊) BsIDH purified by unfolding and refolding method, (○) LpIDH2 purified by unfolding and refolding method. The amount of enzyme in each reaction was 1 µL of 1 mg/mL concentration.

4.4.2 Optimum pH and pH-rate profiles

The pH (a measure of H^+ ion concentration) can influence the structure and activity of an enzyme. A change in pH can influence the state of ionization of acidic or basic amino acid side chains in the active site, which can lead to either loss of substrate recognition by the enzyme or failure to convert substrates into products. Extremely high or low pH conditions can disrupt the three-dimensional conformations of a protein making it completely inactive. Therefore, it is important to determine the optimum pH for an enzyme-catalyzed reaction before performing kinetic studies.

The optimum pH for the reactions catalyzed by LcIDH1, LcIDH2 and BsIDH were determined according to the procedure described in section **3.8.3**. The pH-rate profiles for LcIDH1 and LcIDH2 are indicated in **Figures 4.13 and 4.14** respectively**.** From the pH-rate profiles, it is clear that LcIDH1 has a maximum activity at pH 9.3 while

LcIDH2 has a maximum activity at pH 9.5, when measured at 50 mM *myo*-inositol and 2 mM NAD^+, in 100 mM 2-(cyclohexylamino)-ethanesulfonic acid, CHES (buffer pH range: 8.6-10) at 25^oC.

The pH-rate profile for BsIDH was determined to compare the maximum activities of LcIDH1 and LcIDH2 with that of BsIDH. The pH-rate profile for BsIDH was previously reported and the kinetic studies were performed in Tris-HCl pH 9.0 (*56, 61*). According to the reported pH profile, Tris-HCl buffer was used for the reactions that were performed at pH greater than 9.0. However, the useful pH range for Tris-HCl is 7.0-9.0, which suggests that Tris-HCl cannot show its buffering capacity beyond this range. This could be the possible reason for decrease in forward reaction rates after pH 9.0 that was observed in the pH-rate profile of BsIDH. In this research, the pH-rate profile for BsIDH was established as described in section **3.8.3**. BsIDH showed maximum activity at pH 10.0, when assayed in 100 mM glycine-NaOH buffer (buffer pH range: 8.8-10.6) at 25^oC. In buffer comparison experiments, LcIDH1 and LcIDH2 showed higher activities in CHES than glycine-NaOH and BsIDH showed higher activity in glycine-NaOH than CHES and Tris-HCl, see **Figure 4.15.** Note that the activity below pH 9.0 was much lower.

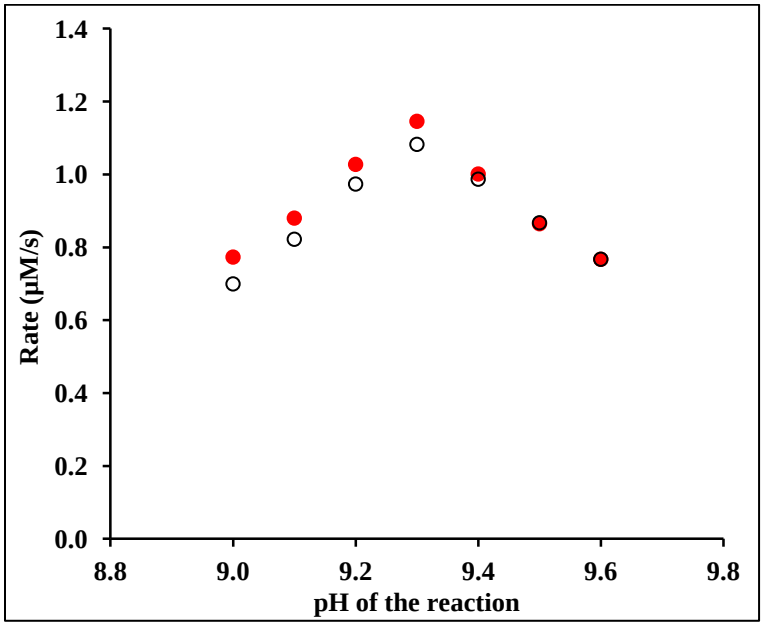

Figure 4.13: The pH-rate profile of LcIDH1. Conditions: 50 mM *myo*-inositol, 2 mM NAD^+ and 100 mM buffer (●) CHES, (○) glycine-NaOH at 25 ^oC.

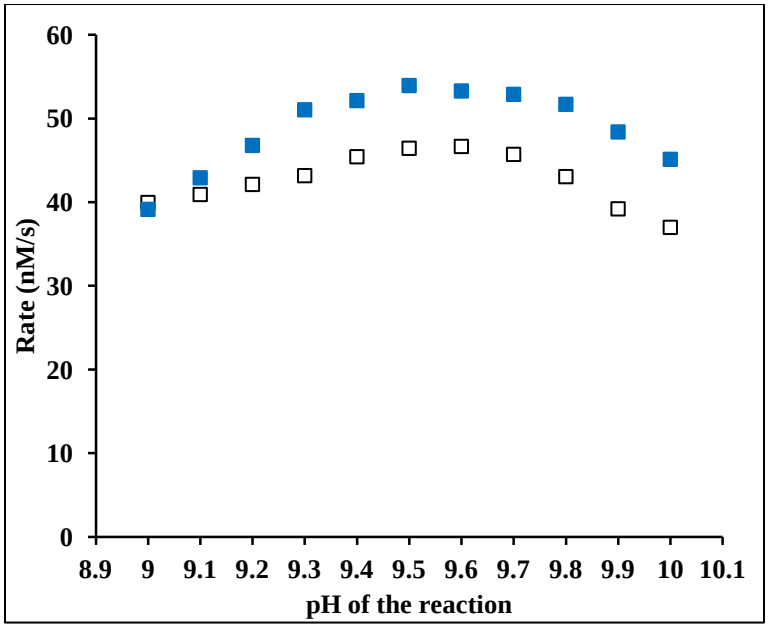

Figure 4.14: The pH-rate profile of LcIDH2. Conditions: 50 mM *myo*-inositol, 2 mM NAD^+ and 100 mM buffer (■) CHES, (□) glycine-NaOH at 25 ^oC.

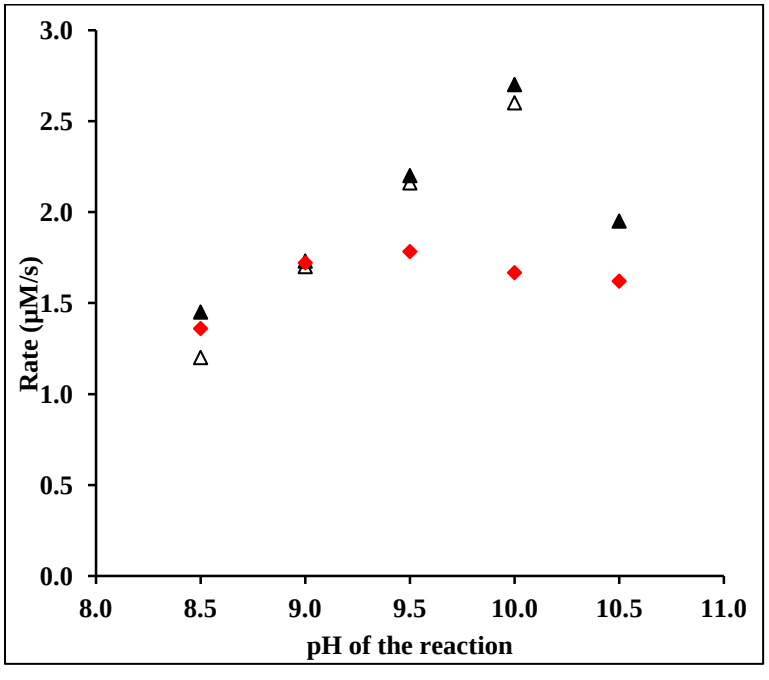

Figure 4.15: The pH-rate profile of BsIDH. Conditions: 50 mM *myo*-inositol, 2 mM NAD^+ and 100 mM buffer (▲) glycine-NaOH, (Δ) CHES, and (♦) Tris-HCl at 25 ^oC.

4.4.3 True kinetic constants (K_m , k_{cat} and k_{cat}/K_m)

True kinetic constants for the reaction catalyzed by LcIDH1, LcIDH2 and BsIDH were determined according to the procedure described in section **3.8.4**. The initial velocity data was calculated as described in section **3.8.2.** Leonora software was used to generate the true kinetic constants (*80*). Leonora uses a non-linear least-squares method to fit the initial velocity data to **Equation 3.3** in **3.8.4** assuming there is no product accumulation and generates the kinetic constants, K_m (for both substrates), and K_i for NAD^+. The turnover number, k_{cat} was calculated using the V_{max} and total enzyme concentration E_t, while the specificity constant, k_{cat}/K_m was calculated using k_{cat} and K_m values. Michaelis-Menten saturation curves and double reciprocal plots (Lineweaver-Burk Plots) for LcIDH1, LcIDH2 and BsIDH are indicated in **Appendix-C.** True kinetic constants for LcIDH1, LcIDH2 and BsIDH with *myo*-inositol and NAD^+, and LcIDH1 with D-glucose and NAD^+ are indicated in **Table 4.1**.

Table 4.1: True kinetic constants for LcIDH1, LcIDH2 and BsIDH

Kinetic constants	LcIDH1	LcIDH2	BsIDH
***myo*-inositol:**			
V_{max} *(nM/s)*	382 ± 4	71 ± 3	(15.5 ± 0.6) × 10^3
K_m (NAD^+) *(mM)*	0.55 ± 0.02	0.03 ± 0.02	0.23 ± 0.04
K_m(*myo*-inositol)*(mM)*	1.7 ± 0.3	6.7 ± 0.9	3.1 ± 0.7
k_{cat} *(s^{-1})*	13.2 ± 0.2	1.8 ± 0.1	294 ± 16
k_{cat}/K_m (NAD^+) *(M^{-1} s^{-1})*	(24 ± 1) × 10^3	(50 ± 9) × 10^3	(1277 ± 62) × 10^3
k_{cat}/K_m (*myo*-inositol) *(M^{-1} s^{-1})*	(7.8 ± 1.4) × 10^3	(0.26 ± 0.038) × 10^3	(96 ± 5) × 10^3
K_i *(NAD^+)*	8.3 ± 0.2	14.5 ± 0.7	10.3 ± 0.6
D-glucose:			
V_{max} *(nM/s)*	1670 ± 160	Not determined	Not determined
K_m (NAD^+) *(mM)*	0.61 ± 0.13		
K_m(D-glucose)*(mM)*	19.5 ± 11.7		
k_{cat} *(s^{-1})*	4.9 ± 0.5		
k_{cat}/K_m (NAD^+) *(M^{-1} s^{-1})*	(7.96 ± 1.83) × 10^3		
k_{cat}/K_m (D-glucose) *(M^{-1} s^{-1})*	250 ± 16		
K_i *(NAD^+)*	4.1 ± 0.5		

From the double reciprocal plots (see appendix-B), it can be observed that the trend lines representing the data points intersects on the left side of the y-axis, which suggests that LcIDH1 and LcIDH2 follow a sequentially ordered Bi-Bi mechanism similar to that reported for BsIDH (*56, 58*). The kinetic results shown in **Table 4.1**, suggests that LcIDH1 and LcIDH2 from *L. casei* BL23 exhibit very different inositol dehydrogenase activities. The K_m value for LcIDH1 is 4 times lower and the k_{cat} value 7.3 times higher when compared to that of LcIDH2. These differences make LcIDH1 a more efficient enzyme for the oxidation of *myo*-inositol, as indicated by its specificity constant value, which is nearly 30 times higher compared to LcIDH2. By comparing the true kinetic constants of LcIDH1 to that of BsIDH, it can be observed that LcIDH1 is a much less efficient enzyme, and this difference is seen almost entirely in the turnover number (k_{cat}). LcIDH2 showed 2-fold higher value of K_m and almost 150-fold smaller k_{cat} value when compared to BsIDH. By comparing the true kinetic constants with *myo*-inositol and D-glucose, it is apparent that LcIDH1 oxidize D-glucose with less efficiency, suggesting *myo*-inositol is the preferred substrate.

4.4.4 Exploring alternate substrates

It was reported that BsIDH can stereoselectively oxidize other structurally related compounds in addition to *myo*-inositol (**section 1.4**) (*56, 58, 59*). Further, assays showed that LpIDH1, LpIDH3 and LpIDH4 from *L. plantarum* WCFS1 are inactive when *myo*-inositol was used as the substrate. Therefore, it was hypothesized that IDH-related enzymes from *L. plantarum* WCFS1 and *L.casei* BL23 may also exhibit a broad substrate spectrum. To investigate this, the dehydrogenase activity assays were performed with compounds such as *scyllo*-inositol, D-c*hiro*-inositol, D-glucose, L-glucose and D-xylose, D-galactose, D-mannose, D-sorbitol, D-mannitol, *scyllo*-inosose and 4-*O*-benzyl-*myo*-inositol. Each assay was performed at 50 mM substrate and 2 mM NAD^+ in 100 mM Tris-HCl pH 9.0, CHES pH 9.3 and 9.5, and glycine-NaOH pH 10.0. The activity of BsIDH was also tested with these compounds. The compounds that are tested in this study are indicated in **Figure 4.16.** Further, apparent kinetic constants were determined for the compounds with which the IDH-related enzymes showed activity.

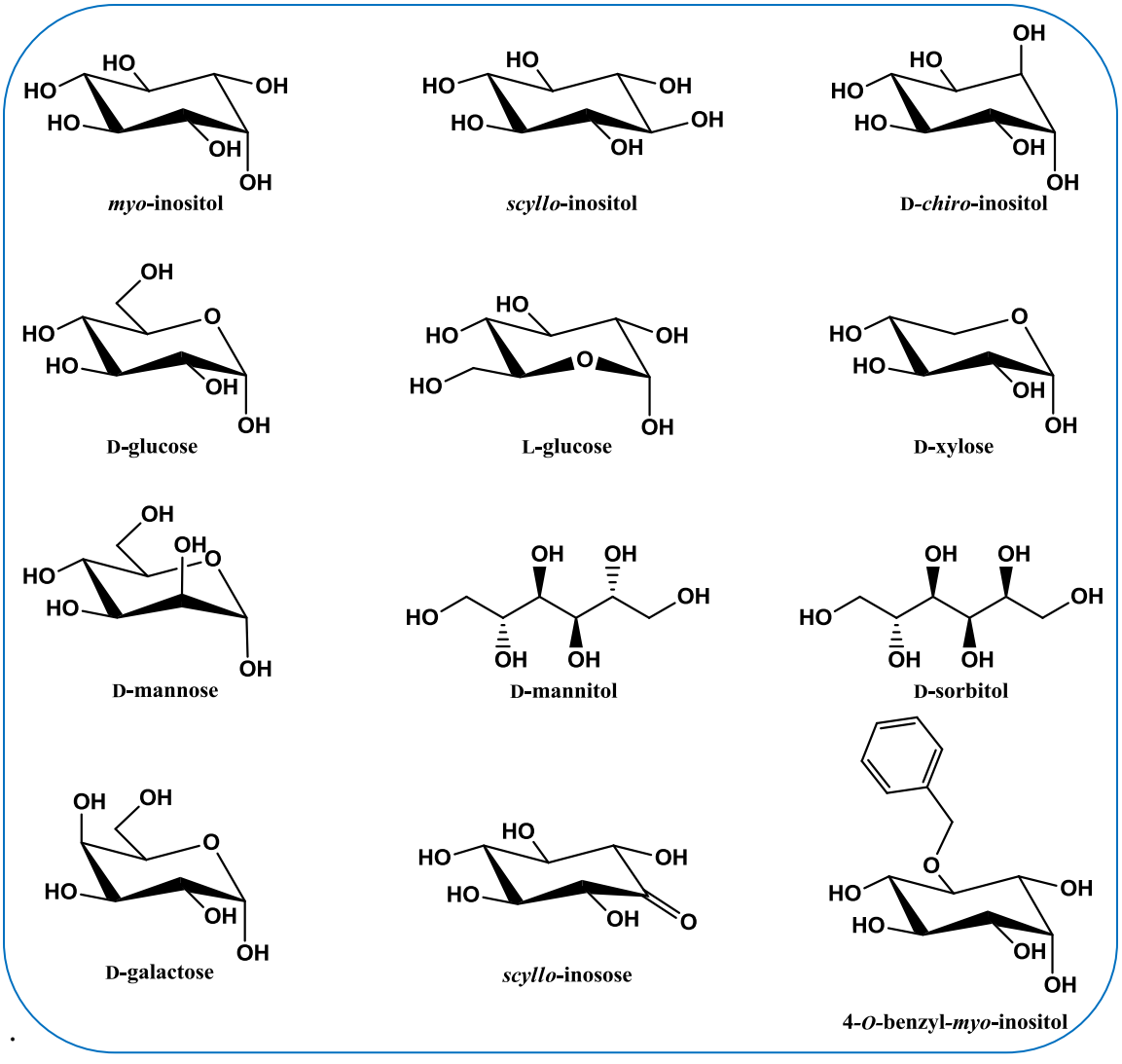

Figure 4.16: *myo*-Inositol and other related compounds tested for dehydrogenase activity

4.4.4.1 Apparent kinetics constants

Apparent kinetic constants were calculated for the active IDH-related enzymes with the compounds that are recognized as the substrates. Kinetic assays were performed as described in section **3.8.5.** The initial velocity data was fitted to **Equation 3.4** using Leonora. Kinetic assays with 4-*O*-benzyl-*myo*-inositol were performed in 20% DMSO as reported previously (*60*). Michaelis-Menten saturation curves and the Lineweaver-Burk plots for LcIDH1 with different substrates are provided in **Appendix-D.** Apparent kinetic constants for LcIDH1 with different substrates are indicated in **Tables 4.2.**

Table 4.2: Apparent kinetic constants for LcIDH1

Substrates	V_{max}^{app} (nM/s)	K_m^{app} (mM)	k_{cat}^{app} (s^{-1})	$(k_{cat}/K_m)^{app}$ (M^{-1} s^{-1})
***myo*-inositol**	**300 ± 1**	**7.0 ± 0.1**	**10.3 ± 0.7**	**1500 ± 100**
D-*chiro*-inositol	**173 ± 6**	**47 ± 3**	**5.9 ± 0.4**	**130 ± 10**
D-glucose	**115 ± 10**	**31 ± 8**	**3.9 ± 0.4**	**130 ± 40**
D-xylose	**165 ± 7**	**225 ± 23**	**5.7 ± 0.2**	**25 ± 3**
4-*O*-benzyl-*myo*-inositol*	**75 ± 3**	**28 ± 2**	**1.9 ± 0.1**	**33 ± 2**

Note: * = The reaction was performed in 20% DMSO in 100 mM CHES pH 9.3

Michaelis-Menten saturation curves and the Lineweaver-Burk plots for LcIDH2 with different substrates are indicated in **Appendix-D.** Apparent kinetic constants of LcIDH2 with different substrates are indicated in **Tables 4.3.**

Table 4.3: Apparent kinetic constants of LcIDH2

Substrates	V_{max}^{app} (nM/s)	K_m^{app} (mM)	k_{cat}^{app} (s^{-1})	$(k_{cat}/K_m)^{app}$ (M^{-1} s^{-1})
***myo*-inositol**	**67 ± 2**	**12.2 ± 1.3**	**1.7 ± 0.1**	**135 ± 15**
D-chiro-inositol	**24 ± 2**	**527 ± 58**	**0.6 ± 0.1**	**1.1 ± 0.1**
D-glucose	**64 ± 1**	**181 ± 6**	**1.6 ± 0.1**	**8.8 ± 0.4**
D-xylose	**42.4 ± 0.6**	**142 ± 6**	**1.1 ± 0.1**	**7.4 ± 0.3**
4-*O*-benzyl-*myo*-inositol*	**No Activity**			
***scyllo*-inositol**	**71.4 ± 0.4**	**0.35 ± 0.07**	**1.8 ± 0.1**	**5000 ± 150**
L-glucose	**48.6 ± 1.4**	**108 ± 5**	**1.21 ± 0.03**	**11.2 ± 0.4**

Note: * = The reaction was performed in 20% DMSO in 100 mM CHES pH 9.5.

Michaelis-Menten saturation curves and the Lineweaver-Burk plots for BsIDH with different substrates are indicated in **Appendix-D.** Apparent kinetic constants for BsIDH with different substrates are indicated in **Tables 4.4.**

Table 4.4: Apparent kinetic constants of BsIDH

Substrates	V_{max}^{app} (nM/s)	K_m^{app} (mM)	k_{cat}^{app} (s^{-1})	$(k_{cat}/K_m)^{app}$ (M^{-1} s^{-1})
***myo*-inositol**	**14700 ± 100**	**7.9 ± 0.1**	**270 ± 2**	**34200 ± 500**
D-*chiro*-inositol	**1200 ± 20**	**18 ± 1**	**22.02 ± 0.02**	**1220 ± 68**
D-glucose	**678.1 ± 14.3**	**60.5 ± 2.3**	**12.4 ± 0.3**	**205 ± 9**
D-xylose	**1210 ± 30**	**200 ± 8**	**22.2 ± 0.5**	**111 ± 5**
4-*O*-benzyl-*myo*-inositol*	**389 ± 5**	**11.2 ± 0.5**	**15.1 ± 0.2**	**1310 ± 60**

Note: * = The reaction was performed in 20% DMSO in 100 mM glycine-NaOH pH 10.

Apparent kinetic constants for LcIDH1, LcIDH2 and BsIDH with different substrates are graphically represented for convenient comparison. **Figure 4.17** represents the comparison of k_{cat} values and **Figure 4.18** represents the comparison of the specificity constants values.

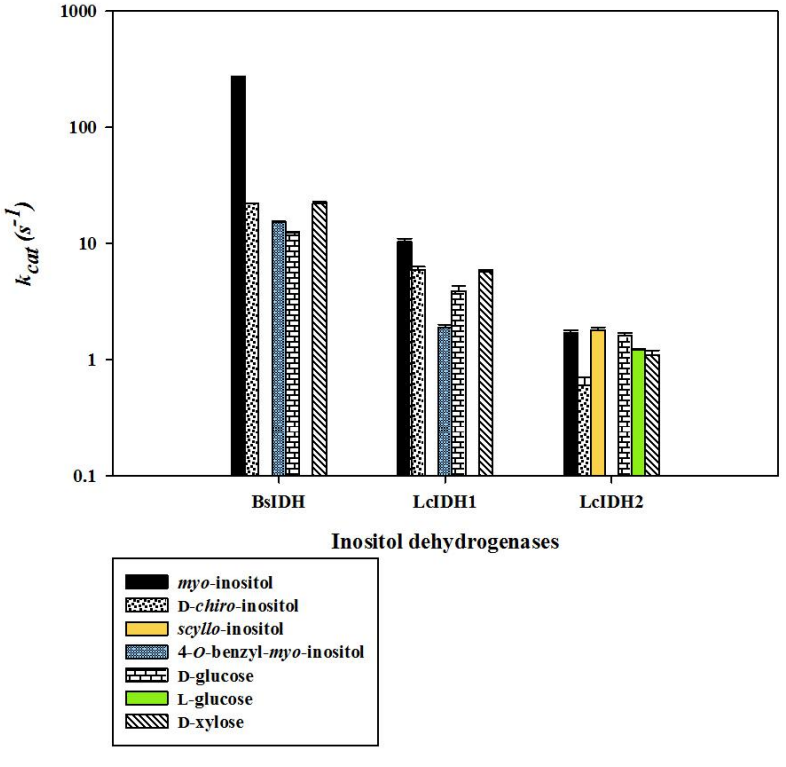

Figure 4.17: Comparison of apparent k_{cat} values of BsIDH, LcIDH1 and LcIDH2 with different substrate. Assay conditions: 50 mM substrate, 2 mM NAD^+ and 100 mM glycine-NaOH pH 10 (BsIDH); 100 mM CHES pH 9.3 (LcIDH1) and pH 9.5 (LcIDH2).

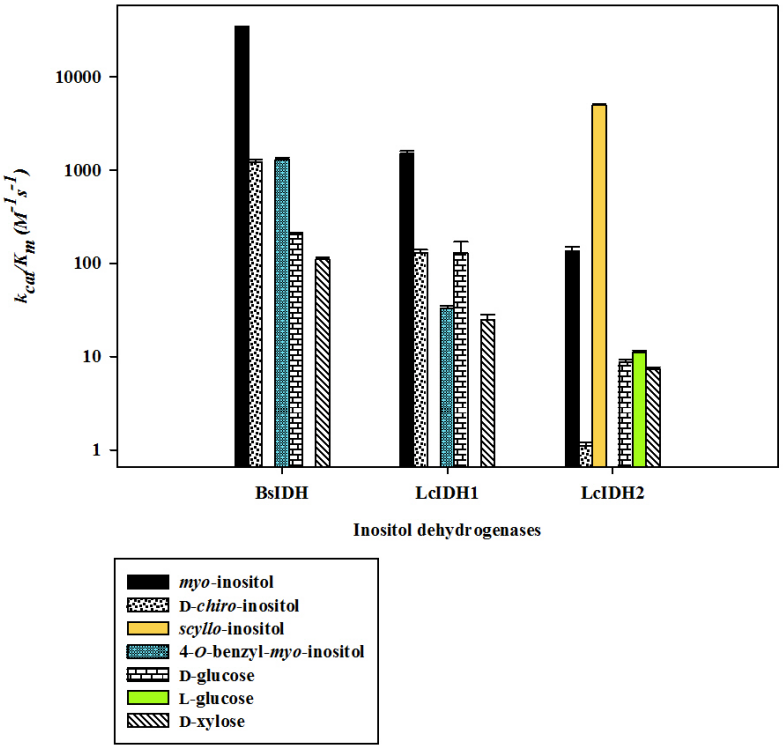

Figure 4.18: Comparison of specificity constants of BsIDH, LcIDH1 and LcIDH2 with different substrate. Assay conditions: 50 mM substrate, 2 mM NAD^+ and 100 mM glycine-NaOH pH 10 (BsIDH); 100 mM CHES pH 9.3 (LcIDH1) and pH 9.5 (LcIDH2).

IDH-related enzymes from *L. plantarum* WCFS1 did not show activity with any of the compounds (**Figure 4.16)** tested. As described in section **1.5.1**, LpIDH1 showed activity with *scyllo*-inosose, which is the product in the first step of *myo*-inositol catabolism. Recently, IDH-related enzymes were classified into four subgroups and proposed that IDH enzymes from *L. plantarum* WCFS1 are different to each other in their sequence and structure. Each of the four enzymes belongs to a different IDH subgroup (*63*). Except for LpIDH1, there is no structural information for these enzymes. Therefore, the protein sequences of these enzymes were compared to sequence and structure of BsIDH by a multiple sequence alignment approach, to predict the activity differences between these enzymes.

LcIDH1 activity is very similar to BsIDH, in that both BsIDH and LcIDH1 showed activity with D-c*hiro*-inositol, D-glucose, D-xylose, and 4-*O*-benzyl-*myo*-inositol in addition to *myo*-inositol, but were unable to show any activity with compounds such as *scyllo*-inositol, and L-glucose. For both BsIDH and LcIDH1 *myo*-inositol is the natural substrate as indicated by their high apparent specificity constant values **(Table 4.2 and**

4.4) compared to the other substrates. The apparent specificity constant for the oxidation of D-*chiro*-inositol is nearly equal to that of 4-*O*-benzyl-*myo*-inositol for BsIDH. LcIDH1 catalyzed the oxidation of D-*chiro*-inositol and D-glucose with equal efficiency. Both enzymes are least active with D-xylose. This is because of a very high value of K_m^{app} and a low apparent turnover number **(Table 4.2 and 4.4)**. The oxidation of 4-*O*-benzyl-*myo*-inositol by LcIDH1 suggests that it also possess a hydrophobic pocket next to the active site similar to BsIDH, and the sequence alignment of LcIDH1 with BsIDH indicates that residues proposed for this hydrophobic pocket are conserved (**Figure 1.4).** It was proposed that the Y235 or W272 make stacking interactions with the benzyl group when 4-*O*-benzyl-*myo*-inositol binds in the active site (*60*). These observations suggest that LcIDH1 has a broad substrate spectrum and stereoselectivity similar to BsIDH.

LcIDH2 activity is quite different from BsIDH and LcIDH1 activities. It oxidized *scyllo*-inositol, and L-glucose in addition to *myo*-inositol, D-c*hiro*-inositol, D-glucose, D-xylose, but no activity was observed with 4-*O*-benzyl-*myo*-inositol. From **Figure 4.17,** it is apparent that the k_{cat}^{app} values for the oxidation of *scyllo*-inositol, *myo*-inositol, and D-glucose are nearly equal. However, the apparent specificity constant for *scyllo*-inositol is 37 times and 570 times higher when compared to *myo*-inositol and D-glucose respectively, (**Figure 4.18**). These differences can be seen entirely in large variations in K_m^{app} values of LcIDH2 towards these substrates **(Table 4.3)**. The apparent specificity constants for the oxidation of D-xylose and D-glucose are nearly equal and are comparable to that of L-glucose, which is the enantiomer of D-glucose. This suggests that the active site of LcIDH2 is structurally different from LcIDH1 and BsIDH. A very high K_m^{app} and a much low apparent turnover number (**Table 4.3**) make LcIDH2 much less efficient for the oxidation of D-*chiro*-inositol. The loss of activity with 4-*O*-benzyl-*myo*-inositol suggests that LcIDH2 does not accommodate the 4-*O*-substituted inositol derivatives as its substrates and the active site of LcIDH2 is different from that of LcIDH1 and BsIDH. It was reported that the C2 hydroxyl group of *myo*-inositol is oxidized by BsIDH (*56*). Since LcIDH2 is able to oxidize s*cyllo*-inositol and *myo*-inositol, it is not clear which hydroxyl group is the target during the oxidation of these substrates and also other substrates. Furthermore, the true kinetic constants were determined for *scyllo*-inositol and compared with those of *myo*-inositol. Michaelis-

Menten saturation curves, and the Lineweaver-Burk plots are shown in **Appendix-C** and the kinetic data is shown in **Table 4.5.**

Table 4.5: True kinetic constants of LcIDH2 with *myo*-inositol and *scyllo*-inositol

inetic constants	*myo*-inositol (MI)	*scyllo*-inositol (SI)
V_{max} (nM/s)	71 ± 3	76 ± 2
K_m (NAD^+) (mM)	0.09 ± 0.01	0.11 ± 0.02
K_m (S) (mM)	6.7 ± 0.9	0.12 ± 0.02
k_{cat} (s^{-1})	1.8 ± 0.1	1.9 ± 0.1
k_{cat}/K_m (NAD^+) (M^{-1} s^{-1})	(20 ± 3) × 10^3	(17.3 ± 0.2) × 10^3
k_{cat}/K_m (S) (M^{-1} s^{-1})	261 ± 38	(15.8 ± 0.2) × 10^3
K_i (NAD^+)	14.5 ± 0.7	0.29 ± 0.02

From **Table 4.5**, the values for V_{max}, k_{cat}, K_m (NAD^+) and k_{cat}/K_m (NAD^+) looks similar, but a significant difference in K_m and the specificity constant, k_{cat}/K_m can be observed between these substrates. The K_m for *scyllo*-inositol is 0.12 mM, which is 60 times less when compared to the K_m for *myo*-inositol. The specificity constant, k_{cat}/K_m for *scyllo*-inositol is also very high relative to that for *myo*-inositol. On the basis of these differences, it is conclusive that LcIDH2 has 60 times higher binding affinity for *scyllo*-inositol than *myo*-inositol and LcIDH2 can catalyze the oxidation of *scyllo*-inositol with high efficiency compared to the oxidation of *myo*-inositol.

4.4.5 Preparation of *scyllo*-inosose, 2-^{2}H-*myo*-inositol, and *myo*-inositol

scyllo-Inosose was prepared from the commercial *myo*-inositol as described in section **3.2.1.** *scyllo*-Inosose was produced as a white solid when *Gluconobacter oxydans* ATCC # 621H was cultured in revitalizing media containing *myo*-inositol for 96 h and followed by methanol precipitation. The product was confirmed by ^{1}H NMR and melting point, which are close to the previously reported once.

Sodium borodeuteride (NaB^2H_4) reduced the carbonyl group of *scyllo*-inosose to produce 2-^{2}H-*myo*-inositol. The deuterium atom was stereoselectively added on to the C2, which is *anti* to the hydroxyl groups on the adjacent carbon atoms. The pure 2-^{2}H-

myo-inositol was obtained after acetylation and deacetylation steps. Similarly, reduction of *scyllo*-inosose with $NaBH_4$ resulted in *myo*-inositol. **Scheme 4.1** represents different steps in the preparation of *scyllo*-inosose, 2-^{2}H-*myo*-inositol and *myo*-inositol.

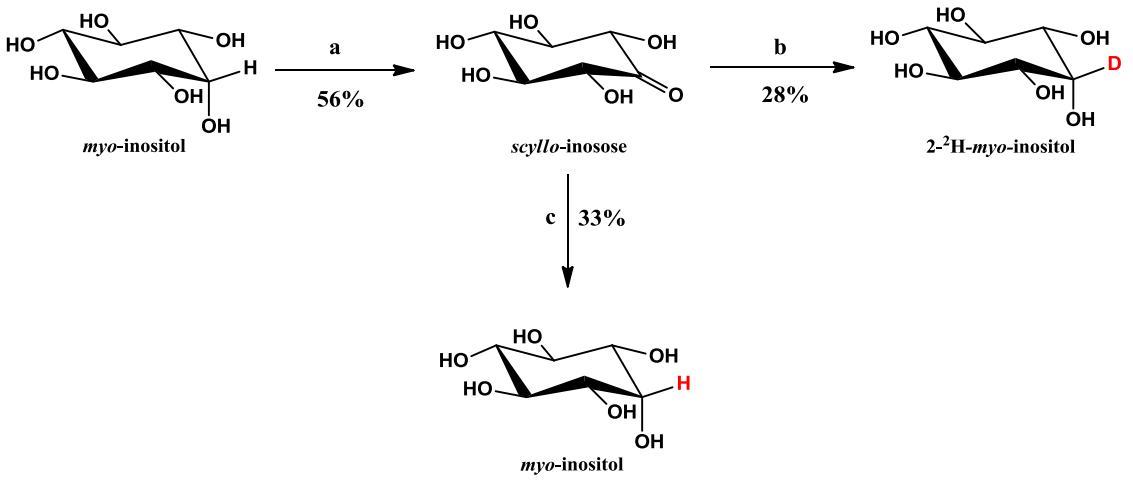

Scheme 4.1: Preparation of *scyllo*-inosose, 2-^{2}H-*myo*-inositol, and *myo*-inositol. a) *G. oxydans* ATCC # 621H, 30 ^oC, 96 h. **b)** (1) $NaBD_4$, ddH_2O, r. t., overnight; (2) Ac_2O, pyridine, 100^oC 24 h; (3) $NaOCH_3$, CH_3OH, reflux 20 min, Dowex 50X8 (H^+ form) 200-400 mesh, acetone wash. **c)** (1) $NaBH_4$, ddH_2O, r. t., overnight; (2) Ac_2O, pyridine, 100^oC 24 h; (3) $NaOCH_3$, CH_3OH, reflux 20 min, Dowex 50X8 (H^+ form) 200-400 mesh, acetone wash.

4.4.6 Kinetic isotopic effect (KIE)

According to a sequentially ordered Bi-Bi mechanism, the enzyme first binds to the coenzyme NAD^+ followed by *myo*-inositol or other related compounds and forms a ternary-complex, (E-NAD^+-Substrate) (*70*). During this ternary-complex state, the conversion of substrates into products or vice-versa constitutes the chemical step of the reaction. After catalysis the ternary-complex breaks down, first releasing *scyllo*-inosose followed by NADH in the forward reaction. A detailed kinetic mechanism for BsIDH has been determined and demonstrated that the chemical step (hydride transfer) is not the rate-limiting step, but the breakdown of the ternary-complex and the liberation of NADH limits the rate of the reaction (*58*). Later, this was confirmed by kinetic isotopic effect studies (*61*).

In this research, the kinetic results suggest that LcIDH1 and LcIDH2 may follow a sequentially ordered Bi-Bi mechanism during catalysis. However, LcIDH1 exhibited less efficiency when compared to BsIDH. It was assumed that the chemical step might be responsible for the reduced activity. Therefore, a primary kinetic isotopic effect

experiments for LcIDH1 were performed to identify the rate-limiting step, using commercial *myo*-inositol, and synthetic *myo*-inositol and 2-^{2}H-*myo*-inositol. The latter compounds were prepared according to previously described methods (*61*). The apparent kinetics constants for LcIDH1 were determined as described in section **3.8.5** and the results are indicated in **Table 4.6** and the Michaelis-Menten saturation curves and the double reciprocal plots were indicated in **Appendix-E**.

Table 4.6: Apparent kinetic constants for LcIDH1 with commercial *myo*-inositol and the synthetic *myo*-inositol, and 2-^{2}H-*myo*-inositol

Substrates	V_{max}^{app} (nM/s)	K_m^{app} (mM)
Commercial *myo*-inositol	**104 ± 6**	**5.8 ± 1.1**
Synthetic *myo*-inositol	**116 ± 5**	**5.1 ± 0.1**
2-^{2}H-*myo*-inositol	**71 ± 2**	**4.7 ± 0.6**

From the kinetic results provided in **Table 4.6**, the primary KIE value, [V_{max}^{app} (synthetic *myo*-inositol)/ V_{max}^{app} (2-^{2}H-*myo*-inositol)] obtained was 1.6 ± 0.1, which is equal to the KIE value of 1.5 ± 0.1 obtained when assayed with commercial *myo*-inositol. Based on these results, it is apparent that the chemical step in the reaction is at least partly rate-limiting and this may contribute to the lower activity of LcIDH1. This is consistent with some other reports of dehydrogenase-catalyzed reactions, in which the primary KIE value for deuterium-substituted substrates is in the range of 1-2, indicating that the chemical step is either not rate-limiting or partially rate-limiting and the release of products is the primarily the rate limiting step (*91-95*).

4.5 Rationale for sequence/structure and activity differences

According to the structural classification of IDH-related enzymes (**section 1.5**), there are six consensus sequence motifs that are important for coenzyme binding and the formation of substrate binding pocket among the IDH-related enzymes (*63*). Four IDH subgroups were classified and proposed that LpIDH1 to LpIDH4 from *L. plantarum* WCFS1 represents a member of one of the subgroup Furthermore, it was reported that LcIDH1 is closely related to BsIDH and LpIDH2, and LcIDH2 is related to IDH from *Clostridia*, *B. cereus*, and *B. halodurans*, *Mycoplasma hyopneumoniae (mioJ1)* and more distantly related to LpIDH1 (*27*). Therefore, a multiple sequence alignment of LpIDH1 to

LpIDH4, and LcIDH1, and LcIDH2 was performed and the aligned sequences were compared to the structure of BsIDH as described in section **2.6,** to understand the sequence and activity differences between the IDH-related enzymes. A multiple sequence alignment result of IDH-related enzymes from *L. plantarum* WCFS1, *and L. casei* BL23 with BsIDH is shown in **Figure 4.19.**

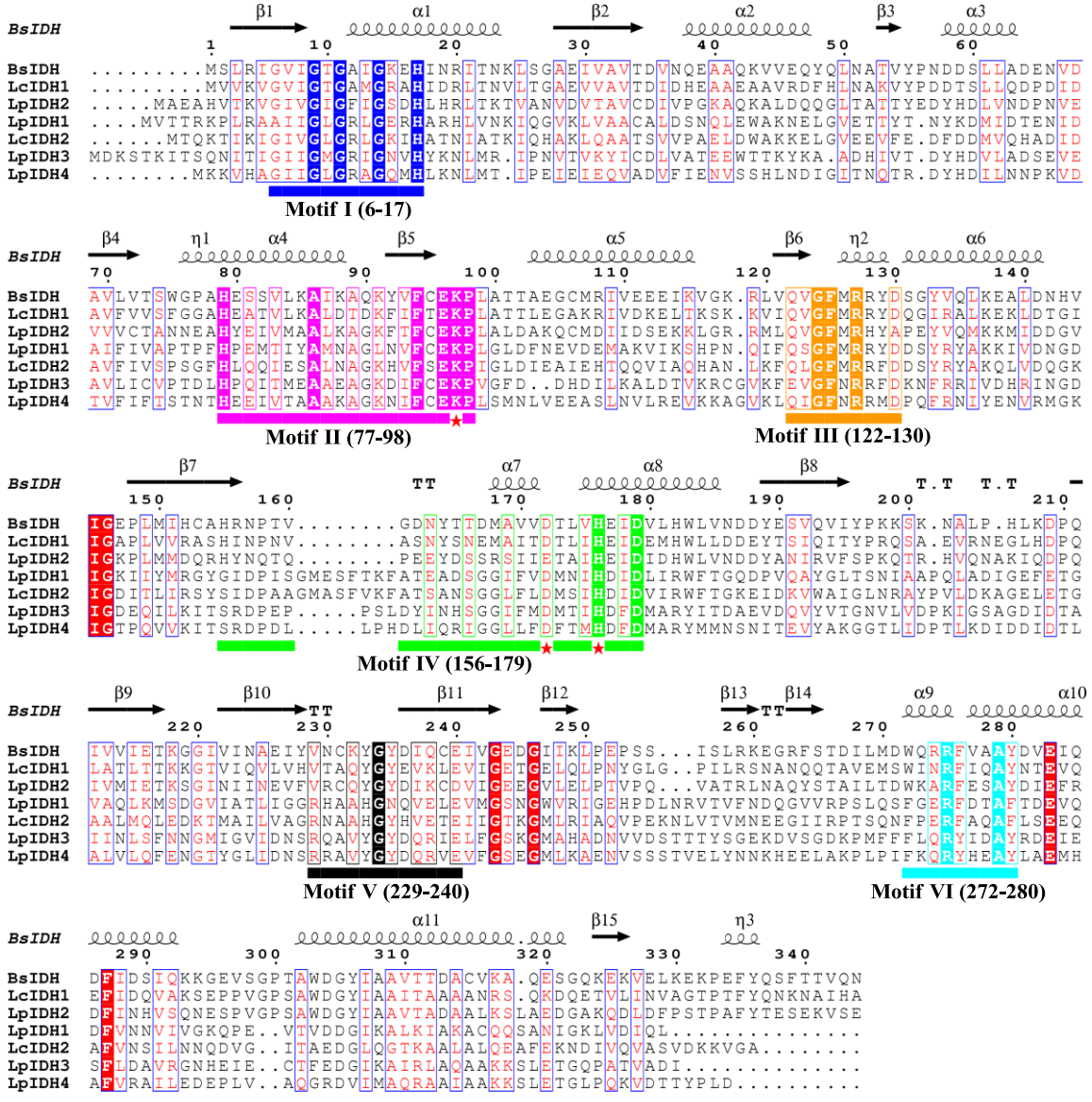

Figure 4.19: Multiple sequence alignment of IDH-related enzymes from *L. plantarum* WCFS1 *and L. casei* BL23 with BsIDH. The consensus sequence motifs are highlighted in different colors, (I - blue; II – pink; III – orange; IV – green; V – black and VI – cyan).The active site residues K97, D172 and H178 are indicated with star in red. Strictly identical residues are highlighted in red background (for example X), similar residues are shown as red letters in blue frame. The secondary structural elements are assigned based in the structure of BsIDH (PDB code: 3NT4).

From **Figure 4.19,** the major difference between the aligned sequences can be observed in sequence motif IV. Three alignment patterns can be observed among the aligned sequences. BsIDH, LpIDH2 and LcIDH1 shows a gap of 8 residues compared to LpIDH1 and LcIDH2. LpIDH3 and LpIDH4 are different from the above protein sequences. The main differences in the six sequence motifs are considered for each subgroup to understand the sequence and activity differences. The structure of BsIDH holo enzyme showing six consensus sequence motifs is shown in **Figure 4.20** and the amino acid residues for all the proteins in each motif are shown in **Figure 4.21.**

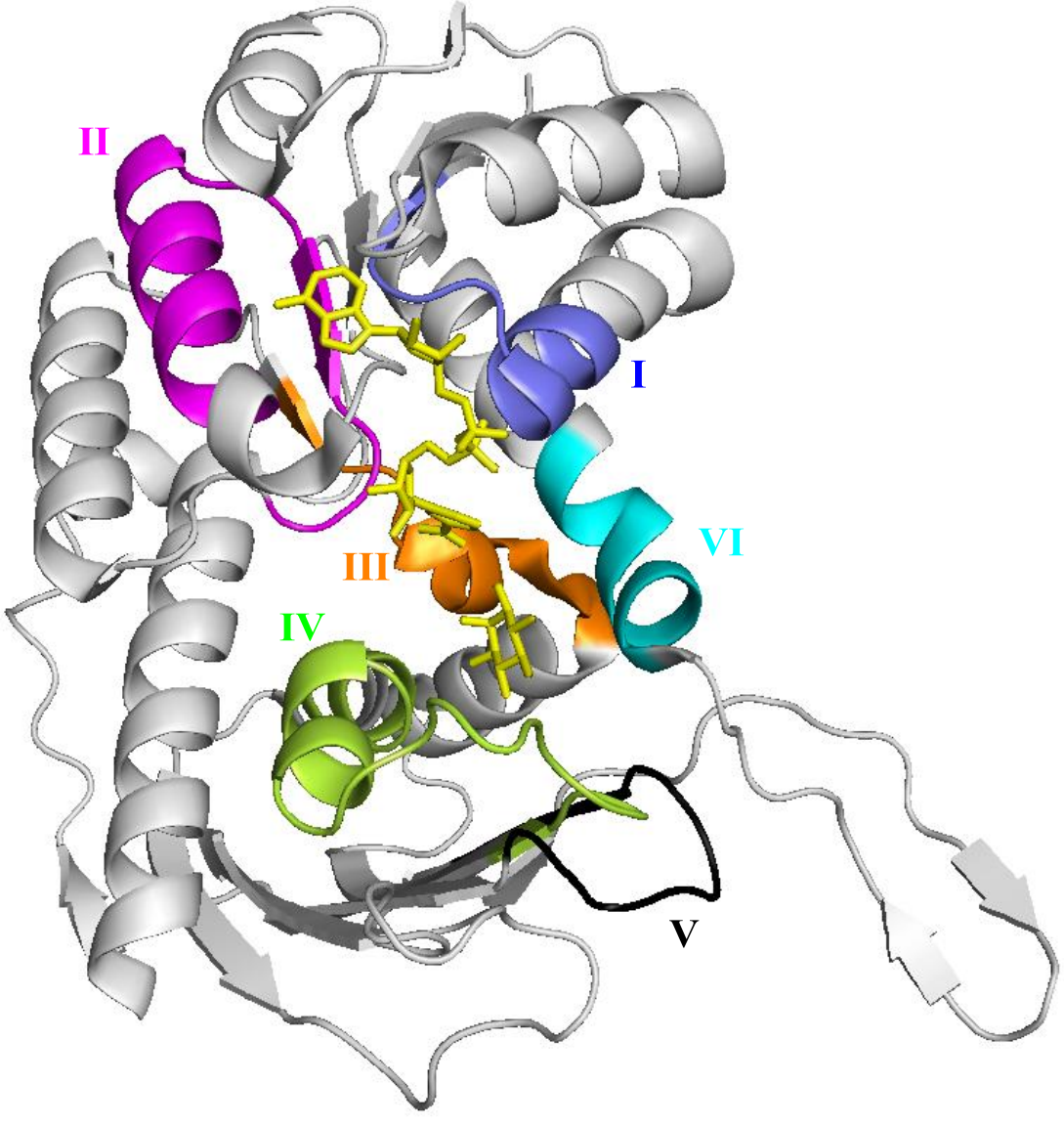

Figure 4.20: Structure in BsIDH (PDB code: 3NT4) showing the proposed consensus sequence motifs. The sequence motifs are numbered and the bound NAD^+ and *myo*-inositol are indicated in yellow.

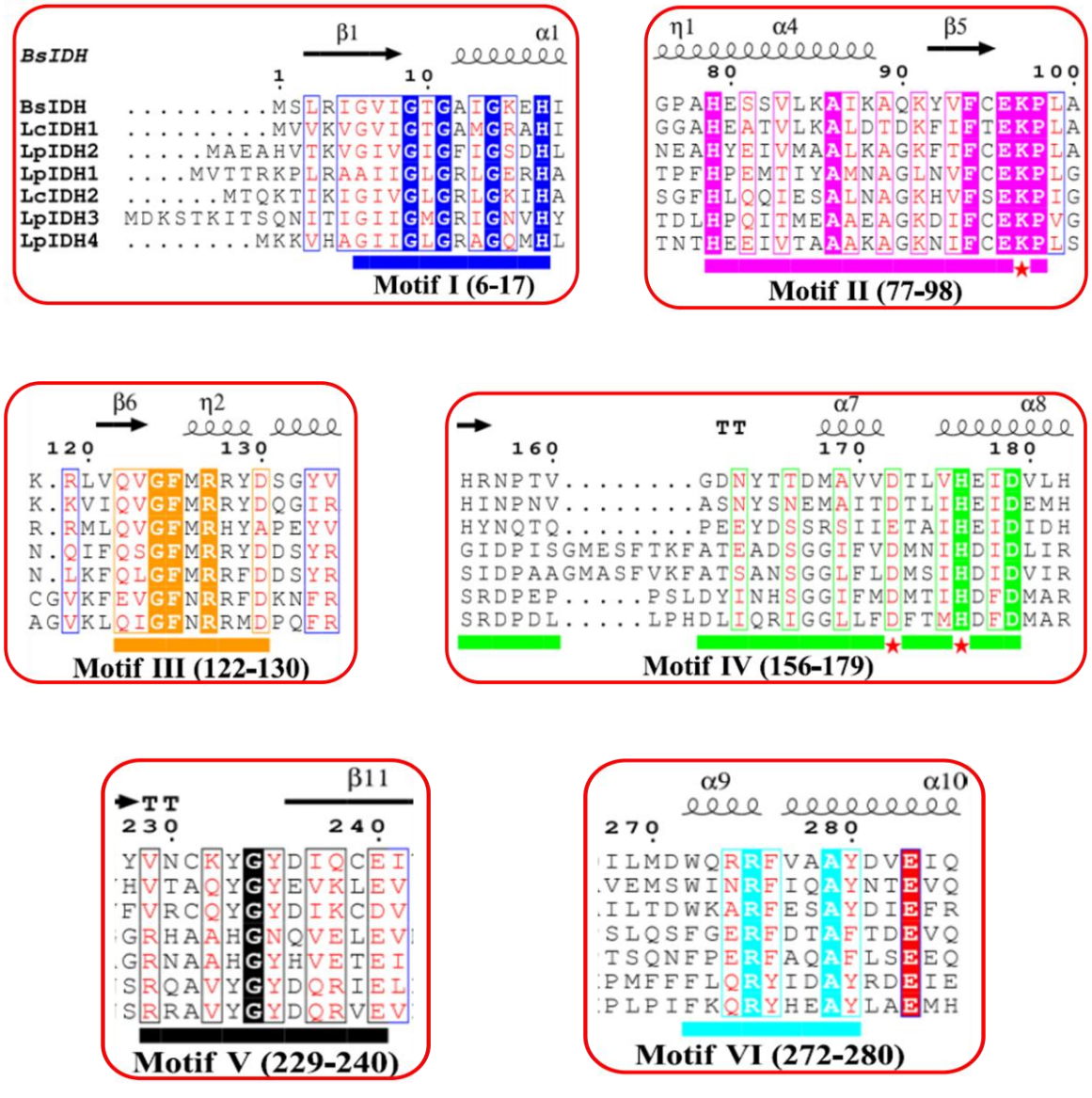

Figure 4.21: The proposed sequence motifs showing the amino acid residues for IDH-related enzymes. The active site residues are indicated with red star.

IDH subgroup I: It consists of BsIDH and LpIDH2 (*63*). LpIDH2 demonstrated 43% and 39% sequence identity with BsIDH and LcIDH1 respectively. In motif IV, the catalytic residue at position 172 is glutamic acid instead of aspartic acid, but other residues, K97 and H176 and most of the amino acid residues important for coenzyme binding and the substrate binding are highly conserved in all six consensus sequence motifs suggesting that LpIDH2 may be a *myo*-inositol dehydrogenase enzyme for *L. plantarum* WCFS1. Unfortunately, it could not express in its soluble form..

LcIDH1 demonstrated 47% sequence identity with BsIDH. In motif I, **(See Figure 4.21)** all the glycine residues are conserved, it was reported that the amide group of the protein chain forms hydrogen bonds with the diphosphate part of coenzyme (*96, 97*). In motif II of BsIDH the amino acid sequence CEKP (residues 95-98) is important for the binding of ribose part of NAD/H (*98*). LcIDH1 contains threonine in place of cysteine at residue 95 and K97, one of the proposed catalytic residues for BsIDH is also conserved in LcIDH1. Motif III is strictly conserved. The catalytic residues D172, H176 and most of the adjacent residues are conserved in motif IV. Further Y233, G243 and Y235 of motif V and W272 and most other residues of motif VI are also conserved in both BsIDH and LcIDH1. It was proposed that the side chain of Y235 or W272 make a stacking hydrophobic interaction with the substituent of 4-*O*-substituted-*myo*-inositol derivatives (*60*). Kinetic results have demonstrated that it is the real *myo*-inositol dehydrogenase enzyme for *L. casei* BL23. Furthermore, dehydrogenase activity with other substrates such as D-*chiro*-inositol, D-glucose, D-xylose, and 4-*O*-benzyl-*myo*-inositol suggested that it also possesses a broad substrate spectrum similar to BsIDH. Although, residues that are important for coenzyme and substrate binding are conserved, there may be small differences in the overall structure of LcIDH1 that resulted in the less activity compared to BsIDH.

IDH subgroup II: LpIDH1 from *L. plantarum* WCFS1 was assigned to this group (*63*). The amino acid resides in sequence motifs I and II that are important for coenzyme binding and the catalytic residues K97, D172 and H178 are conserved, but the amino acid sequence in motif IV is different in which an extra 8 residues (GMESFTKF) form an α-helix 7 in LpIDH1. This α-helix 7 close the active site making it less solvent exposed and might prevent the substrate access into the active site **Figure 4.22 (right).**

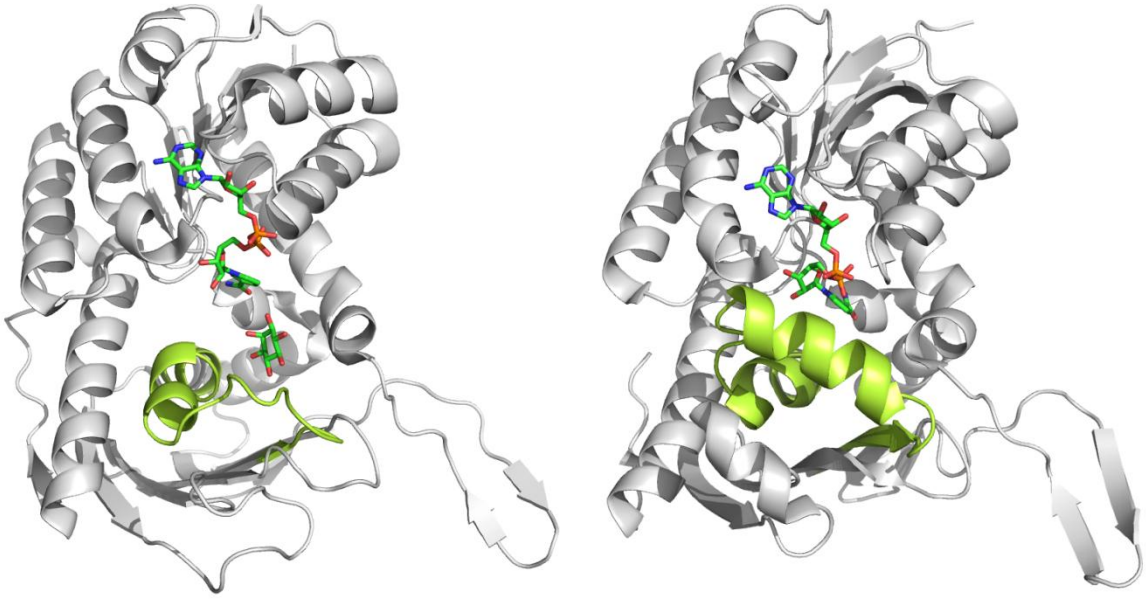

Figure 4.22: Comparison of the structures of BsIDH (PDB code: 3NT4) and LpIDH1 (PDB code: 3CEA) on right. BsIDH is on left and LpIDH1 is on right and the consensus sequence motif IV is highlighted in green.

From the **Figure 4.22**, it can be observed that the orientation of NAD^+ is different when compared to BsIDH. Furthermore, it is reported that the binding pocket of LpIDH1 is different from that of BsIDH and the spatial orientation of the active site residues would generate different interactions with substrates (*63*). In motif V the YGY (residues 233-235) of BsIDH is aligned with HGN of LpIDH1 and also W272 of BsIDH is aligned with phenylalanine in motif VI **(See Figure 4.21).** Furthermore, by comparing the structures of BsIDH and LpIDH1, it can be concluded that the active site of BsIDH looks wide and much solvent exposed, while the active site of LpIDH1 is closed and less accessible to the substrates.

LpIDH1 showed 46% sequence identity with LcIDH2, which demonstrated to be a *scyllo*-inositol dehydrogenase in this research. Based on the sequences identity result and the previous studies on LpIDH1 showing the activity with *scyllo*-inosose, it was assumed that *scyllo*-inositol which is structurally related to *scyllo*-inosose could also be a possible substrate, but the experiments have demonstrated that LpIDH1 cannot oxidize any of the structurally related compounds except *scyllo*-inosose. The above mentioned structural features might be a possible reason for its loss of dehydrogenase activity.

Based on the sequence alignment results it can be assumed that LcIDH2 may belong to IDH subgroup II. However, the kinetic results demonstrated that it is entirely different from LpIDH1 and other IDH enzymes. It also has an extra 8 amino acid residues before the active site in motif IV, which is similar to LpIDH1. In motif V residue Y235 is conserved, but in motif VI it has phenylalanine aligned with W272 of BsIDH. On the basis of these differences it can be assumed that LcIDH2 cannot accommodate 4-*O*-substituted inositol derivatives into its active site. In this research it was observed that LcIDH1 is inactive with 4-*O*-benzyl-*myo*-inositol. This supports the above assumption. Further, dehydrogenase activity with *scyllo*-inositol and L-glucose suggests that LcIDH1 may have different structural features compared to BsIDH and LcIDH1.

Recently, two *scyllo*-inositol dehydrogenases (the products of *iolX* and *iolW*) were identified from *B. subtilis (29)* and also a putative gene *smc01163* was found to be essential for the growth of *Sinorhizobium meliloti* on *scyllo*-inositol (*99*). Therefore, the sequence of LcIDH2 was compared to protein sequences of *iolX, iolW* and *smc01163,* as shown in **Figure 4.23.** LcIDH2 demonstrated 29%, 15% and 17% sequence identity with the protein sequences of *iolX, iolW* and *smc01163* respectively. The main differences in the sequence can be seen in α-helix1, between α-helix 7 and α-helix 8, and between α-helix 9 and β-strand 9. In spite of having differences, all these enzymes except LpIDH1, are demonstrated to be *scyllo*-inositol dehydrogenases.

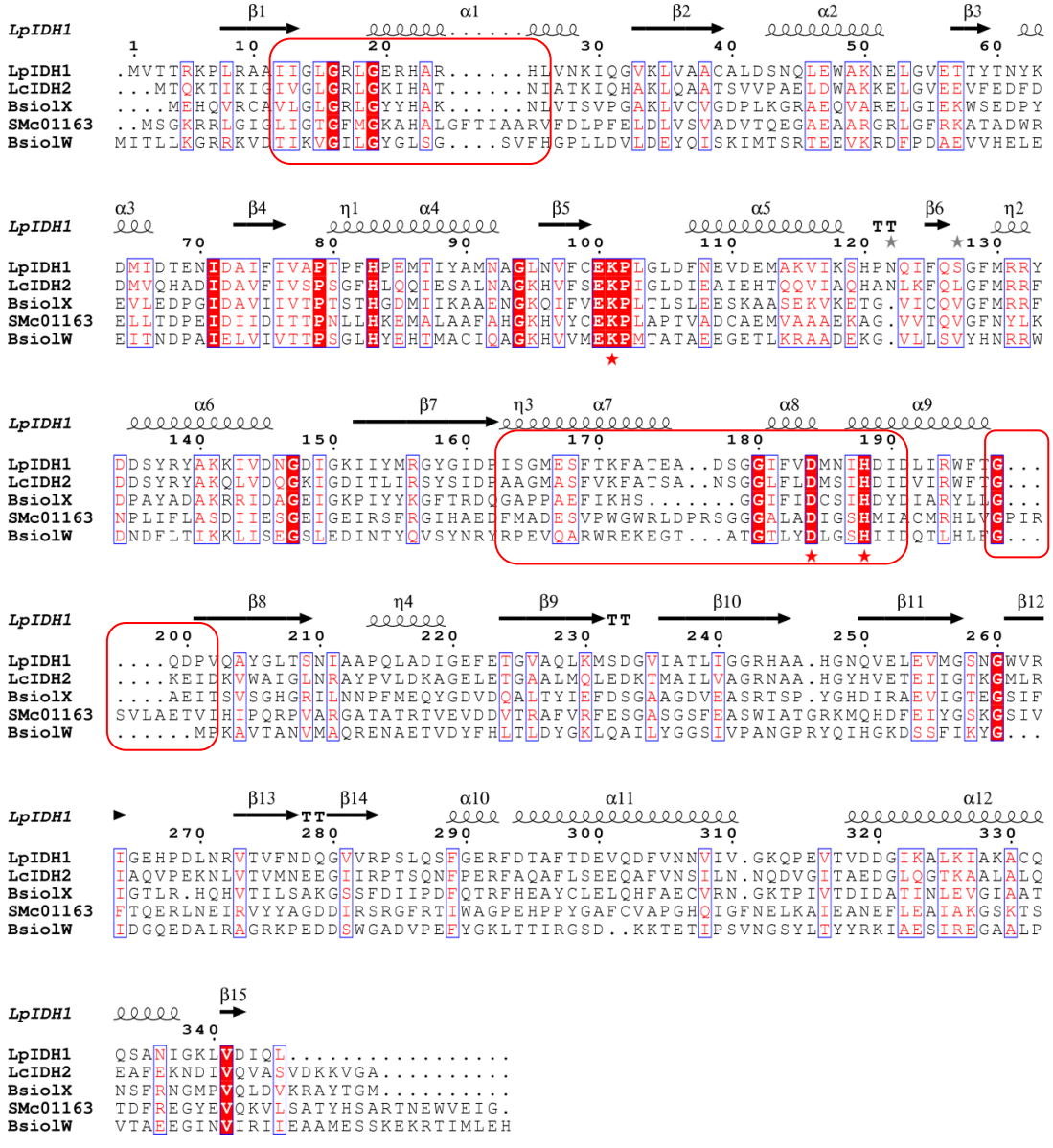

Figure 4.23: Multiple sequence alignment of LcIDH2 with other *scyllo*-inositol dehydrogenases and LpIDH1. *BsiolX* and *BsiolW* are from *B. subtilis*; *SMc01163* from *S. meliloti* and LpIDH1 from *L. plantarum* WCFS1. The proposed active site residues are indicated with star in red. Strictly identical residues are highlighted in red background (for example X), similar residues are shown as red letters in blue frame. The secondary structural elements are assigned based in the structure of LpIDH1 (PDB code: 3CEA).The major differences between these protein sequences are highlighted in red outline.

IDH subgroup III: LpIDH3 and IDH-related enzymes from *C. glutamicum* (CgIDH), *Thermotoga maritima* (TmIDH), IDHA from *Rhizobium* and *Brucella species* were included in this group (*63*). LpIDH3 demonstrated 35% and 44% sequence identity with CgIDH and TmIDH respectively and only 17% of sequence identity with BsIDH, but most of the residues in motifs I, II and III and the identified catalytic residues (K97, D172 and H176) are conserved. However, it was proposed that sequence motif IV has a

proline-rich loop before α-helix 7 (PP-II helix), a pattern associated with formation of a flexible left-handed helix that is often exposed to outer surfaces of proteins (*66, 67*). This flexibility suggests that PP-II helix may cause the α-helix 7 to change its position, thus altering the structure upon coenzyme or substrate binding (*63*), which is different from BsIDH. This may be a possible reason for the loss of activity of LpIDH3. CgIDH and TmIDH have same structural features, and as there is no structure available for LpIDH3, the structure of CgIDH was shown along with BsIDH in **Figure 4.24.**

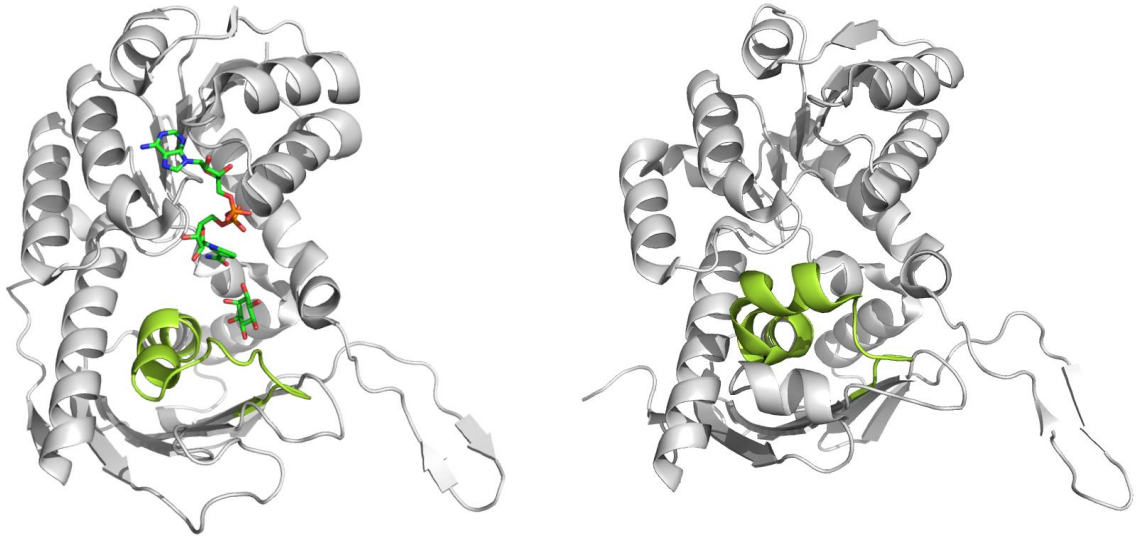

Figure 4.24: Comparison of the structures of BsIDH (PDB code: 3NT4) and CgIDH (PDB code: 3EUW). BsIDH is on left and CgIDH is on right and the sequence motif IV is highlighted in green.

IDH subgroup IV: LpIDH4 was included in this group (*63*). It demonstrated low sequence identity of 19% with BsIDH, but it exhibited 42% identity with LpIDH3. Most of the residues in all the sequence motifs except motif IV are similar to group III members. In motif IV the amino acid residues adjacent to the conserved active site residues, D172 and H176 are entirely different, which may cause different interactions with either the nicotinamide ring of NAD^+ or the substrate, or may prevent the substrate binding. Also it can be assumed that LpIDH4 may have a structure similar to that of group III members.

5. SUMMARY OF RESEARCH AND FUTURE STUDIES

- The genes encoding IDH-related enzymes from *L. plantarum* WCFS1 (*Lp_iolG1-Lp_iolG4*) and *L.casei* BL23 (*Lc_iolG1 & Lc_iolG2*) were successfully cloned into *pQE-80L* vector.
- All the clones, except *pQE-80L-Lp_iolG2*, have expressed the proteins in their soluble form. Expression and purification of LpIDH2 was unsuccessful as it resulted in the formation of insoluble inclusion bodies. However, the inclusion bodies were solubilized using unfolding and refolding method and purified by nickel affinity column chromatography. The other proteins (LpIDH1, LpIDH3, LpIDH4, LcIDH1 and LcIDH2) were purified by using a nickel affinity column chromatography.
- IDH-related enzymes form *L. plantarum* WCFS1 did not exhibited any dehydrogenase activity, but LcIDH1 and LcIDH2 from *L. casei* BL23 showed activity with *myo*-inositol and other structurally related compounds. Similar to BsIDH, LcIDH1 and LcIDH2 are exclusively NAD^+-dependent inositol dehydrogenases. The activity of LcIDH1 is similar to that of BsIDH, while LcIDH2 activity is different from both LcIDH1 and BsIDH. All three enzymes could not recognize compounds such as D-galactose, D-mannose, D-sorbitol, D-mannitol and *scyllo*-inosose as substrates. LpIDH2 purified by unfolding and refolding method also inactive towards the compounds tested. However, BsIDH purified by this method showed a reduced activity.
- pH-rate profiles of the active IDH-related enzymes were established and found that LpIDH1 and LcIDH2 showed maximum activity in CHES at pH 9.3 and 9.5 respectively, while BsIDH showed maximum activity in glycine-NaOH at pH 10 in contrast to previously reported results.
- Kinetic experiments have demonstrated that LcIDH1 is a *myo*-inositol dehydrogenase and LcIDH2 is a *scyllo*-inositol dehydrogenase from *L. casei*

BL23. It is likely that LcIDH1 and LcIDH2 follows a sequentially ordered Bi-Bi mechanism similar to BsIDH. However, further experiments such as dead end inhibition and product inhibition have to be performed to understand the mechanism of catalysis for these enzymes. LcIDH1 and LcIDH2 catalyzed the oxidation of *myo*-inositol with much less efficiency compared to BsIDH. Further, LcIDH2 catalyzed the oxidation of *scyllo*-inositol more efficiently than *myo*-inositol, while LcIDH1 and BsIDH did not show any activity at all. Further, experiments have to be performed to identify the product of the reactions catalyzed by LcIDH1 and LcIDH2.

- By exploring the alternative substrates, it was found that LcIDH1 has a broad substrate spectrum and stereoselectivity similar to BsIDH, while LcIDH2 behaved differently compared to LcIDH1 and BsIDH.
- Kinetic isotopic effect studies for LcIDH1 with 2-^{2}H-*myo*-inositol and synthetic *myo*-inositol have demonstrated that the release of the product is primarily the rate-limiting step and the chemical step may be partially rate-limiting. Further experiments have to be performed to clearly understand whether the chemical step contribute to the rate-limiting or not.
- From the multiple sequence alignment results, it can be concluded that the IDH-related enzymes from *L. plantarum* WCFS1 are not active with *myo*-inositol and other related compounds because of the differences in their protein sequences. Furthermore, these enzymes showed low sequence identity with BsIDH. However, LpIDH1 was found to be active with *scyllo*-inosose as previously demonstrated in our lab. Further, it showed 46% sequence identity with LcIDH2 but failed to oxidize *scyllo*-inositol.

  In this research, it was found that *L. casei* BL23 possesses two functionally different inositol dehydrogenases. LcIDH1 is a *myo*-inositol dehydrogenase, while LcIDH2 is a *scyllo*-inositol dehydrogenase. Although, LcIDH1exhibited 47% sequence identity with BsIDH and the catalytic residues are highly conserved, the kinetic results demonstrated that LcIDH1 is a less efficient enzyme. This enzyme can be assigned to IDH subgroup I.

  According to sequence alignment results, LcIDH2 can be assigned to IDH subgroup II. But functionally LcIDH2 can oxidize *scyllo*-inositol more efficiently

than *myo*-inositol and other compounds, which is different from LcIDH1 and BsIDH. However, the substrate spectrum is different for LcIDH2 and it is not clear that which hydroxyl group of *scyllo*-inositol, *myo*-inositol and other substrates is oxidized. Hence, future studies for LcIDH2 include identification of the reaction end products for the oxidation of *myo*-inositol and *scyllo*-inositol, crystallization experiments to identify the structural features. Furthermore site-directed mutagenesis experiments can be performed for the conformation of active site residues of both LcIDH1 and LcIDH2.

6. REFERENCES

1. Kersting, M. C., Boyette, M., Massey, J. H., and Ryals, P. E. (2003) Identification of the inositol isomers present in Tetrahymena, *J. Eukaryot. Microbiol. 50*, 164-168.

2. Fisher, S. K., Novak, J. E., and Agranoff, B. W. (2002) Inositol and higher inositol phosphates in neural tissues: homeostasis, metabolism and functional significance, *J. Neurochem. 82*, 736-754.

3. Michell, R. H. (2008) Inositol derivatives: evolution and functions, *Nat. Rev. Mol. Cell Biol. 9*, 151-161.

4. Berridge, M. J., and Irvine, R. F. (1984) Inositol trisphosphate, a Novel 2nd Messenger in Cellular Signal Transduction, *Nature 312*, 315-321.

5. Biden, T. J., Prentki, M., Irvine, R. F., Berridge, M. J., and Wollheim, C. B. (1984) Inositol 1,4,5-trisphosphate mobilizes intracellular Ca^{2+} from permeabilized insulin-secreting cells, *Biochem. J. 223*, 467-473.

6. Burgess, G. M., Irvine, R. F., Berridge, M. J., McKinney, J. S., and Putney, J. W. (1984) Actions of inositol phosphates on Ca^{2+} pools in guinea-pig hepatocytes, *Biochem. J. 224*, 741-746.

7. Hokin, L. E. (1985) Receptors and Phosphoinositide-Generated Second Messengers, *Annu. Rev. Biochem. 54*, 205-235.

8. Munnik, T., Irvine, R. F., and Musgrave, A. (1998) Phospholipid Signalling in Plants, *BBA-Lipids Lipid Met. 1389*, 222-272.

9. Stevenson, J. M., Pepera, I. Y., Heilmann, I., Persson, S., and Boss, W. F. (2000) Inositol signaling and plant growth, *Trends Plant Sci. 5*, 252-258.

10. Shen, X. T., Xiao, H., Ranallo, R., Wu, W. H., and Wu, C. (2003) Modulation of ATP-dependent chromatin-remodeling complexes by inositol polyphosphates, *Science 299*, 112-114.

11. Larner, J. (2002) D-*chiro*-inositol: Its functional role in insulin action and its deficit in insulin resistance, *Int. J. Exp. Diabetes Res. 3*, 47-60.

12. Iuorno, M. J., Jakubowicz, D. J., Baillargeon, J. P., Dillon, P., Gunn, R. D., Allan, G., and Nestler, J. E. (2002) Effects of D-*chiro*-inositol in lean women with the polycystic ovary syndrome, *Endocr. Pract. 8*, 417-423.

13. Loewus, F. A., And Loewus, M. W. (1983) *myo*-inositol: Its Biosynthesis And Metabolism, *Annu. Rev. Plant Phys. 34*, 137-161.

14. Loewus, F. A. (1983) Phytate metabolism with special reference to its *myo*-inositol component, *Recent adv. Phytochem. 17*, 173-192.

15. Graf, E., Empson, K. L., and Eaton, J. W. (1987) Phytic Acid: A Natural Antioxidant, *J. Biol. Chem. 262*, 11647-11650.

16. Graf, E., and Eaton, J. W. (1993) Suppression of Colonic-Cancer by Dietary Phytic Acid, *Nutr. Cancer 19*, 11-19.

17. Molina, Y., Ramos, S. E., Douglass, T., and Klig, L. S. (1999) Inositol synthesis and catabolism in *Cryptococcus neoformans*, *Yeast. 15*, 1657-1667.

18. Berman, T., and Magasani, B. (1966) The Pathway of *myo*-inositol degradation in *Aerobacter aerogenes*: Dehydrogenation and Dehydration, *J. Biol.Chem. 241*, 800-806.

19. Anderson, W. A., and Magasani.B. (1971) The Pathway of *myo*-inositol degradation in *Aerobacter aerogenes*: Conversion of 2-*deoxy*-5-keto-D-gluconic acid to glycolytic intermediates, *J. Biol. Chem. 246*, 5662-5675.

20. Vidal Leiria, M., and Van Uden, N. (1973) Inositol Dehydrogenase from Yeast *Cryptococcus melibiosum*, *Biochim. Biophys. Acta Enzymol. 293*, 295-303.

21. Poole, P. S., Blyth, A., Reid, C. J., and Walters, K. (1994) *myo*-inositol Catabolism and Catabolite Regulation in *Rhizobium Leguminosarum Bv. Viciae*, *Microbiology 140*, 2787-2795.

22. Yoshida, K. I., Aoyama, D., Ishio, I., Shibayama, T., and Fujita, Y. (1997) Organization and transcription of the *myo*-inositol operon, *iol*, of *Bacillus subtilis*, *J. Bacteriol. 179*, 4591-4598.

23. Galbraith, M. P., Feng, S. F., Borneman, J., Triplett, E. W., de Bruijn, F. J., and Rossbach, S. (1998) A functional *myo*-inositol catabolism pathway is essential for rhizopine utilization by *Sinorhizobium meliloti*, *Microbiology 144*, 2915-2924.

24. McClelland, M., Sanderson, K. E., Spieth, J., Clifton, S. W., Latreille, P., Courtney, L., Porwollik, S., Ali, J., Dante, M., Du, F. Y., Hou, S. F., Layman, D., Leonard, S., Nguyen, C., Scott, K., Holmes, A., Grewal, N., Mulvaney, E., Ryan, E., Sun, H., Florea, L., Miller, W., Stoneking, T., Nhan, M., Waterston, R., and Wilson, R. K. (2001) Complete genome sequence of *Salmonella enterica* serovar Typhimurium LT2, *Nature. 413*, 852-856.

25. Jiang, G. Q., Krishnan, A. H., Kim, Y. W., Wacek, T. J., and Krishnan, H. B. (2001) A functional *myo*-inositol dehydrogenase gene is required for efficient nitrogen

fixation and competitiveness of *Sinorhizobium fredii* USDA191 to nodulate Soybean (*Glycine max [L]*. Merr.), *J. Bacteriol. 183*, 2595-2604.

26. Krings, E., Krumbach, K., Bathe, B., Kelle, R., Wendisch, V. F., Sahm, H., and Eggeling, L. (2006) Characterization of *myo*-inositol utilization by *Corynebacterium glutamicum*: The stimulon, identification of transporters, and influence on L-lysine formation, *J. Bacteriol. 188*, 8054-8061.

27. Yebra, M. J., Zuniga, M., Beaufils, S., Perez-Martinez, G., Deutscher, J., and Monedero, V. (2007) Identification of a gene cluster enabling *Lactobacillus casei* BL23 to utilize *myo*-inositol, *Appl. Environ. Microbiol. 73*, 3850-3858.

28. Yoshida, K. I., Yamaguchi, M., Morinaga, T., Ikeuchi, M., Kinehara, M., and Ashida, H. (2006) Genetic modification of *Bacillus subtilis* for production of D-*chiro*-inositol, an investigational drug candidate for treatment of type 2 diabetes and polycystic ovary syndrome, *Appl. Environ. Microbiol. 72*, 1310-1315.

29. Morinaga, T., Ashida, H., and Yoshida, K.I. (2010) Identification of two *scyllo*-inositol dehydrogenases in *Bacillus subtilis*, *Microbiology. 156*, 1538-1546.

30. Yoshida, K. I., Yamaguchi, M., Morinaga, T., Kinehara, M., Ikeuchi, M., Ashida, H., and Fujita, Y. (2008) *myo*-inositol catabolism in *Bacillus subtilis*, *J. Biol. Chem. 283*, 10415-10424.

31. Yoshida, K. I., Yamaguchi, M., Ikeda, H., Omae, K., Tsurusaki, K. I., and Fujita, Y. (2004) The fifth gene of the *iol* operon of *Bacillus subtilis*, *iolE*, encodes 2-keto-*myo*-inositol dehydratase, *Microbiology. 150*, 571-580.

32. Stines-Chaumeil, C., Talfournier, F., and Branlant, G. (2006) Mechanistic characterization of the MSDH (methylmalonate semialdehyde dehydrogenase) from *Bacillus subtilis*, *Biochem. J. 395*, 107-115.

33. Nakano, M., Morita, T., Yamamoto, T., Sano, H., Ashiuchi, M., Masui, R., Kuramitsu, S., and Yagi, T. (1999) Purification, molecular cloning, and catalytic activity of *Schizosaccharomyces pombe* pyridoxal reductase: A possible additional family in the aldo-keto reductase superfamily, *J. Biol. Chem. 274*, 23185-23190.

34. Salminen, S., von Wright, A. and Ouvehand, A. C., (2004) *Lactic acid Bacteria: Microbiological and Functional Aspects*, 3rd edition., Marcel Dekker, Inc., New York.

35. Collins, M. D., Rodrigues, U., Ash, C., Aguirre, M., Farrow, J. A. E., Martinezmurcia, A., Phillips, B. A., Williams, A. M., and Wallbanks, S. (1991) Phylogenetic analysis of the genus *Lactobacillus* and related lactic acid bacteria as determined by reverse-transcriptase sequencing of 16s rRNA, FEMS *Microbiol. Lett. 77*, 5-12.

36. Schleifer, K. H., and Ludwig, W. (1996) Phylogeny of the genus *Lactobacillus* and related genera, *Syst. Appl. Microbiol. 18*, 461-467.

37. Cleveland, J., Montville, T. J., Nes, I. F., and Chikindas, M. L. (2001) Bacteriocins: safe, natural antimicrobials for food preservation, *Int. J. Food Microbiol. 71*, 1-20.

38. Nettles, C. G., and Barefoot, S. F. (1993) Biochemical and genetic characteristics of Bacteriocins of food-associated lactic acid bacteria, *J. Food Protect. 56*, 338-356.

39. Guarner, F., and Schaafsma, G. J. (1998) Probiotics, *Int. J. Food Microbiol. 39*, 237-238.

40. Mattila-Sandholm, T., Myllarinen, P., Crittenden, R., Mogensen, G., Fonden, R., and Saarela, M. (2002) Technological challenges for future probiotic foods, *Int. Dairy J. 12*, 173-182.

41. Millette, M., Luquet, F.-M., Ruiz, M. T., and Lacroix, M. (2008) Characterization of probiotic properties of *Lactobacillus* strains, *Dairy Sci. Technol. 88*, 695-705.

42. Poolzobel, B. L., Neudecker, C., Domizlaff, I., Ji, S., Schillinger, U., Rumney, C., Moretti, M., Vilarini, I., ScassellatiSforzolini, R., and Rowland, I. (1996) *Lactobacillus* and *Bifidobacterium* mediated antigenotoxicity in the colon of rats, *Nutr.Cancer 26*, 365-380.

43. Takano, T., Arai, K., Murota, I., Hayakawa, K., Mizutani, T., and Mitsuoka, T. (1985) Effects of feeding sour milk on longevity and tumorigenesis in mice and rats, *Bifidobacteria and Microflora 4*, 31-37.

44. Gilliland, S. E., Nelson, C. R., and Maxwell, C. (1985) Assimilation of cholesterol by *Lactobacillus acidophilus*, *Appl. Environ. Microbiol. 49*, 377-381.

45. Nielsen, J. W., and Gilliland, S. E. (1985) Variations in cholesterol assimilation by individual strains of *Lactobacillus acidophilus* and *Lactobacillus casei* from human intestines, *J. Dairy Sci. 68*, 83.

46. Beena, A., and Prasad, V. (1997) Effect of yogurt and bifidus yogurt fortified with skim milk powder, condensed whey and lactose-hydrolysed condensed whey on serum cholesterol and triacylglycerol levels in rats, *J. Dairy Res. 64*, 453-457.

47. Nakajima, H., Suzuki, Y., Kaizu, H., and Hirota, T. (1992) Cholesterol lowering activity of ropy fermented milk, *J. Food Sci. 57*, 1327-1329.

48. Mohan, B., Kadirvel, R., Natarajan, A., and Bhaskaran, M. (1996) Effect of probiotic supplementation on growth, nitrogen utilisation and serum cholesterol in broilers, *British Poultry Sci. 37*, 395-401.

49. Hata, Y., Yamamoto, M., Ohni, M., Nakajima, K., Nakamura, Y., and Takano, T. (1996) Placebo-controlled study of the effect of sour milk on blood pressure in hypertensive subjects, *Am. J. Clin. Nutr. 64*, 767-771.

50. Seppo, L., Jauhiainen, T., Poussa, T., and Korpela, R. (2003) A fermented milk high in bioactive peptides has a blood pressure-lowering effect in hypertensive subjects, *Am. J. Clin. Nutr. 77*, 326-330.

51. Yamamoto, N., and Takano, T. (1999) Antihypertensive peptides derived from milk proteins, *Nahrung 43*, 159-164.

52. Kleerebezem, M., Boekhorst, J., van Kranenburg, R., Molenaar, D., Kuipers, O. P., Leer, R., Tarchini, R., Peters, S. A., Sandbrink, H. M., Fiers, M., Stiekema, W., Lankhorst, R. M. K., Bron, P. A., Hoffer, S. M., Groot, M. N. N., Kerkhoven, R., de Vries, M., Ursing, B., de Vos, W. M., and Siezen, R. J. (2003) Complete genome sequence of *Lactobacillus plantarum* WCFS1, *P. Natl. Acad. Sci. USA. 100*, 1990-1995.

53. Pouwels, P. H., Leer, R. J., Shaw, M., den Bak-Glashouwer, M. J. H., Tielen, F. D., Smit, E., Martinez, B., Jore, J., and Conway, P. L. (1998) Lactic acid bacteria as antigen delivery vehicles for oral immunization purposes, *Int. J. Food Microbiol. 41*, 155-167.

54. Vesa, T., Pochart, P., and Marteau, P. (2000) Pharmacokinetics of *Lactobacillus plantarum* NCIMB 8826, *Lactobacillus fermentum* KLD, and *Lactococcus lactis* MG 1363 in the human gastrointestinal tract, *Aliment. Pharm. Therap. 14*, 823-828.

55. Maze, A., Boel, G., Zuniga, M., Bourand, A., Loux, V., Jesus Yebra, M., Monedero, V., Correia, K., Jacques, N., Beaufils, S., Poncet, S., Joyet, P., Milohanic, E., Casaregola, S., Auffray, Y., Perez-Martinez, G., Gibrat, J.-F., Zagorec, M., Francke, C., Hartke, A., and Deutscher, J. (2010) Complete genome sequence of the probiotic *Lactobacillus casei* strain BL23, *J. Bacteriol. 192*, 2647-2648.

56. Ramaley, R., Fujita, Y., and Freese, E. (1979) Purification and properties of *Bacillus subtilis* Inositol Dehydrogenase, *J. Biol.Chem. 254*, 7684-7690.

57. Daniellou, R., Phenix, C. P., Tam, P. H., Laliberte, M. C., and Palmer, D. R. J. (2005) Stereoselective oxidation of protected inositol derivatives catalyzed by inositol dehydrogenase from *Bacillus subtilis*, *Org. Biomol. Chem. 3*, 401-403.

58. Daniellou, R., Zheng, H. Y., and Palmer, D. R. J. (2006) Kinetics of the reaction catalyzed by inositol dehydrogenase from *Bacillus subtilis* and inhibition by fluorinated substrate analogs, *Can. J. Chem. 84*, 522-527.

59. Daniellou, R., and Palmer, D. R. J. (2006) Appel-Lee synthesis of glycosyl inositols, substrates for inositol dehydrogenase from *Bacillus subtilis*, *Carbohydr. Res. 341*, 2145-2150.

60. Daniellou, R., Zheng, H., Langill, D. M., Sanders, D. A. R., and Palmer, D. R. J. (2007) Probing the promiscuous active site of *myo*-inositol dehydrogenase using synthetic substrates, homology modeling, and active site modification, *Biochemistry. 46*, 7469-7477.

61. Zheng, H. (2010) Mechanistic, Inhibitory, and Mutagenic Studies of Inositol Dehydrogenase from *Bacillus subtilis*, PhD thesis, University of Saskatchewan, Saskatoon.

62. Morinaga, T., Yamaguchi, M., Makino, Y., Nanamiya, H., Takahashi, K., Yoshikawa, H., Kawamura, F., Ashida, H., and Yoshida, K.I. (2006) Functional *myo*-inositol catabolic genes of *Bacillus subtilis* natto are involved in depletion of pinitol in natto (Fermented soybean), *Biosci. Biotechnol. Biochem. 70*, 1913-1920.

63. van Straaten, K. E., Zheng, H., Palmer, D. R. J., and Sanders, D. A. R. (2010) Structural investigation of *myo*-inositol dehydrogenase from *Bacillus subtilis*: implications for catalytic mechanism and inositol dehydrogenase subfamily classification, *Biochem. J. 432*, 237-247.

64. van Straaten, K. E., Hoffort, A., Palmer, D. R. J., and Sanders, D. A. R. (2008) Purification, crystallization and preliminary X-ray analysis of inositol dehydrogenase (IDH) from *Bacillus subtilis*, *Acta Crystallogr. Sect F. Str. Biol. Cryst. Commu. 64*, 98-101.

65. Kroeger, C., and Fuchs, T. M. (2009) Characterization of the *myo*-inositol utilization island of *Salmonella enterica* serovar Typhimurium, *J. Bacteriol. 191*, 545-554.

66. Williamson, M. P. (1994) The structure and function of Proline-rich regions in proteins, *Biochem. J. 297*, 249-260.

67. Stapley, B. J., and Creamer, T. P. (1999) A survey of left-handed polyproline II helices, *Protein Sci. 8*, 587-595.

68. Zhang, W. Y., Sun, Z. H., Yu, D. L., Airideng, C., Chen, W., Meng, H., and Zhang, H. P. (2010) Comparative analysis of *iol* clusters in *Lactobacillus casei* strains, *World J.Microbiol. Biotechnol. 26*, 1949-1955.

69. Angyal, S. J., Ranga, D., Defaye, J., and Gadelle, A. (1979) The behavior of inososes in neutral and basic aqueous solution, *Carbohydr. Res, 76*, 121-130,.

70. Copeland., R. A. (2000) *Enzymes: A Practical Introduction to Structure, Mechanism, and Data Analysis.*, 2nd Edition., J. Wiley, New York.

71. Wiberg, K. B. (1955) The Deuterium Isotope Effect, *Chem. Rev. 55*, 713-743.

72. Lars C. S. Melander, W. H. S. (1980) *Reactions of Isotopic Molecules*, Wiley Interscience publication, New York.

73. Purich, D. L. (1996) *Isotopic Effects: Determination of Enzyme Transition State Structure, Contemporary Enzyme Kinetics and Mechanism*, 2nd Edition., Academic press.

74. Hansen, C. A., Dean, A. B., Draths, K. M., and Frost, J. W. (1999) Synthesis of 1,2,3,4-tetrahydroxybenzene from D-glucose: Exploiting *myo*-inositol as a precursor to aromatic chemicals, *J. Am Chem. Soc. 121*, 3799-3800.

75. Kanehisa, M., Goto, S., Sato, Y., Furumichi, M., And Tanabe, M. (2012) KEGG For integration and interpretation of large-scale molecular data sets, *Nucleic Acids Res. 40*, D109-114

76. Thompson, J. D., Higgins, D. G., And Gibson, T. J. (1994) Clustal-W - Improving The Sensitivity Of Progressive Multiple Sequence Alignment Through Sequence Weighting, Position-Specific Gap Penalties And Weight Matrix Choice, *Nucleic Acids Res. 22*, 4673-4680.

77. Larkin, M. A., Blackshields, G., Brown, N. P., Chenna, R., Mcgettigan, P. A., Mcwilliam, H., Valentin, F., Wallace, I. M., Wilm, A., Lopez, R., Thompson, J. D., Gibson, T. J., And Higgins, D. G. (2007) Clustal W And Clustal X Version 2.0, *Bioinformatics. 23*, 2947-2948.

78. Gouet, P., Courcelle, E., Stuart, D. I., And Metoz, F. (1999) Espript: Analysis Of Multiple Sequence Alignments in Postscript, *Bioinformatics. 15*, 305-308.

79. Gouet, P., Robert, X., and Courcelle, E. (2003) Espript/Endscript: Extracting and rendering sequence and 3D information from Atomic Structures of Proteins, *Nucleic Acids Res. 31*, 3320-3323.

80. Cornish-Bowden, A. (1995) *Analysis of enzyme kinetic data*, Oxford University Press, New York.

81. Bujard, H., Gentz, R., Lanzer, M., Stüber, D. Müller, M., Ibrahimi, I. Häuptle, M.T., and Dobberstein, B. (1987) A T5 promotor based transcription-translation system for the analysis of proteins in vivo and in vitro, *Methods Enzymol. 155, 416-433*.

82. Farabaugh, P. J. (1978) Sequence of *LacI* Gene, *Nature 274*, 765-769.

83. Sutcliffe, J. G. (1979) Complete nucleotide sequence of the *Escherichia coli* plasmid pBR322., *Cold spring Harb. Symp. Quant. Biol. 43*, 77-90

84. Schwarz, E., Scherrer, G., Hobom, G., and Kössel, H. (1978) Nucleotide sequence of cro, cII and part of the O gene in phage lambda DNA., *Nature, 272(5652), 410-414*.

85. Rychlik, W., Spencer, W. J., and Rhoads, R. E. (1990) Optimization of the Annealing temperature for DNA amplification invitro, *Nucleic Acids Res. 18*, 6409-6412.

86. Fink, A. L. (1998) Protein aggregation: folding aggregates, inclusion bodies and amyloid, *Fold Des. 3(1)*, R9-R23.

87. Kopito, R. R. (2000) Aggresomes, inclusion bodies and protein aggregation, *Trends Cell Biol. 10*, 524-530.

88. Porath, J., Carlsson, J., Olsson, I., and Belfrage, G. (1975) Metal Chelate Affinity Chromatography, a new approach to protein fractionation, *Nature 258*, 598-599..

89. Sulkowski, E. (1985) Purification of proteins by IMAC, *Trends Biotechnol. 3*, 1-7.

90. Singh, S. M., and Panda, A. K. (2005) Solubilization and refolding of bacterial inclusion body proteins, *J. Biosci. Bioeng. 99*, 303-310.

91. Fonseca, I. O., Silva, R. G., Fernandes, C. L., de Souza, O. N., Basso, L. A., and Santos, D. S. (2007) Kinetic and chemical mechanisms of shikimate dehydrogenase from *Mycobacterium tuberculosis*, *Arch. Biochem. Biophys. 457*, 123-133.

92. Jacques, S. L., Ejim, L. J., and Wright, G. D. (2001) Homoserine dehydrogenase from Saccharomyces cerevisiae: kinetic mechanism and stereochemistry of hydride transfer, *Biochim. Biophys. Acta, Protein Str.Mol. Enzymol. 1544*, 42-54.

93. Grubmeyer, C., and Teng, H. (1999) Mechanism of *Salmonella typhimurium* histidinol dehydrogenase: Kinetic isotope effects and pH profiles, *Biochemstry. 38*, 7355-7362.

94. Lindstad, R. I., Hermansen, L. F., and McKinleymckee, J. S. (1992) The kinetic mechanism of sheep liver sorbitol dehydrogenase, *Eur. J. Biochem. 210*, 641-647.

95. Pourmotabbed, T., Shih, M. J., and Creighton, D. J. (1989) Bovine liver formaldehyde dehydrogenase. Kinetic and molecular properties, *J. Biol. Chem. 264*, 17384-17388.

96. Bellamacina, C. R. (1996) The nicotinamide dinucleotide binding motif: A comparison of nucleotide binding proteins, *FASEB J. 10*, 1257-1269.

97. Bottoms, C. A., Smith, P. E., and Tanner, J. J. (2002) A structurally conserved water molecule in Rossmann dinucleotide-binding domains, *Protein Sci. 11*, 2125-2137.

98. Kingston, R. L., Scopes, R. K., and Baker, E. N. (1996) The structure of glucose-fructose oxidoreductase from *Zymomonas mobilis*: An osmoprotective periplasmic enzyme containing non-dissociable NADP, *Structure 4*, 1413-1428.

99. Kohler, P. R. A., Zheng, J. Y., Schoffers, E., and Rossbach, S. (2010) Inositol Catabolism, a key Pathway in *Sinorhizobium meliloti* for Competitive Host Nodulation, *Appl. Environ. Microbiol. 76*, 7972-7980.

APPENDIX-A

Composition of LB media, Terrific Broth and MRS Broth

LB media		**Terriffic Broth**		**MRS Broth**	
Ingredients	/L	Ingredients	/L	Ingredients	/L
Tryptone	10 g	Tryptone	10 g	Peptone	10 g
Yeast extract	5 g	Yeast extract	5 g	Meat extract	8 g
NaCl	10 g	glycerol	10 g	Yeast extract	4 g
		KH_2PO_4	2.31g	D(+)-glucose	20 g
pH was adjusted to 7.0 with 5 N NaOH.		K_2HPO_4	12.54 g	K_2HPO_4	2 g
				$CH_3COONa.3H_2O$	5 g
				Triammonium citrate	2 g
				$MgSO_4.7H_2O$	0.2 g
				$MnSO_4.4H_2O$	0.05 g
				Tween 80	1 mL
All the media was sterilized by autoclaving for 15-20 min at 121^oC or 15 psi					

APPENDIX-B

DNA maps of recombinant constructs

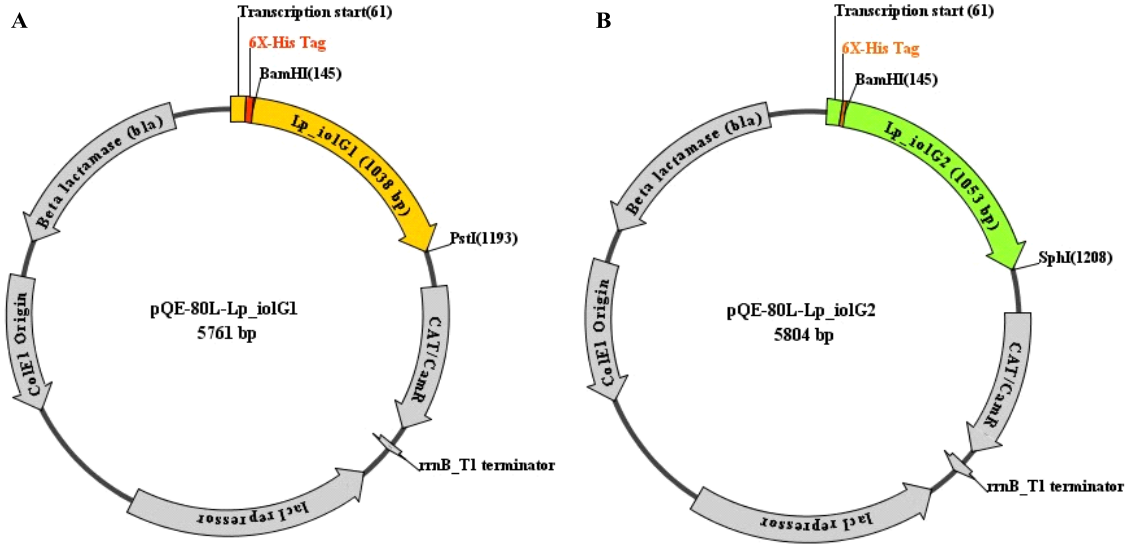

A): ***pQE-80L–Lp_iolG1.*** *Lp_iolG1* gene ligated into *BamHI* & *PstI* sites;
B): ***pQE-80L–Lp_iolG2.*** *Lp_iolG2* gene ligated into *BamHI* & *SphI* sites.

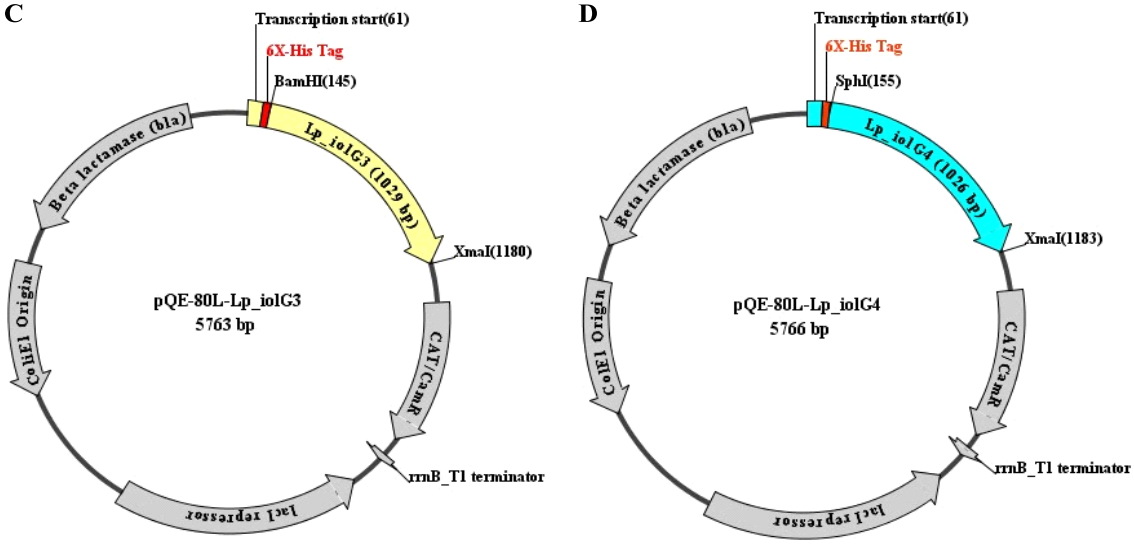

C): ***pQE-80L–Lp_iolG3.*** *Lp_iolG3* gene ligated into *BamHI* & *XmaI* sites**;**
D): ***pQE-80L–Lp_iolG4.*** *Lp_iolG4* gene ligated into *SphI* & *XmaI* sites.

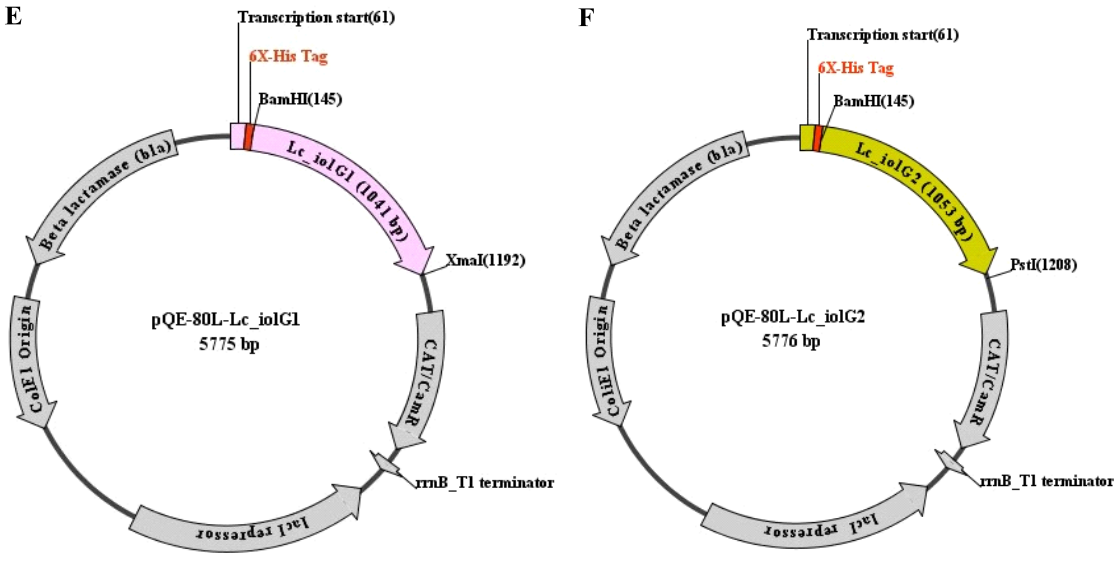

E): *pQE-80L–Lc_iolG1.* *Lc_iolG1* gene ligated into *BamHI* & *XmaI* sites;
F): *pQE-80L–Lc_iolG2* *Lc_iolG2* gene ligated into *BamHI* & *PstI* sites.
All the images were generated using DNADynamo software.

APPENDIX-C
(True kinetics)

Michaelis-Menten saturation curves and double-reciprocal plots (Lineweaver-Burk plots): 1). LcIDH1 with *myo*-inositol and NAD^+:

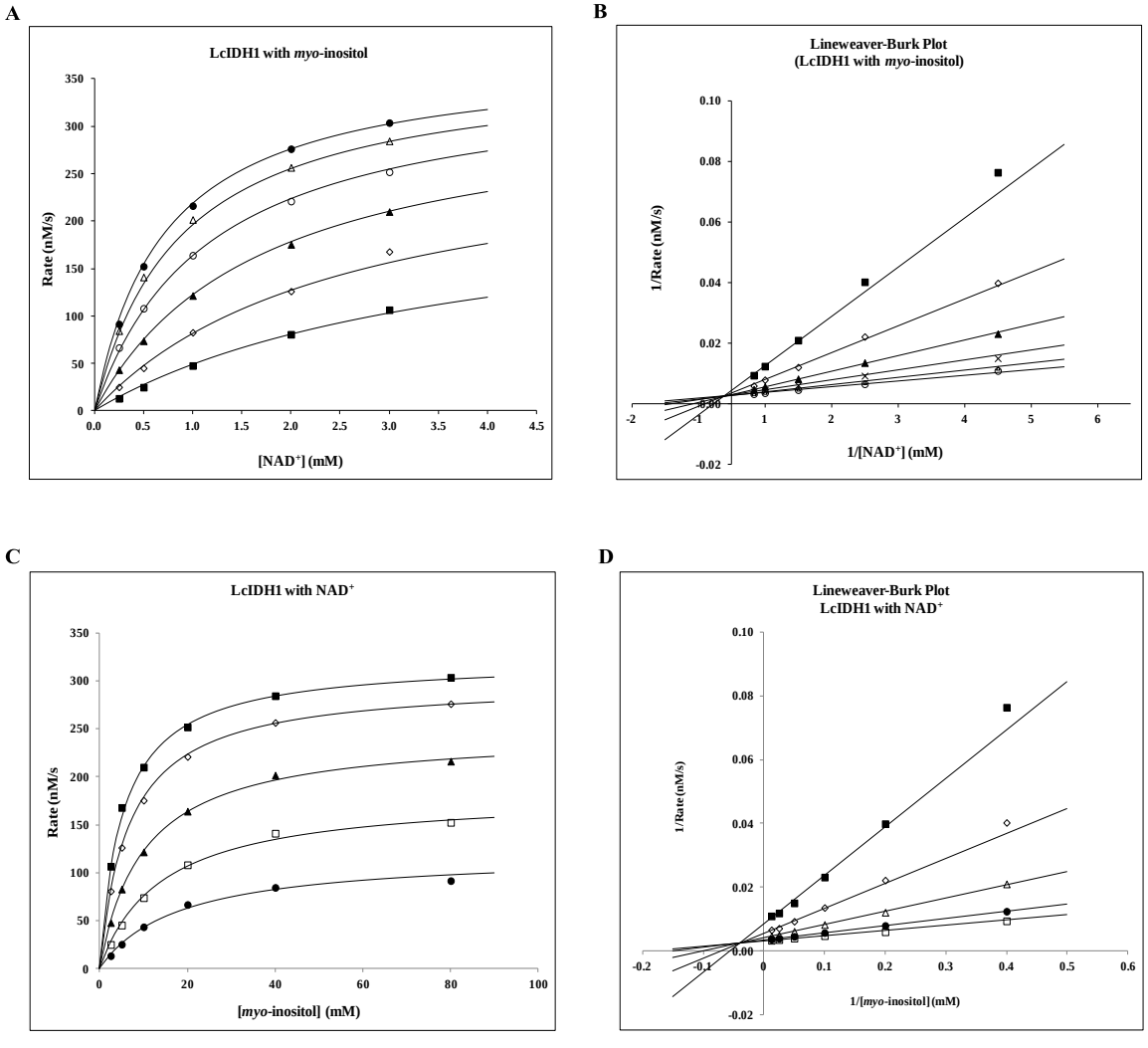

A): (■) 2.5 mM, (◊) 5 mM, (▲) 10 mM, (○) 20 mM, (Δ) 40 mM, and (●) 80 mM *myo*-inositol at different fixed concentrations of NAD^+, 100 mM CHES pH 9.3 at 25 ^oC;

B): (■) 2.5 mM, (◊) 5 mM, (▲) 10 mM, (×) 20 mM, (Δ) 40 mM, and (○) 80 mM *myo*-inositol at different fixed concentrations of NAD^+, 100 mM CHES pH 9.3 at 25 ^oC;

C): (●) 0.25 mM, (□) 0.5 mM, (▲) 1.0 mM, (◊) 2.0 mM, and (■) 3.0 mM NAD^+ at different fixed concentrations of *myo*-inositol, 100 mM CHES pH 9.3 at 25 ^oC.

D): (■) 0.25 mM, (◊) 0.5 mM, (Δ) 1.0 mM, (●) 2.0 mM, and (□) 3.0 mM NAD^+ at different fixed concentrations of *myo*-inositol, 100 mM CHES pH 9.3 at 25 ^oC.

2). LcIDH1 with D-glucose and NAD^+:

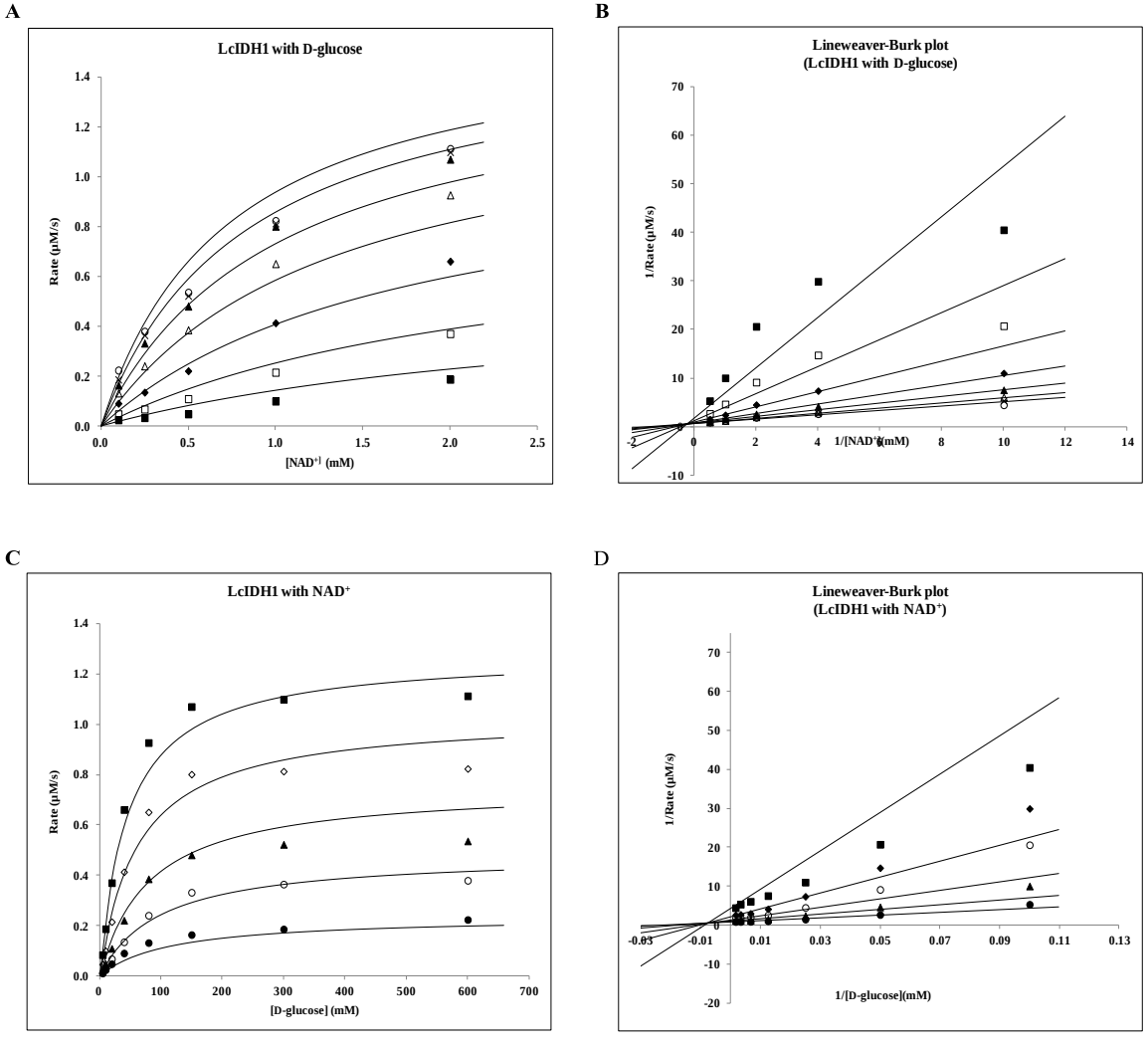

A): (■) 10 mM, (□) 20 mM, (♦) 40 mM, (∆) 80 mM, (▲) 150 mM, (×) 300 mM and (○) 600 mM D-glucose at different fixed concentrations of NAD^+, 100 mM CHES pH 9.3 at 25 ^oC.

B): (■) 10 mM, (□) 20 mM, (♦) 40 mM, (▲) 80 mM, (∆) 150 mM, (×) 300 mM and (○) 600 mM D-glucose at different fixed concentrations of NAD^+, 100 mM CHES pH 9.3 at 25 ^oC.

C): (●) 0.1 mM, (○) 0.25 mM, (▲) 0.5 mM, (◊) 1.0 mM, and (■) 2.0 mM NAD^+ at different fixed concentrations of D-glucose, 100 mM CHES pH 9.3 at 25 ^oC.

D): (■) 0.1 mM, (♦) 0.25 mM, (○) 0.5 mM, (▲) 1.0 mM, and (●) 2.0 mM NAD^+ at different fixed concentrations of D-glucose, 100 mM CHES pH 9.3 at 25 ^oC.

3). LcIDH2 with *myo*-inositol and NAD^+:

A

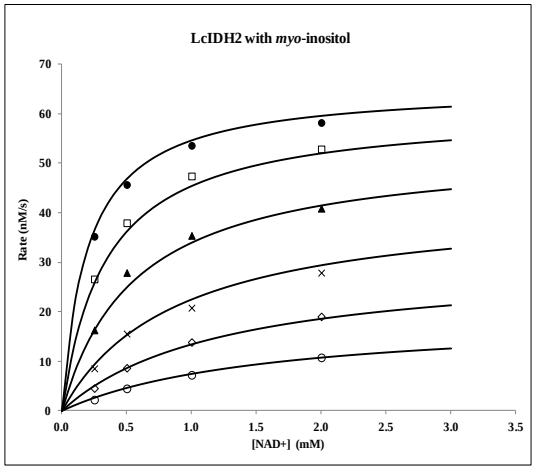

B

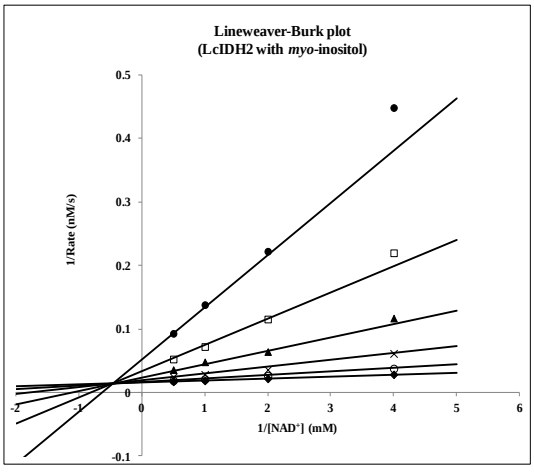

A

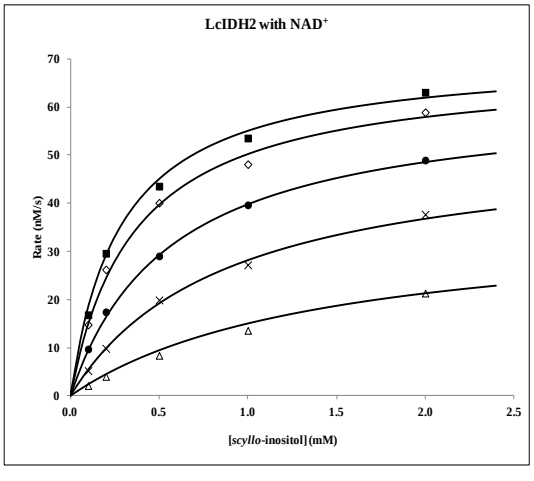

B

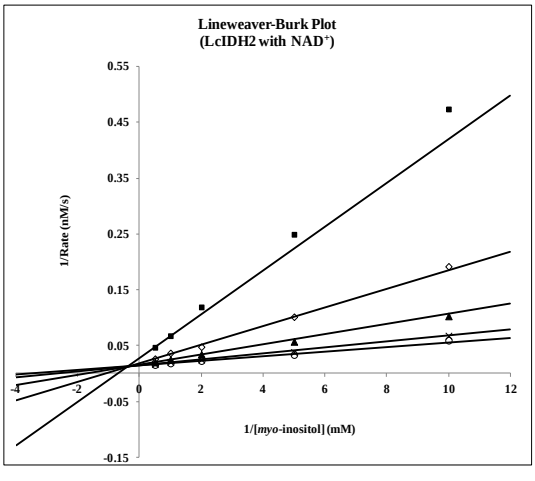

A): (○) 2.5 mM, (◊) 5 mM, (×) 10 mM, (▲) 20 mM, (□) 40 mM, and (●) 80 mM *myo*-inositol at different fixed concentrations of NAD^+, 100 mM CHES pH 9.5 at 25 ^oC.

B): (●) 2.5 mM, (□) 5 mM, (▲) 10 mM, (×) 20 mM, (○) 40 mM, and (♦) 80 mM *myo*-inositol at different fixed concentrations of NAD^+, 100 mM CHES pH 9.5 at 25 ^oC.

C): (Δ) 0.1 mM, (×) 0.2 mM, (●) 0.5 mM, (◊) 1.0 mM, and (■) 2.0 mM NAD^+ at different fixed concentrations of *myo*-inositol, 100 mM CHES pH 9.5 at 25 ^oC.

D): (■) 0.1 mM, (◊) 0.2 mM, (▲) 0.5 mM, (×) 1.0 mM, and (○) 2.0 mM NAD^+ at different fixed concentrations of NAD^+, 100 mM CHES pH 9.5 at 25 ^oC.

4). LcIDH2 with *scyllo*-inositol and NAD^+:

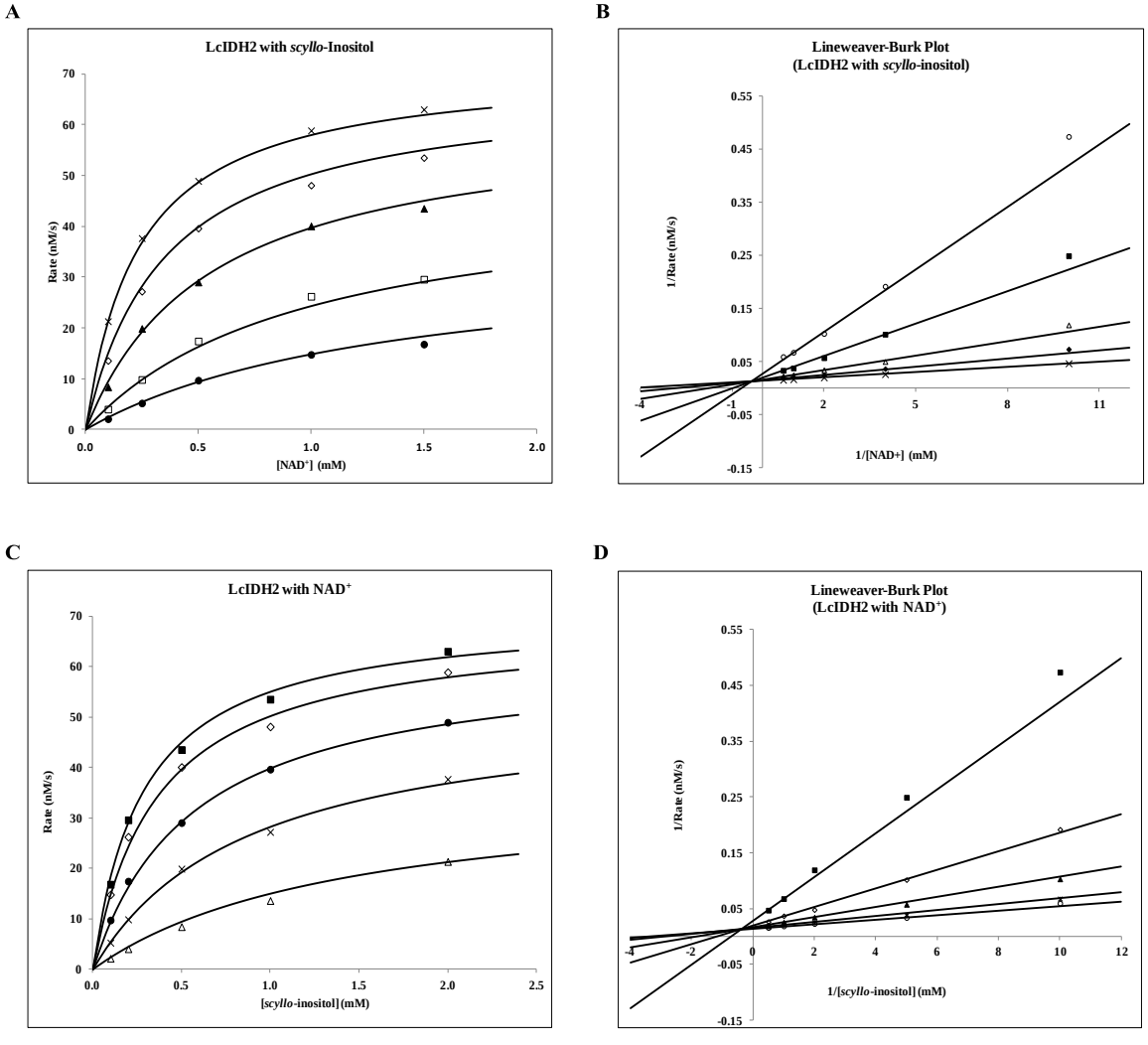

A): (●) 0.1 mM, (□) 0.2 mM, (▲) 0.5 mM, (◊) 1 mM, and (×) 2 mM *scyllo*-inositol at different fixed concentrations of NAD^+, 100 mM CHES pH 9.5 at 25 ^oC.

B): (●) 0.1 mM, (■) 0.2 mM, (▲) 0.5 mM, (♦) 1 mM, and (×) 2 mM *scyllo*-inositol at different fixed concentrations of NAD^+, 100 mM CHES pH 9.5 at 25 ^oC.

C): (Δ) 0.1 mM, (×) 0.25 mM, (●) 0.5 mM, (◊) 1 mM, and (■) 1.5 mM NAD^+ at different fixed concentrations of *scyllo*-inositol, 100 mM CHES pH 9.5 at 25 ^oC.

D): (■) 0.1 mM, (◊) 0.25 mM, (▲) 0.5 mM, (×) 1.0 mM, and (○) 1.5 mM NAD^+ at different fixed concentrations of NAD^+, 100 mM CHES pH 9.5 at 25 ^oC.

5). BsIDH with *myo*-inositol and NAD^+:

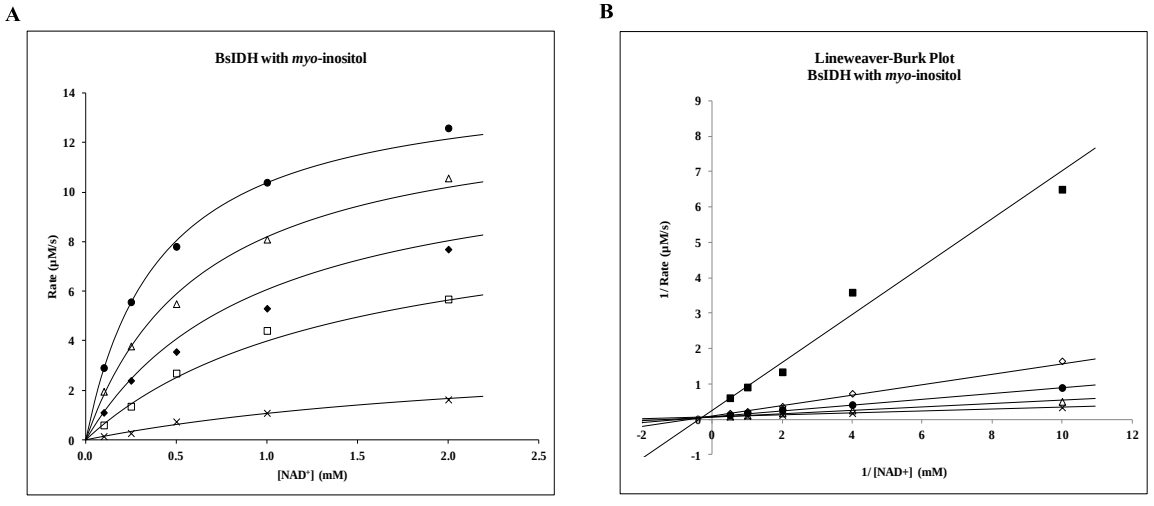

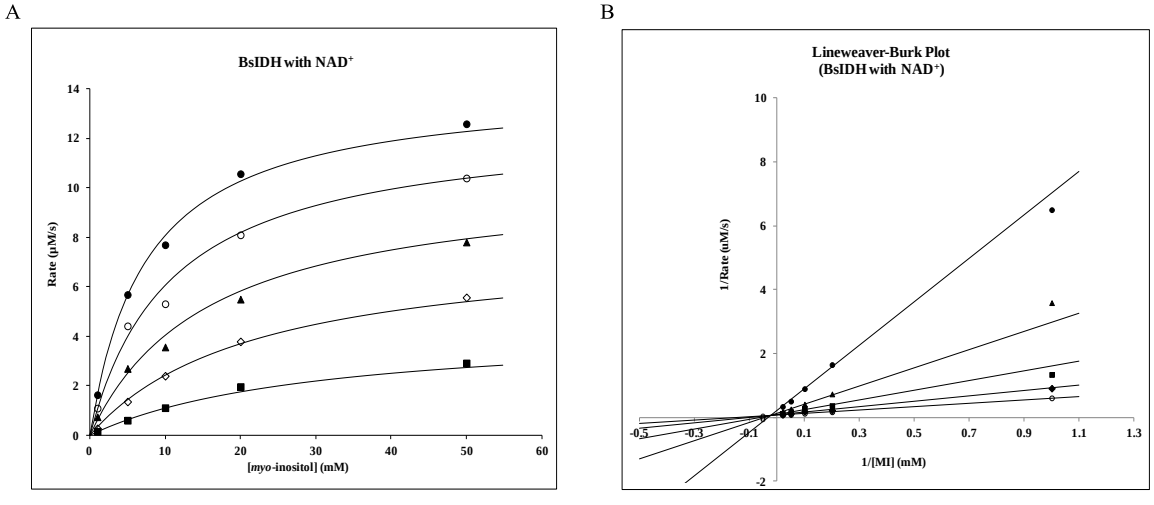

A): (×) 1 mM, (□) 5 mM, (♦) 10 mM, (Δ) 20 mM, and (●) 50 mM *myo*-inositol at different fixed concentrations of NAD^+, 100 mM glycine-NaOH pH 10 at 25 ^oC.

B): (■) 1 mM, (◊) 5 mM, (●) 10 mM, (Δ) 20 mM, and (×) 50 mM *myo*-inositol at different fixed concentrations of NAD^+, 100 mM glycine-NaOH pH 10 at 25 ^oC.

C**):** (■) 0.1 mM, (◊) 0.25 mM, (▲) 0.5 mM, (○) 1.0 mM, and (●) 2.0 mM NAD^+ at different fixed concentrations of *myo*-inositol, 100 mM glycine-NaOH pH 10 at 25 ^oC.

D): (●) 0.1 mM, (▲) 0.25 mM, (■) 0.5 mM, (♦) 1.0 mM, and (○) 2.0 mM NAD^+ at different fixed concentrations of NAD^+, 100 mM glycine-NaOH pH 10 at 25 ^oC.

APPENDIX-D
(Apparent kinetics)

Michaelis-Menten saturation curves and double-reciprocal plots (Lineweaver-Burk plots): 1). LcIDH1 with different substrates at 2mM NAD^+ and100 mM CHES pH 9.3 at 25 ^oC:

A

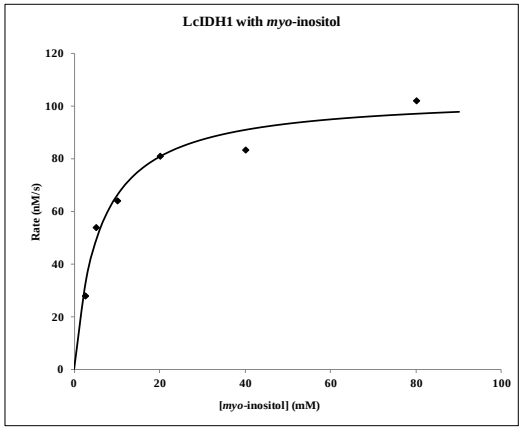

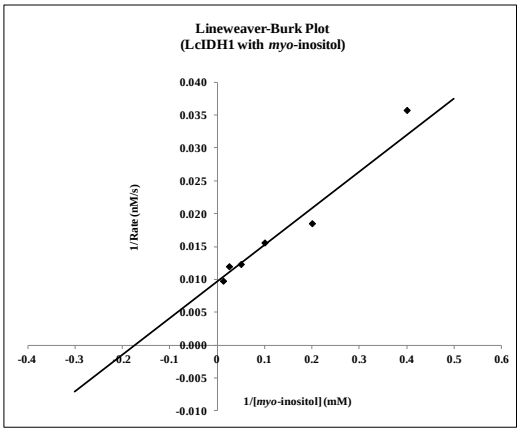

B

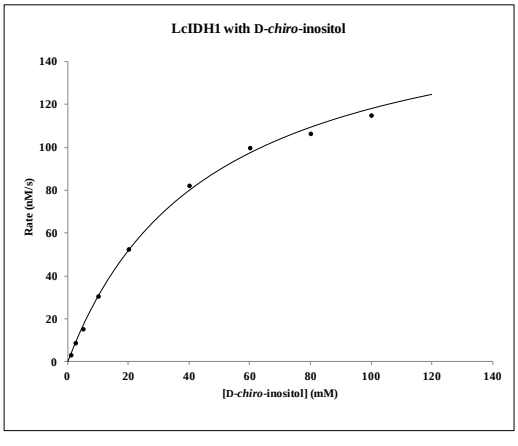

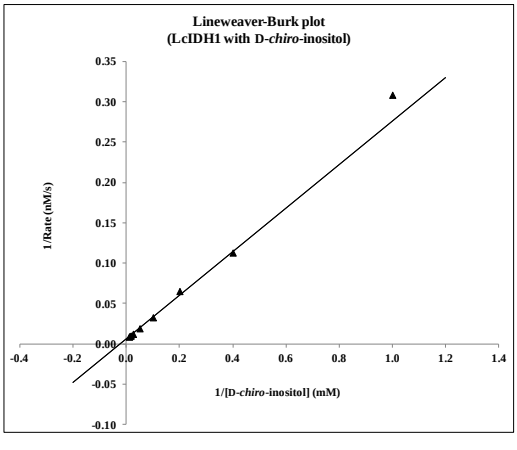

A): 2.5, 5 10, 20, 40, and 80 mM *myo*-inositol;
B): 1, 2.5, 5, 10, 20, 40, 60, 80, and 100 mM D-*chiro*-inositol;

C

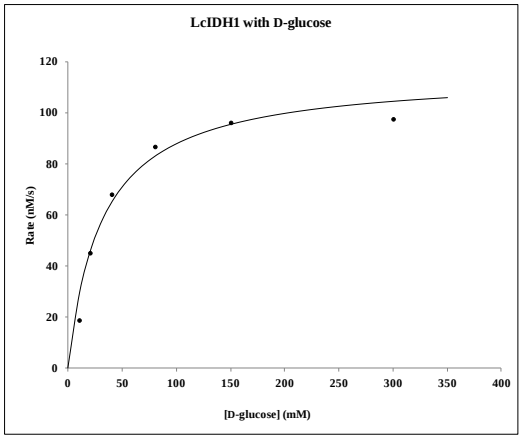

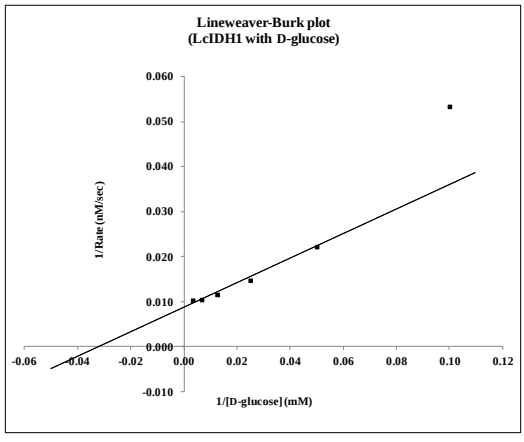

D

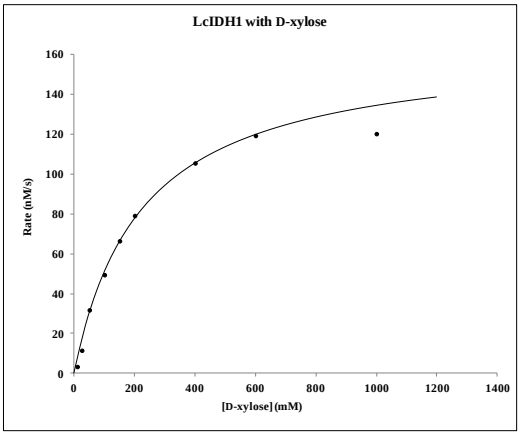

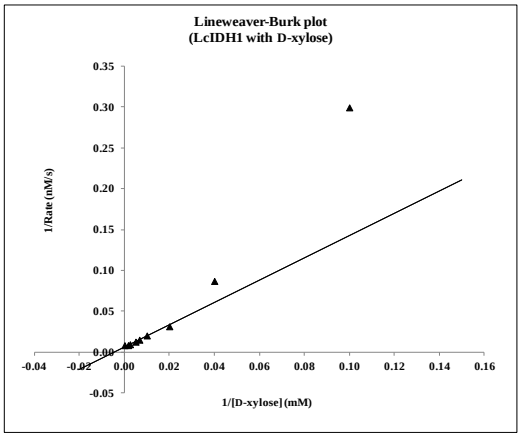

E

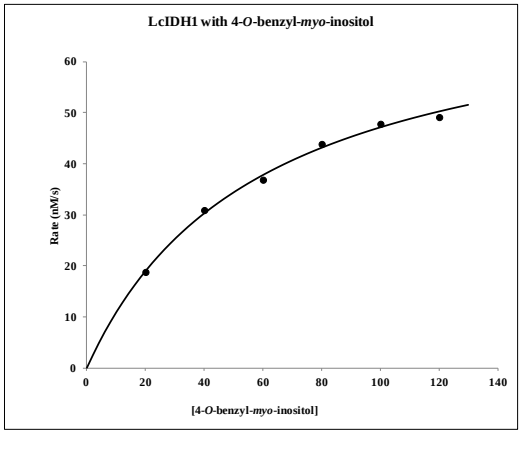

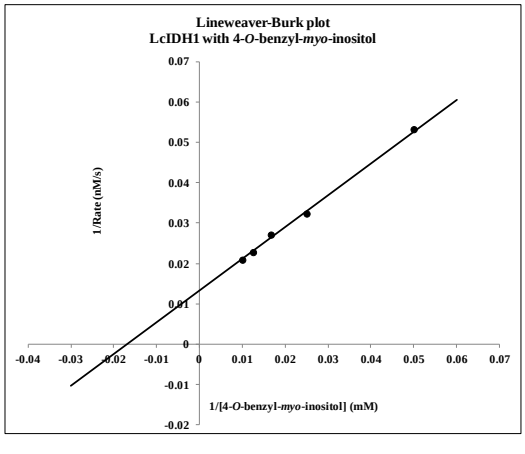

C): 10, 20, 40, 80, 150, and 300 mM D-glucose;
D): 10, 25, 50, 100, 150, 200, 400, 600, 1000 mM D-xylose and
E): 20, 40, 60, 80, 100, 120 mM 4-*O*-benzyl-*myo*-inositol

2). LcIDH2 with different substrates at 2mM NAD^+ and100 mM CHES pH 9.5 at 25°C:

A

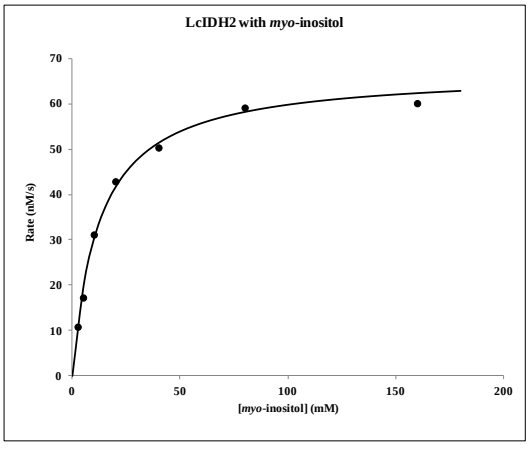

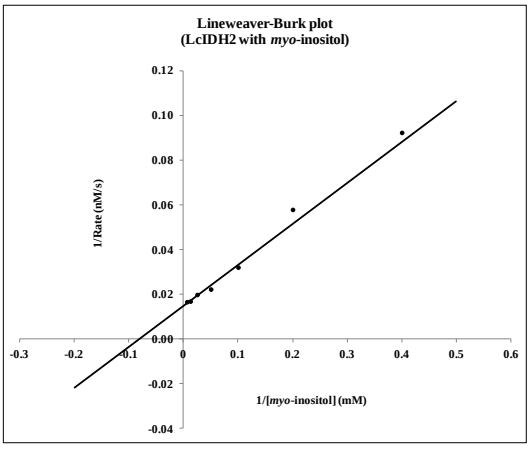

B

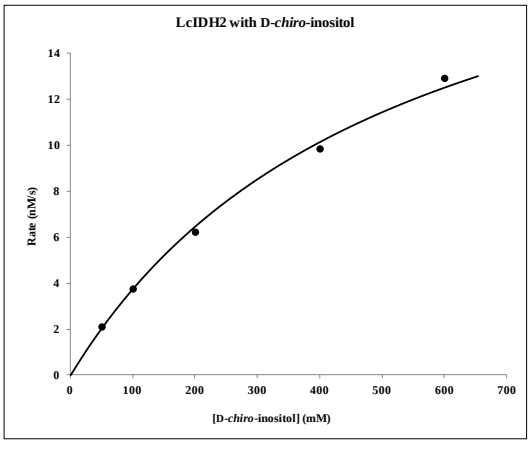

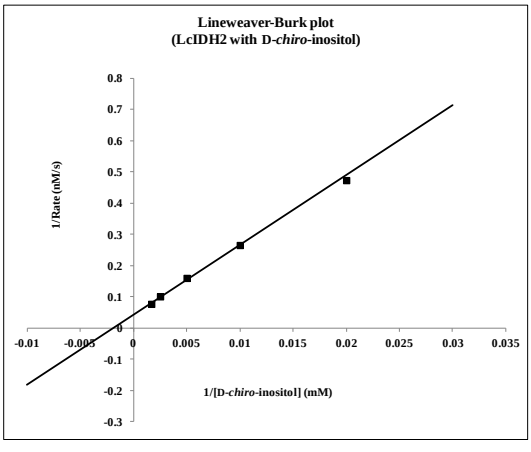

C

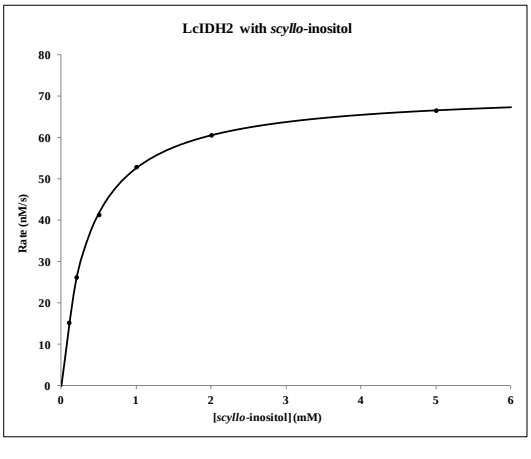

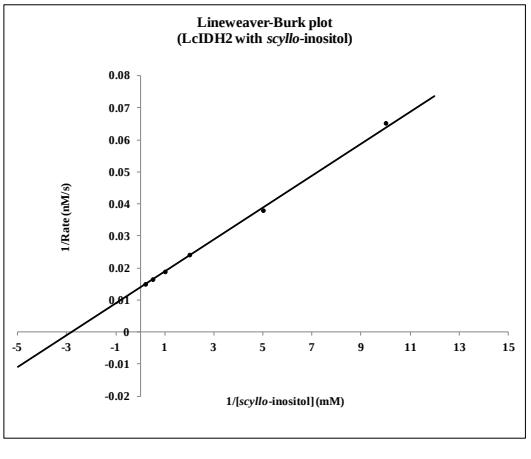

A): 2.5, 5 10, 20, 40, 80, and 160 mM *myo*-inositol;
B): 50, 100, 200, 400, and 600 mM D-*chiro*-inositol;
C): 0.1, 0.2, 0.5, 1, 2, and 5 mM *scyllo*-inositol;

D

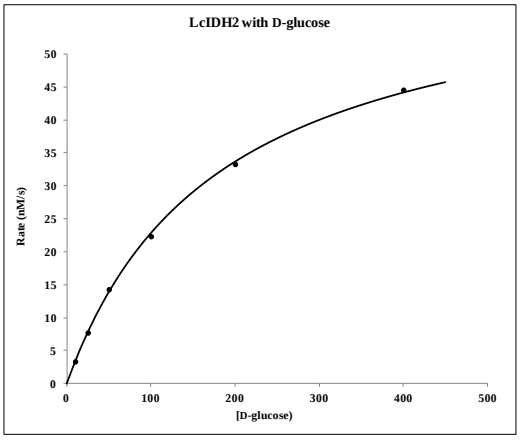

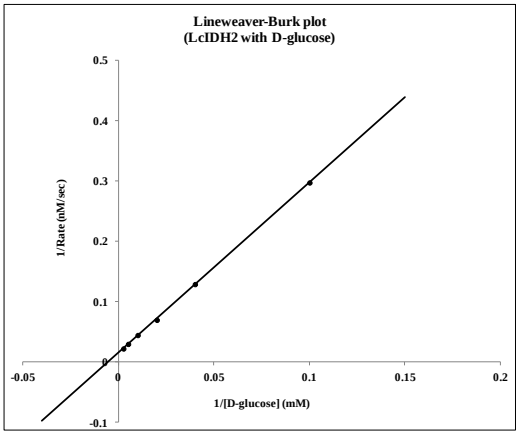

E

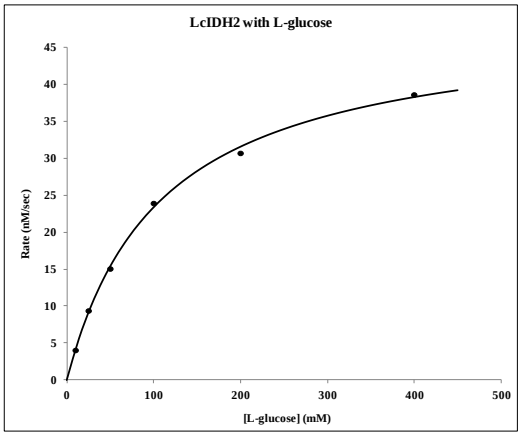

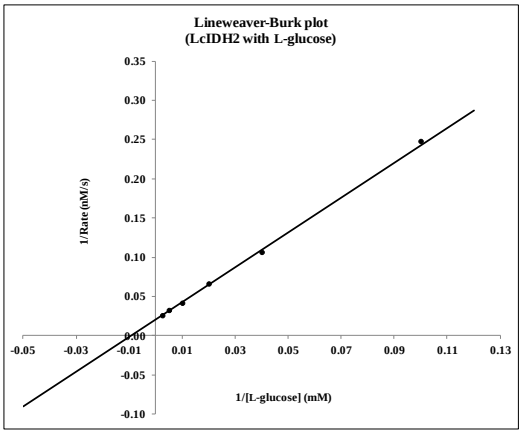

F

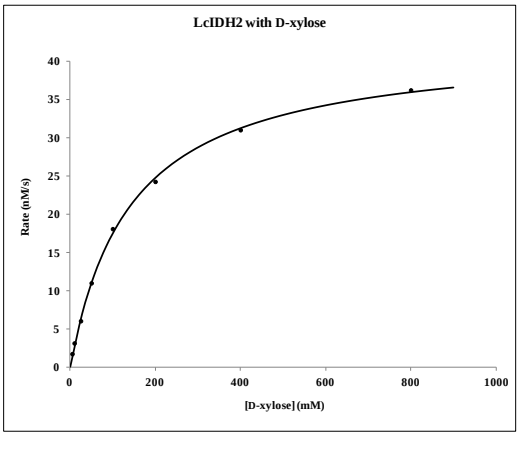

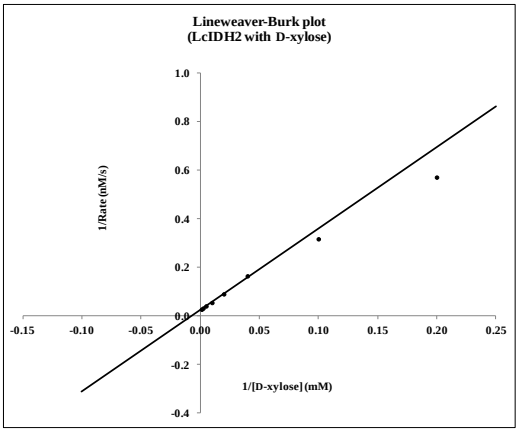

D): 10, 25, 50, 100, 200, and 400 D-glucose;
E): 10, 25, 50, 100, 200, and 400 L-glucose;
F): 5, 10, 25, 50, 100, 200, 400, and 800 mM D-xylose

3). BsIDH with different substrates at 2mM NAD^+ and100 mM glycine-NaOH pH 10 at 25°C:

A

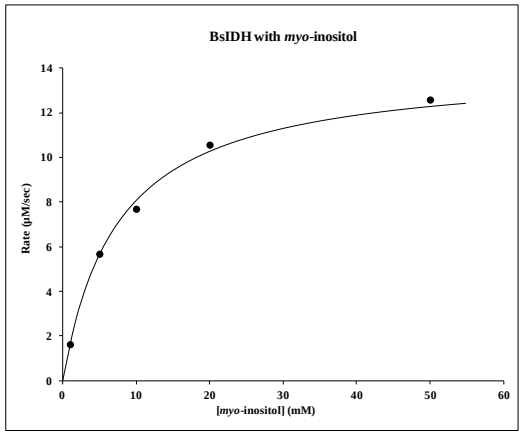

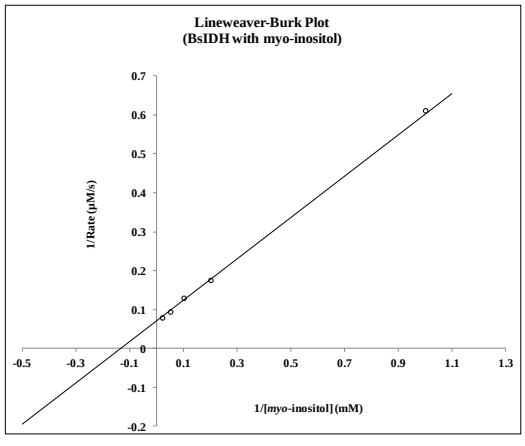

B

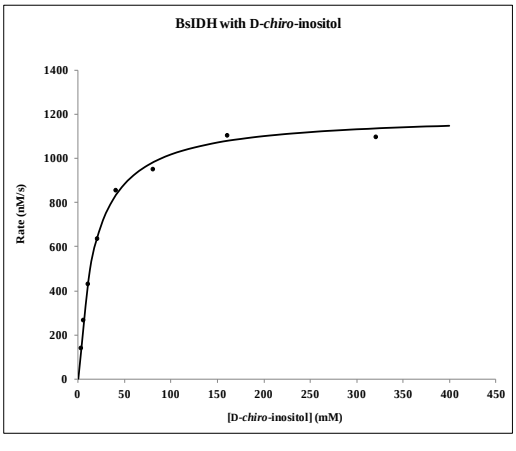

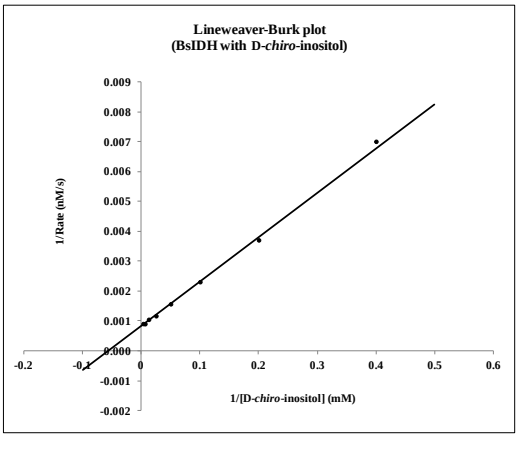

A): 1, 5 10, 20, and 50 mM *myo*-inositol;
B): 2.5, 5, 10, 20, 40, 80, 160, and 320 mM D-*chiro*-inositol;

C

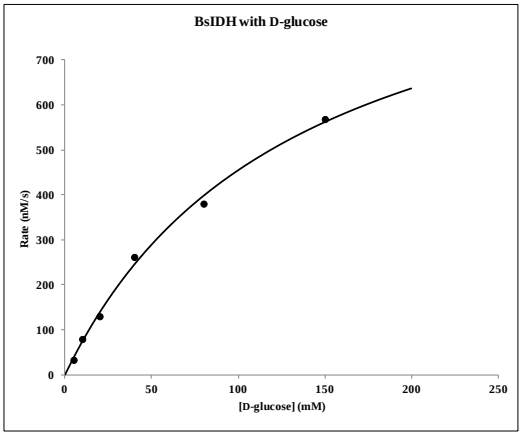

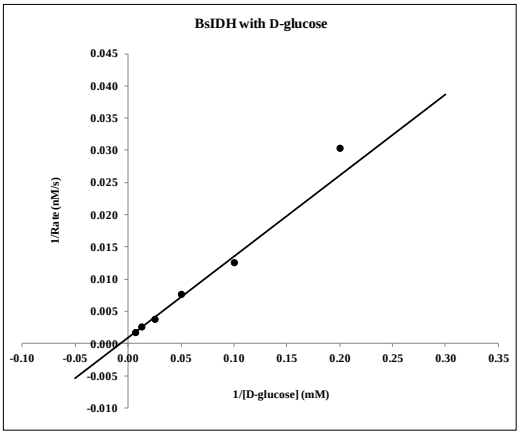

D

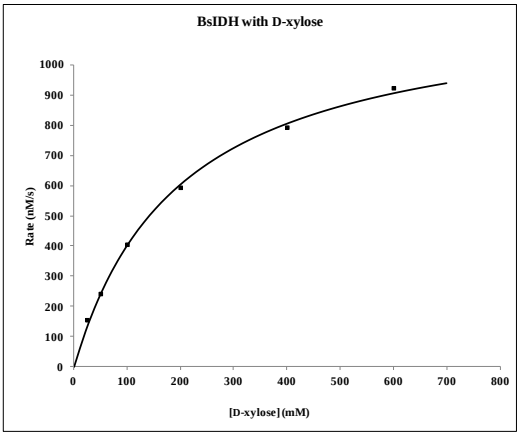

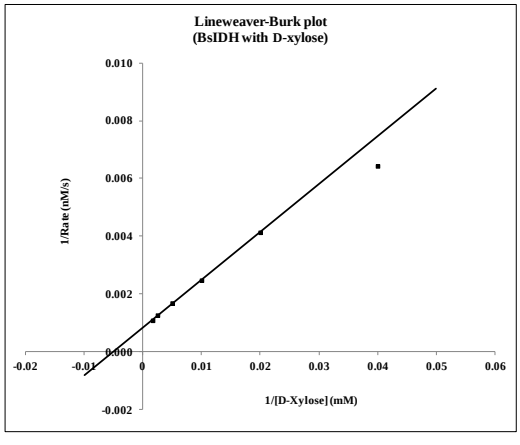

E

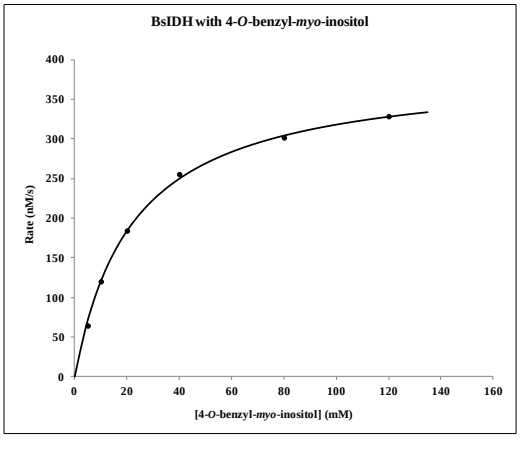

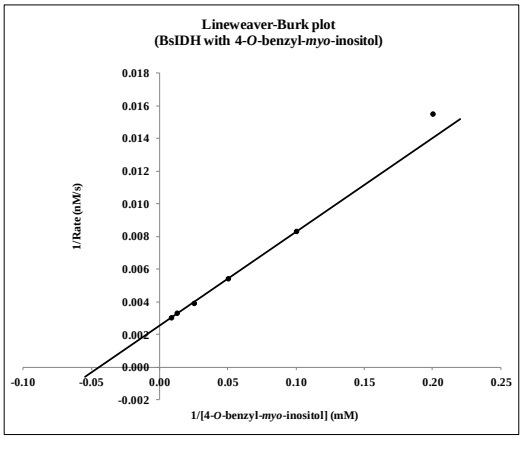

C): 5, 10, 20, 40, 80, and 150 mM D-glucose;
D): 25, 50, 100, 200, 400, and 600 mM D-xylose
E): 5, 10, 20, 40, 80, and 120 mM 4-*O*-benzyl-*myo*-inositol

APPENDIX-E

(Kinetics isotopic effect)

Michaelis-Menten saturation curves and double-reciprocal plots (Lineweaver-Burk plots): 1). LcIDH1 with 2-^{2}H-*myo*-inositol and 2-^{1}H-*myo*-inositol at 2mM NAD^{+} and100 mM CHES pH 9.3 at 25 ^{o}C:

A

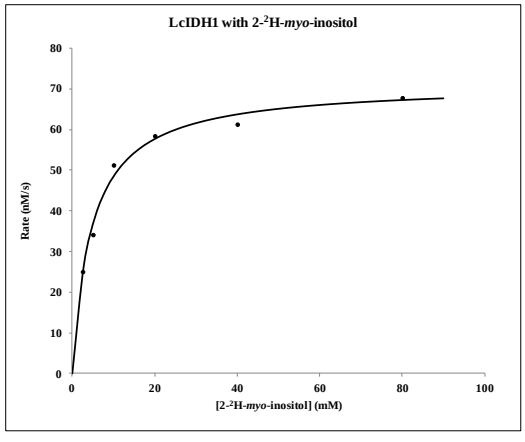

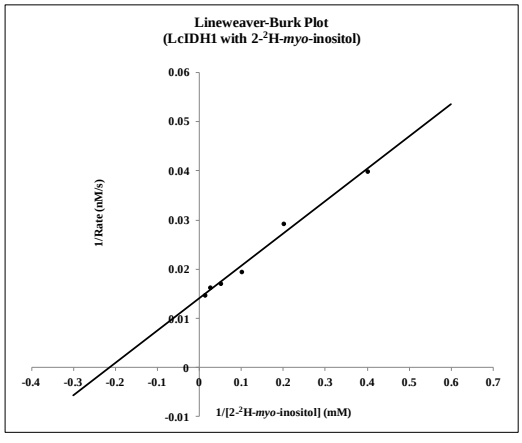

B

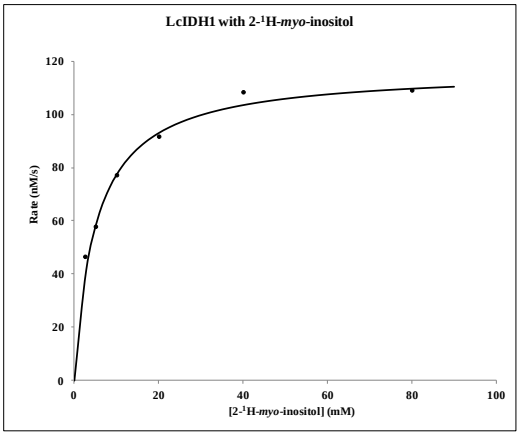

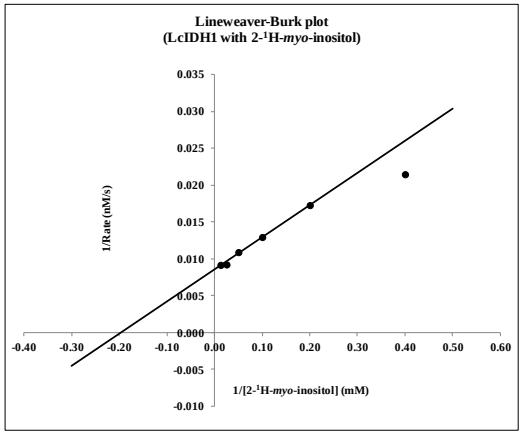

A): 2.5, 5 10, 20, 40, and 80 mM 2-^{2}H-*myo*-inositol and
B): **2.5, 5 10, 20, 40, and 80 mM 2-^{1}H-*myo*-inositol (synthetic *myo*-inositol)**